

# MOUNTAIN-PLAINS CONSORTIUM

MPC 16-315 | C. Pantelides, L. Ibarra, Y. Wang, and A. Upadhyay

Seismic Rehabilitation of  
Skewed and Curved Bridges  
Using A New Generation of  
Buckling Restrained Braces



A University Transportation Center sponsored by the U.S. Department of Transportation serving the Mountain-Plains Region. Consortium members:

Colorado State University  
North Dakota State University  
South Dakota State University

University of Colorado Denver  
University of Denver  
University of Utah

Utah State University  
University of Wyoming

**SEISMIC REHABILITATION OF SKEWED AND CURVED BRIDGES  
USING A NEW GENERATION OF BUCKLING RESTRAINED BRACES**

Chris P. Pantelides  
Professor

Luis Ibarra  
Associate Professor

Yuandong Wang  
Graduate Student

Anurag Upadhyay  
Graduate Student

Department of Civil and Environmental Engineering  
University of Utah  
Salt Lake City

December 2016

## **Acknowledgements**

The authors acknowledge the financial support provided by the Mountain-Plains Consortium (MPC) under project MPC-421.

## **Disclaimer**

The content of this report reflects the views of the authors, who are responsible for the facts and the accuracy of the information presented. This document is disseminated under the sponsorship of the Department of Transportation, University Transportation Centers Program, in the interest of information exchange. The U.S. Government assumes no liability for the contents or use thereof.

NDSU does not discriminate in its programs and activities on the basis of age, color, gender expression/identity, genetic information, marital status, national origin, participation in lawful off-campus activity, physical or mental disability, pregnancy, public assistance status, race, religion, sex, sexual orientation, spousal relationship to current employee, or veteran status, as applicable. Direct inquiries to Vice Provost for Title IX/ADA Coordinator, Old Main 201, NDSU Main Campus, 701-231-7708, [ndsueoaa.ndsu.edu](https://ndsueoaa.ndsu.edu).

## ABSTRACT

The objective of this project is to find effective configurations for using buckling restrained braces (BRBs) in both skewed and curved bridges for reducing the effects of strong earthquakes. Verification is performed by numerical simulation using analytical models of existing bridges when BRBs are implemented for control of seismic forces.

The effect of ground motion incidence angle on the responses of skewed bridges retrofitted with BRBs in the bents is evaluated. A three-span skewed bridge with no retrofit was used as a baseline case. The assessment is carried out in OpenSees using a model that accounts for the BRBs between bent columns, abutment, and shear keys, as well as soil-structure interaction effects. The models are subjected to 21 far-field ground motions, and the maximum response under 11 incidence angles is obtained. The two components in each ground motion set are first rotated to their principal directions to minimize correlation among horizontal orthogonal directions. Thereafter, the ground motion components are scaled to the maximum considered earthquake (MCE) level.

The effect of pounding was investigated for curved bridges considering soil-structure interaction effects. A non-linear finite element model of the bridge was used to investigate structural pounding by performing time history analyses of strong motion earthquake records scaled to site conditions. Pounding between girders and abutments, between girders at expansion joints, and at shear keys was modeled when soil-structure interaction effects were considered using linear link elements. BRBs were modeled between girders and abutment, between girders at expansion joints and in the transverse direction at shear keys using non-linear links. Incremental dynamic analysis was used to assess the bridge performance under various earthquake scenarios with and without BRBs.

# TABLE OF CONTENTS

<b>1. INTRODUCTION.....</b>	<b>1</b>
1.1 Curved Bridge.....	1
1.1.1 Bridge Retrofit .....	2
1.1.2 Soil Structure Interaction .....	3
1.2 Skewed Bridge.....	3
1.2.1 Critical Seismic Analysis of Bridges Using Orthogonal Effects .....	4
1.2.2 Bridge Retrofit with BRB .....	5
<b>2. DESIGN OF BRIDGE.....</b>	<b>6</b>
2.1 Design of Curved Bridge .....	6
2.2 Design of Skewed Bridge .....	10
<b>3. FINITE ELEMENT MODEL.....</b>	<b>14</b>
3.1 Curved Bridge.....	14
3.1.1 Finite Element Model in SAP 2000® .....	14
3.1.2 Ground Motion Data .....	22
3.2 Skewed Bridge.....	30
3.2.1 Skewed Bridge Characteristics .....	30
3.2.2 Skewed Bridge Numerical Model.....	31
3.2.3 Performance Limit States.....	37
3.2.4 Bridge Seismic Performance.....	38
3.2.5 Optimization of BRB Core in Straight Bridge Under ASCE 41-13 Scaled Method.....	38
3.2.6 Principal Direction of Skewed Bridge Under ASCE 41-06 Scaled Method.....	38
<b>4. ANALYSIS RESULTS.....</b>	<b>41</b>
4.1 Analysis Results of the Curved Bridge.....	41
4.1.1 Moment Curvature Analysis .....	41
4.1.2 Static Pushover Analysis.....	41
4.1.3 Results of Non-linear Analysis .....	42
4.1.4 Time History Analysis .....	44
4.1.5 Application of Buckling Restrained Braces .....	54
4.2 Analysis Results of the Skewed Bridge.....	61
4.2.1 Static Pushover Analysis.....	61
4.2.2 Results of Skewed Bridge Performance Analysis.....	64
4.2.3 Results of BRB Core Optimization Under ASCE 41-13 Method.....	66
4.2.4 Results of Parametric Analysis under ASCE 41-06 Method .....	68
<b>5. SIMPLIFIED BRB DESIGN PROCEDURE FOR ABUTMENT POUNDING.....</b>	<b>79</b>
5.1 Calculation for Initial BRB Strength .....	81

<b>6. CONCLUSIONS .....</b>	<b>83</b>
6.1 Curved Bridge.....	83
6.2 Skewed Bridge.....	83
<b>REFERENCES.....</b>	<b>85</b>
<b>APPENDIX A. CURVED BRIDGE DRAWINGS AND SITE PHOTOGRAPH .....</b>	<b>91</b>
<b>APPENDIX B. CURVED BRIDGE SOIL SPRING CONSTANTS .....</b>	<b>98</b>
<b>APPENDIX C. SKEWED BRIDGE DRAWINGS AND SITE PHOTOGRAPHS .....</b>	<b>106</b>

## LIST OF TABLES

Table 2.1	Sectional and reinforcement details for curved bridge columns .....	7
Table 2.2	Details of pile groups and pile caps at various bents of curved bridge .....	9
Table 2.3	BRB dimensions for skewed bridge .....	12
Table 3.1	Ground motions used for time-history analysis of curved bridge .....	24
Table 3.2	BRB dimensions for skewed bridge .....	37
Table 3.3	Limit state definition .....	37
Table 4.1	Periods and mass participation ratios of first 30 modes of curved bridge.....	44
Table 4.2	Effect of Soil-Structure Interaction on first three modes of curved bridge .....	47
Table A.1	Details of pile groups and pile caps at various bents of curved bridge .....	95
Table A.2	Steel girder sections used in curved bridge .....	96
Table B.1	Calculation of $Y_s$ , $Y_c$ and $P$ at various pile depth of curved bridge.....	103
Table B.2	Calculation of P-y curve at depth $Z = 2$ m. for curved bridge.....	104
Table B.3	Tri-linear curve points for P-y curve at $Z=2$ m. for curved bridge.....	105

## LIST OF FIGURES

Figure 2.1	Dimensions of the concrete deck of curved bridge.....	6
Figure 2.2	Plan of bent beam 10 of curved bridge .....	6
Figure 2.3	Details of bent 10 of curved bridge: (a) Elevation; (b) Typical column section details (size and number of rebar are given in Table 2.1).....	8
Figure 2.4	Expansion joint detail for curved bridge.....	8
Figure 2.5	Restrainer rods at expansion joints of curved bridge.....	9
Figure 2.6	Pile cap for bent 10 of curved bridge.....	10
Figure 2.7	Bent design details (adapted from Caltrans 2008).....	10
Figure 2.8	Bent detail: (a) Column cross section; (b) Footing plan (Caltrans 2008) .....	11
Figure 2.9	Idealized pushover curves for column bent system with BRB .....	12
Figure 2.10	Proposed connection: (a) Post-installed adhesive anchor rods; (b) steel plate jacket; (c) additional outside steel frame .....	13
Figure 3.1	Spans of curved bridge modeled in SAP 2000® (top) and computer model (bottom).....	15
Figure 3.2	Column section and reinforcement assignment in SAP 2000® model of curved bridge...	16
Figure 3.3	I-section assignment for one of the girders in SAP 2000® model of curved bridge .....	16
Figure 3.4	T-section assignment using section builder in SAP 2000® model of curved bridge.....	17
Figure 3.5	Rigid links to model diaphragm connections in SAP 2000® model of curved bridge.....	17
Figure 3.6	Analysis model for transverse direction of expansion bearing for curved bridge .....	18
Figure 3.7	Analysis model for friction in longitudinal direction of expansion bearing for curved bridge .....	18
Figure 3.8	Simplified pile-cap model for curved bridge in SAP 2000® .....	19
Figure 3.9	Expansion joint with restrainer rod in SAP 2000® model of curved bridge .....	20
Figure 3.10	Impact element (I.E.): (a) location; (b) analysis model for curved bridge expansion joint.....	20
Figure 3.11	Simplified SAP 2000® model of the curved bridge bent .....	21
Figure 3.12	BRB hysteresis (Wenjing Xu 2016) .....	22
Figure 3.13	DBE and Risk-targeted MCE for the site of curved bridge .....	23
Figure 3.14	Spectral acceleration response spectra of the ground motions for analysis of curved bridge .....	23
Figure 3.15	Chalfant Valley 1986, USA (CDMG Station 54428) .....	25
Figure 3.16	Duzce 1999, Iran (Station - Lamont 1061) .....	25
Figure 3.17	Kobe 1995, Japan (Station - KJMA).....	26
Figure 3.18	Manjil, 1990, Iran (Station - Abbar) .....	26
Figure 3.19	Landers 1992, USA (Station - 000 SCE Station 24).....	27
Figure 3.20	ChiChi 1999, Taiwan (Station - TCU074).....	27
Figure 3.21	Iwate 2008, Japan (Station – Tamati Ono) .....	28
Figure 3.22	Imperial Valley 1979, USA (Station - Cerro Prieto) .....	28
Figure 3.23	Northridge 1994, Newhall, USA (Station - LA County Fire Station, 180) .....	29
Figure 3.24	Irpenia 1980, Italy (Station - Rionero In Vulture) .....	29
Figure 3.25	Parkfield, 1966, USA (Cholame – Shandon Array).....	30
Figure 3.26	Typical forces distribution on skewed bridge.....	31



Figure 3.27	Typical forces distribution on straight/non-skewed bridge.....	31
Figure 3.28	Retrofitted bridge model in OpenSees.....	32
Figure 3.29	Mode shapes of original straight bridge and 36° skewed bridge .....	35
Figure 3.30	Mode shapes of retrofit straight bridge and 36° skewed with BRB.....	36
Figure 3.31	Transverse response spectra for unscaled Landers 1992 Earthquake .....	38
Figure 3.32	Response spectrum for far-field FEMA: (2009) set (a) original spectrum; (b) scaled spectrum .....	39
Figure 3.33	GM set rotation direction.....	40
Figure 4.1	Moment-curvature analysis for column 10 of curved bridge.....	41
Figure 4.2	Pushover curves for various columns of curved bridge.....	42
Figure 4.3	First six mode shapes of curved bridge.....	43
Figure 4.4	Response acceleration of girder G1 relative to abutment for Irpenia, Italy ground motion .....	45
Figure 4.5	Maximum displacement of girder G1 towards the abutment without considering SSI....	46
Figure 4.6	Axial force in restrainer rod; from IDA using Chalfant Valley ground acceleration ignoring SSI .....	46
Figure 4.7	Effect of SSI on relative displacement between girder G1 and abutment .....	47
Figure 4.8	Relative displacement and pounding force for girder G1 at abutment for scaled Kobe ground motion for as-built bridge.....	48
Figure 4.9	Pounding between abutment and girders for Kobe ground motion .....	48
Figure 4.10	Pounding between abutment and girder for Cape-Mendocino ground motion.....	49
Figure 4.11	Pounding between abutment and girder for Chalfant Valley ground motion .....	49
Figure 4.12	Pounding between abutment and girder for ChiChi, Tiwan ground motion.....	49
Figure 4.13	Pounding between abutment and girder for Chuetsu-oki Japan ground motion.....	50
Figure 4.14	Pounding between abutment and girder for Duzce, Turkey ground motion.....	50
Figure 4.15	Pounding between abutment and girder for Parkfield ground motion.....	50
Figure 4.16	Axial force time-history in one of the restrainer rods at expansion joint for scaled Kobe ground motion .....	51
Figure 4.17	Pounding between girders at expansion joint for scaled Kobe ground motion.....	52
Figure 4.18	Location of concrete shear key of curved bridge.....	53
Figure 4.19	Shear keys on curved bridge bent .....	53
Figure 4.20	Pounding force time-history between concrete shear keys and steel girder G1 of curved bridge for Kobe ground motion .....	54
Figure 4.21	Application of longitudinal BRB at the abutment of curved bridge .....	55
Figure 4.22	Retrofit scheme using BRBs at abutment of curved bridge.....	55
Figure 4.23	Bilinear backbone curve used for longitudinal BRB .....	56
Figure 4.24	IDA results of retrofitted curved bridge abutment.....	56
Figure 4.25	Peak relative displacements of girder (G1) of curved bridge for ground motions at various angles of incidence .....	57
Figure 4.26	Response acceleration time history of end of girder G1 of curved bridge for Irpenia, Italy ground motion .....	57
Figure 4.27	Performance of longitudinal BRB at curved bridge abutment for scaled ground motions.....	58

Figure 4.28	Displacement time-history of longitudinal BRB at curved bridge abutment for scaled ground motions. ....	59
Figure 4.29	Backbone curve for lateral BRBs for curved bridge retrofit.....	60
Figure 4.30	Peak displacement of girder relative to concrete shear key for IDA of curved bridge using Kobe ground motion.....	60
Figure 4.31	Hysteresis of one of the lateral BRBs at curved bridge abutment for scaled Kobe ground motion.....	61
Figure 4.32	Calibration of BRB model using experimental results from Xu (2016) .....	62
Figure 4.33	Pushover curves of columns bents retrofitted with BRB.....	63
Figure 4.34	BRB hysteretic response for the three dual systems .....	64
Figure 4.35	Responses of straight bridge under Landers 1992 Earthquake, 23 Coolwater Station ...	665
Figure 4.36	Comparison of different BRB designs for transverse global responses.....	67
Figure 4.37	Comparison of different BRB designs for column bent responses .....	68
Figure 4.38	Comparison of total demand of straight and skewed bridges under 10 incidence angles .....	69
Figure 4.39	Comparison of bent shear of straight and skewed bridges under 10 incidence angles .....	70
Figure 4.40	Combinational PGA.....	71
Figure 4.41	Comparison of abutment transverse shear of straight and skewed bridges under 10 incidence angles .....	72
Figure 4.42	Comparison of abutment longitudinal pounding force of straight and skewed bridges under 10 incidence angles.....	73
Figure 4.43	Comparison of bent drift of straight and skewed bridges under 10 incidence angles.....	74
Figure 4.44	Comparison of side column shear of straight and skewed bridges under 10 incidence angles .....	75
Figure 4.45	Comparison of column concrete strain of straight and skewed bridges under 10 incidence angles .....	76
Figure 4.46	Comparison of column steel strain of straight and skewed bridges under 10 incidence angles .....	77
Figure 4.47	Comparison of column moment capacity to demand ratio of straight and skewed bridges under 10 incidence angle.....	78
Figure 5.1	Design procedure for BRBs at bridge abutments of curved bridge .....	80
Figure 5.2	Design Response Spectrum in AASHTO .....	81
Figure 5.3	BRB backbone curve for SAP 2000® non-linear analysis .....	82
Figure A.1	Plan and elevation of curved bridge spans.....	92
Figure A.2	Elevation of bent 10 of curved bridge.....	93
Figure A.3	Dimensions of the concrete deck of curved bridge.....	93
Figure A.4	Top view of the bent 10 beam of curved bridge .....	94
Figure A.5	Pile group and pile cap at bent 11 of curved bridge.....	94
Figure A.6	Section of steel girder used in the curved bridge .....	95
Figure A.7	Site photograph of curved bridge (Bents 11, 12, 13 and 14) .....	96
Figure A.8	Site photograph of diaphragms connecting the girders of curved bridge .....	97
Figure A.9	Site photograph of fixed bearing condition at bent 9 of curved bridge .....	97
Figure B.1	Location of Bore holes at curved bridge site .....	99
Figure B.2	Soil bore log data at curved bridge site.....	100

Figure B.3	Equations used to calculate foundation-soil spring constants (FEMA 356) .....	101
Figure B.4	P-y curve calculation procedure.....	102
Figure B.5	P-y curve for pile at $Z=2$ .....	105
Figure C.1	Elevation and side view of skewed bridge.....	106
Figure C.2	Picture of on-site bridge (Image capture July 2012, Map data 2015 Google) .....	106
Figure C.3	Bent design details (adapted from Caltrans, 2008).....	106
Figure C.4	Bent detail: (a) Column cross section; (b) Footing plan (adapted from Caltrans, 2008) .....	107
Figure C.5	Abutment plan and elevation .....	107

## EXECUTIVE SUMMARY

Nonlinear time history analyses indicate that seismic behavior of skewed bridges can be significantly different from that of straight bridges due to torsional effects caused by the combination of longitudinal and transverse seismic responses. The skew configuration decreases the difference in responses among different angles due to the combinational effects of longitudinal and transverse directions. After the retrofit implementation, the BRBs in column bents can mitigate the influence of incidence angle. Therefore, to predict the maximum bridge response, it is usually sufficient to apply the minor principal direction ground motion in the bridge longitudinal axis, and the major principal direction orthogonal to the longitudinal axis. The study shows that the effect of ground motion incidence angles on the bridge response is smaller for higher skew angles and for BRB retrofitted bridges. Other findings of the project include:

1. BRBs reduce the bent drift by up to 60% for the evaluated skewed bridges, keeping the bent drift under the operational limit. BRBs reduce the total bridge shear demand by 10% to 25% through hysteretic behavior.
2. The BRB retrofit reduces the demands on the abutment transverse system and shear key components of skewed bridges, which are often damaged during earthquakes.
3. The BRBs retrofit strategy reduces the effect of ground motion input directionality on the output parameters.
4. Skew bridges lead to bent drifts 50% to 100% larger than those of straight bridges, as well as 10% to 20% larger shear demands and about 100% larger steel strains. These larger demands may compromise the structural integrity of the abutment and shear keys, and may lead to deck unseating.
5. The ground motion incidence angle has a greater influence on straight bridges than skewed bridges, since the latter bridges capture frequency content from both horizontal ground motions.
6. The maximum median response for different incidence angles can be reasonably predicted by applying the GM minor principal direction on the bridge longitudinal axis, and the major principal direction in the orthogonal direction, even if for skewed bridges it does not correspond to the bent direction.

Nonlinear time history analyses were carried out for a curved bridge studied in this research to investigate the benefits of a retrofit using BRBs on the seismic response. The findings for the curved bridge study are as follows:

1. When the bridge model was analyzed without soil-structure interaction (SSI) effects under the DBE earthquake level, girder displacements were less than the gap provided at the abutments and at the expansion joints; no pounding was observed and the columns had sufficient strength to resist the seismic forces. In addition, bearing displacements were underestimated if SSI was ignored.
2. The bridge model was re-analyzed including SSI, which lengthened the fundamental period of vibration. Displacement of the girders relative to the abutments increased due to SSI effects to a level higher than the construction gap, leading to pounding between girders and abutments. Restrainer rods at the expansion joints buckled or fractured, which led to pounding between the girders. Shear keys experienced high pounding forces and potential failure due to movement of the girders in the transverse direction.
3. Incremental dynamic analysis showed that BRBs placed between girders and abutments were able to reduce the relative displacement more effectively on the side of the bridge with the smallest radius of curvature; the relative displacement reduction at this location reached a median level of 50% for the 15 earthquakes considered.

4. BRBs placed between girders along the girder axes were able to prevent pounding at the expansion joints. In addition, BRBs placed in the transverse direction were able to prevent concrete shear key damage and potential failure.
5. For the 15 earthquake records examined, nonlinear analysis, including SSI effects, showed that pounding was avoided for the as-built structure for a median spectral acceleration up to 0.91g; for the retrofitted structure with BRBs, pounding was avoided for a median spectral acceleration up to 1.56g. The seismic bridge retrofit using BRBs could be used to prevent damage and potential failure at bridge abutments, expansion joints, and shear keys and unseating of steel girders during strong earthquakes.

# 1. INTRODUCTION

## 1.1 Curved Bridge

Structural pounding related to earthquakes is a well-documented phenomenon in buildings and bridges. Evidence of damage to bridge abutments and decks from structural pounding is abundant. Performance of steel bridges in the 1995 Hyogo-ke Nanbu (Kobe) earthquake was investigated by Bruneau et al. (1996); and in the 2011 Great East Japan earthquake, Buckle et al. (2012) investigated several types of failures occurred during these earthquakes. A large number of bridges experienced damage in the seismic restrainers or in the concrete and steel shear keys, resulting in unseating or total collapse of spans at expansion joints and abutments (Itani et al. [2004], Hao and Chouw [2008]). A number of studies have been carried out to predict the seismic response of existing bridges and specifically the pounding damage at the abutments and expansion joints. Most of these studies did not include soil-structure interaction, which has a significant effect on the response of bridge structures, particularly for soft soils.

A number of studies have analytically evaluated the seismic response of typical Multi Span Simply Supported (MSSS) and Multi Span Continuous (MSC) steel girder bridges in order to better understand the seismic behavior and impact of modeling fidelity on the performance of these bridges. Dicleli and Bruneau (1995) found that bearing stiffness significantly affects the response of MSSS steel girder bridges, and they indicated that if pounding was considered in the longitudinal direction, there could be a large potential for shearing of bearings and span unseating; with MSC bridges, damage to steel bearings is probable but may serve as an effective way of isolating the superstructure and preventing further column damage.

DesRoches and Muthukumar (2002) investigated the effect that pounding and restrainers have on the global demand of bridge frames in multi-frame bridges and showed that the primary factors affecting pounding were the frame stiffness ratio or period ratio of adjacent frames in a bridge and the ground motion effective period ratio. Pounding increases when the two frames are highly out-of-phase and decreases when the frames vibrate near the characteristic time period of the ground motion. Also, the effect of restrainers was evident significantly in highly out-of-phase frames and was marginal in other cases.

Padgett and DesRoches (2008) evaluated the three-dimensional nonlinear seismic performance of retrofit measures for typical steel girder bridges; they showed that the use of elastomeric bearings in MSC bridges increased passive deformations from 17.4 to 29.0 mm due to pounding. Pan et al. (2007, 2010) performed parametric studies to evaluate seismic fragility of MSSS highway bridges and showed that pounding of girders at abutments may lead to a change in curvature ductility of the concrete piers.

Li et al. (2013) studied the effect of abutment excitations on seismic pounding in bridges. Bi and Hao (2013) performed a detailed 3D analysis to understand pounding between girders and between bridge girders and the corresponding abutment of a two-span simply supported bridge subjected to spatially varying ground motions. The results showed that 1D excitations overestimate the pounding forces as 2D excitations lead to eccentric pounding, which has more pounding events but smaller pounding forces. Permanent girder displacements of up to 100 mm were also observed in the analysis. However, soil structure interaction was not considered in the analysis.

Huo and Zhang (2013) used the fragility function method to study the effects of pounding and skewness on the seismic behavior of typical multispan RC highway bridges. Accelerations in pounding cases were five to ten times more than those without pounding, and severity of damage increased with irregularity in the bridge structure. Nielson and DesRoches (2006) studied the influence of modeling assumptions on the

seismic response of multi-span simply supported steel girder bridges in moderate seismic zones. The study showed the importance of the selection of appropriate modeling parameters.

### **1.1.1 Bridge Retrofit**

El-Bahey and Bruneau (2011, 2012) performed non-linear time history analysis using BRBs as structural fuses for the retrofit of bents of concrete bridges and presented a design procedure for BRBs. The design procedure was found satisfactory and was similar to the procedure available in the AISC (2010) manual but with modified values. Capron (1999) retrofitted a bridge using shock transmission type longitudinal restrainers at expansion piers, between concrete blocks and steel bumpers for increased transverse force transfer capacity. Time-history analysis of the retrofitted bridge showed that the restrainers provided significant longitudinal displacement control. Shock transmission devices allow slow thermal expansion movements, but resist relatively fast movements. Kanaji et al. (2003) used BRBs to retrofit the Minato Bridge, one of the longest steel truss bridges.

Andrawes and DesRoches (2007) used shape memory alloy (SMA) seismic restrainers for possible retrofit of a bridge and compared the performance with steel cable restrainers, metallic dampers, and visco-elastic dampers using OpenSees 2D analysis. The sensitivity analysis showed that all devices except the steel restrainers performed well. Tension-only behavior of the steel restrainers combined with the yielding behavior of steel results in an accumulation of residual displacement. Tension-only SMA devices were 34% more effective compared with the steel restrainers. Padgett and DesRoches (2008) and Zhou and Meng (2011) showed that use of cable restrainers to mitigate pounding can be effective in multi-span continuous steel girder bridges.

Raheem (2009) presented results from a non-linear analysis on a multi-span steel girder bridge by idealizing it as a two-dimensional non-linear numerical finite element model utilizing three types of restrainer configurations at the expansion joint. Pounding reduced the segment displacement response when vibrating near the characteristic period of the ground motion and increased the adjacent segment response. The restrainers attached through the bent cap to the girders perform better in preventing unseating of the girders and reducing the displacements between superstructure and substructure. The study showed that by using shock absorbers between the bridge segments or the restrainers' ends as potential practical mitigation measures against impact due to pounding, the sudden changes of stiffness can be smoothed. However, the shock absorbers do not work once restrainer rods fail in earthquakes.

Reno and Pohl (2013) presented a possible retrofit of a steel bridge with BRBs at both the ends to avoid pounding and presented satisfactory results from numerical analysis. However, the study did not state any consideration of soil-structure interaction for the analysis. Sun et al. (2012) used BRBs as possible energy dissipators in dual piers in a cable stayed bridge. However, the study did not find the use of BRBs in dual piers to be effective.

Much of the research used BRBs in the transverse direction as a cross fuse element; Celik and Bruneau used BRBs in both the transverse and longitudinal directions. Celik and Bruneau (2009, 2011) developed closed-form solutions for two retrofit schemes for straight and skewed steel girder bridges using BRBs in ductile end diaphragms. The purpose of the retrofit scheme was to reduce the seismic demand in the superstructure by hysteretic energy dissipation. No time-history analysis was performed to support the closed-form solutions.

### 1.1.2 Soil Structure Interaction

Not many studies regarding pounding damage to bridges considering soil-structure interaction (SSI) have been performed [Ingham et al. (1999), Konagai et al. (2003)]. However, the literature shows that SSI has a significant role in determining the behavior of a bridge. Makris and Zhang (2002) performed a non-linear numerical analysis of a freeway overcrossing equipped with elastomeric bearings and fluid dampers. A parametric study of non-linear seismic response of the bridge accounting for the effects of soil-structure interaction showed that fluid dampers reduced the large displacements and accelerations at the deck ends. Also, soil-structure interaction increased the displacements and forces at the abutments.

Soneji and Jangid (2008) studied the effect of soil-structure interaction on the response of a seismically isolated cable-stayed bridge. Time-history analyses showed that depending on the ground motion, the displacement response of the bridge varied to a large extent when SSI was taken into account. SSI increased the fundamental period of the structure, which changed the spectral acceleration range for response and the displacement controlled behavior dominated. However, as the stiffness of the soil strata increased, the effect of SSI diminished. Konagai et al. (2003) presented a single beam analogy for a pile group, which shows that using appropriate values for soil and pile stiffness, a pile group can be considered as a single pile which makes numerical analysis feasible.

Review of the research shows that there have not been enough investigations of pounding damage in curved steel girder bridges taking soil-structure interaction into consideration. Recognizing the complexities involved with the bridge pounding problem, this study is an attempt to examine the retrofit measures with Buckling Restrained Braces for an existing curved bridge on pile foundations in soft soil.

## 1.2 Skewed Bridge

Surveys of U.S. highway bridges indicate that 24% of the total 607,708 bridges in the United States are structurally deficient or functionally obsolete (US DOT, 2014). Since many bridges are located in seismic regions like California and Utah, they may suffer unrepairable damage or even collapse when subjected to strong earthquakes. Jennings and Wood (1971) reported major damages for a four-span reinforced concrete (RC) skewed bridge at center bent columns and abutments because of in-plane rotational effects in the 1971 San Fernando earthquake. Other seismic-induced failures from the offset angle of skewed bridges were reported, such as unseating or permanent offset of the superstructure, failure of bearings, and shear damages of columns (Wakefield et al. 1991, Catacoli et al. 2012).

Skew bridges increase rotational effects due to the longitudinal forces developed between deck and abutment. These forces would create an additional rotation around the center of gravity center of the entire system.

Maragakis and Jennings (1987) proved that the rigid body motion of the bridge deck along with the impact between the deck and the abutments can lead to severe damage on skew highway bridges. Wakefield et al. (1991) utilized nonlinear models to analyze skewed bridge seismic effects, showing that skewed dynamic responses are dominated by in-plane rigid body motion in translation and rotation direction. The main vulnerability was at the center bent columns in transverse direction of abutment due to deck rotation. Haque and Bhuiyan (2012) performed seismic response analyses of a simple-span concrete deck girder skewed bridge with a wide range of skewed angles, finding that larger skewness increases base shear, deck acceleration, and bearing reactions. The typical seismic damages are caused by complicated dynamic responses. Longitudinal and transverse seismic excitations may induce a longitudinal force ( $F_L$ ) and transverse forces, which must be resisted by the backfill soil passive force ( $P_P$ ) normal to the abutment wall and the shear resistance ( $P_R$ ) on the shear key or wingwall system. However,



compared with the symmetric force distribution of a straight bridge, the asymmetric forces may cause a rotational moment  $M_R$  when the deck collides with the abutment (Watanabe and Kawashima, 2004).

Amjadian and Kalantari (2012) performed parametric studies with different widths of expansion joints (gap), the skewness angle, and the normalized stiffness eccentricity along the longitudinal direction for GMs in longitudinal and transverse directions. They concluded that for larger values of skewness angle and a smaller gap, the rotational effects induced by pounding are significant. A skewed bridge may amplify rotational motions around the center of the superstructure, leading to higher forces on the transverse support of the abutment and less longitudinal stress on the backing soil (Wilson et al. 2014).

### 1.2.1 Critical Seismic Analysis of Bridges Using Orthogonal Effects

In seismic events, a pair of horizontal ground motions can propagate from any direction toward a bridge, resulting in different levels of seismic demand for the structure. The principal axes of a pair of ground motions are uncorrelated (Penzien and Watabe 1975), whereas the major principal axis in general points to the epicenter, which is usually close to a fault normal (FN) direction. Since the recording instrument could have been installed at any orientation, the principal ground acceleration is rarely recorded. Furthermore, the uncertainty of the epicenter and fault makes the principal seismic demand of a certain structure more unpredictable. But even with the set of orthogonal principal ground motions, the responses can still vary when they propagate from different directions. This phenomenon is called orthogonal effect; and the input angle with respect to longitudinal axis is called incidence. For design purposes, calculation of the maximum demand is necessary to ensure the structural safety.

Maleki and Bisadi (2006) conducted linear seismic analyses on skewed bridges with original orthogonal records to determine the critical response under varying ground motion incidence angles. A single-span I-girder skewed bridge of different lengths of 10 m, 20 m and 30 m with varying skewed angles from  $0^\circ$  to  $60^\circ$  was used as a case study. They were not able to determine the critical input angle that produced the maximum response for the case bridge, and they suggested considering at least three input angles of  $0^\circ$ ,  $60^\circ$ , and  $120^\circ$  to obtain the maximum response. Bisadi and Head (2011) performed a parametric study with 100 paired ground motions, 100 different bridge configurations, and ground motion incidence angles varying from  $0^\circ$  to  $180^\circ$  with increments of  $10^\circ$ . The results showed that the critical angle of incidence that caused maximum response was dependent on the characteristics of the ground motions and the bridge. Mackie et al. (2011) performed time history analyses in different bridge structures with different span length by varying the incident angle of ground motions. They concluded that varying the angle from  $0^\circ$  to  $180^\circ$  had negligible effects on the bridge response.

Torbol and Shinozuka (2012) examined orthogonal effect on the fragility curves of straight bridges with FN/FP ground motions for incidence angle varying from  $0^\circ$  to  $360^\circ$ . The results showed that even though the bridges are regular and symmetric, neither longitudinal nor transverse is the weakest direction. Bhatnagar (2013) modeled the skewed Painter Street Bridge to show skewness effects under various incident angles for a suite of orthogonal ground motions. The results proved that variation of the maximum response of skew bridge could be observed with respect to change in angle of incidence, change in skew angle, and a combination of both. However, the uncertainty of response spectrum shape under bridge fundamental structure may bias the results.

### **1.2.2 Bridge Retrofit with BRB**

Buckling restrained braces (BRBs) have been proposed to increase the seismic capacity of bridge decks and RC bridge bent (Celik and Bruneau 2009, El-Bahey and Bruneau 2011). Recently, Dusicka et al. (2015) performed both experimental and numerical analyses to seismically deficient bridge bents retrofitted using BRBs in diagonal configurations. The results showed the effectiveness of using BRBs to achieve high displacement ductility of retrofitted bridge bent while controlling the damage of vulnerable bent columns. Wang et al. (2016, 2017) presented a comprehensive evaluation on the use of BRBs to seismically retrofit existing straight RC bridges. The results proved that the additional BRBs in column bents can reduce bent drift and redistribute stiffness in the transverse direction of the bridge between bent and abutments dissipating shear demand through BRB hysteretic behavior. Upadhyay et al. (2016a, 2016b) showed that pounding between girders and abutment, and between girders at expansion joint of a curved bridge, can be prevented successfully with the help of BRBs.

## 2. DESIGN OF BRIDGE

### 2.1 Design of Curved Bridge

The curved bridge under investigation is a part of the existing I-15 corridor and provides an exit toward West Valley at 3300 South. A plan of the bridge is provided in Appendix A (Figure A.I). The bridge consists of a reinforced concrete deck supported on three steel girders, which are robustly connected with each other via cross-frames every 15 feet. This truss assembly helps the superstructure to act as a continuous deck with effective strength much higher than the individual girder, thus minimizing deck displacements. These cross-frames are connected to the main girders through bolted joints. The diameter of the columns of this bridge varies from 1.981 m to 2.314 m and the height of the columns from 6 m to 13.5 m. Section properties of the columns and reinforcement details along with confining steel are given in Table 2.1 and Figure 2.3. All reinforcing steel complies with ASTM A706 grade 60, and the 28-day compressive strength of concrete is 25 MPa. Pier cap beams are non-prismatic, therefore non-prismatic sections have been generated and assigned to the beam elements representing the beams.

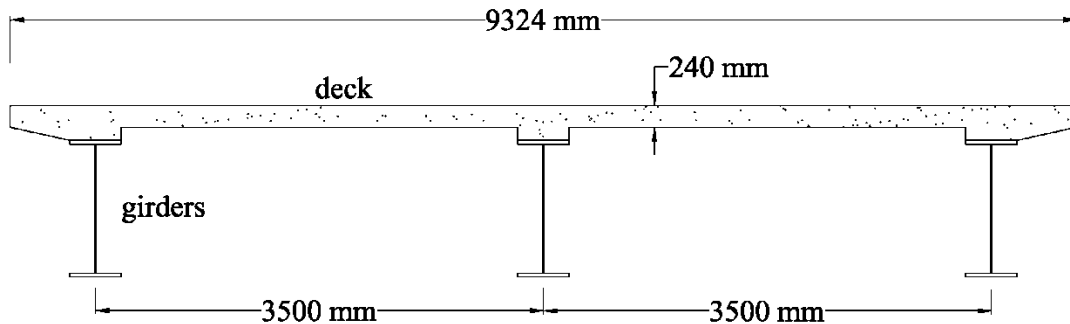
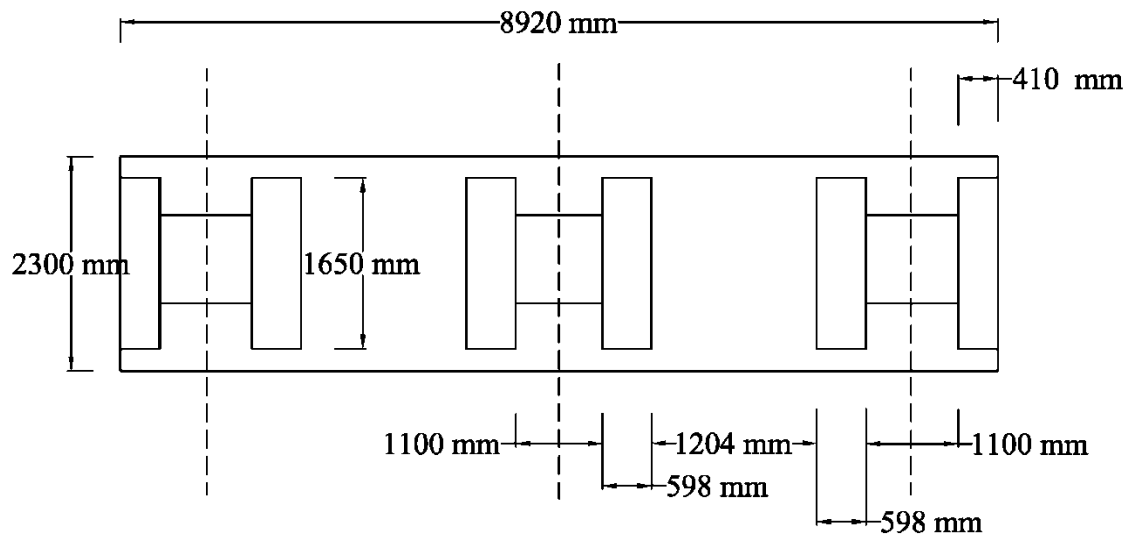


**Figure 2.1** Dimensions of the concrete deck of curved bridge



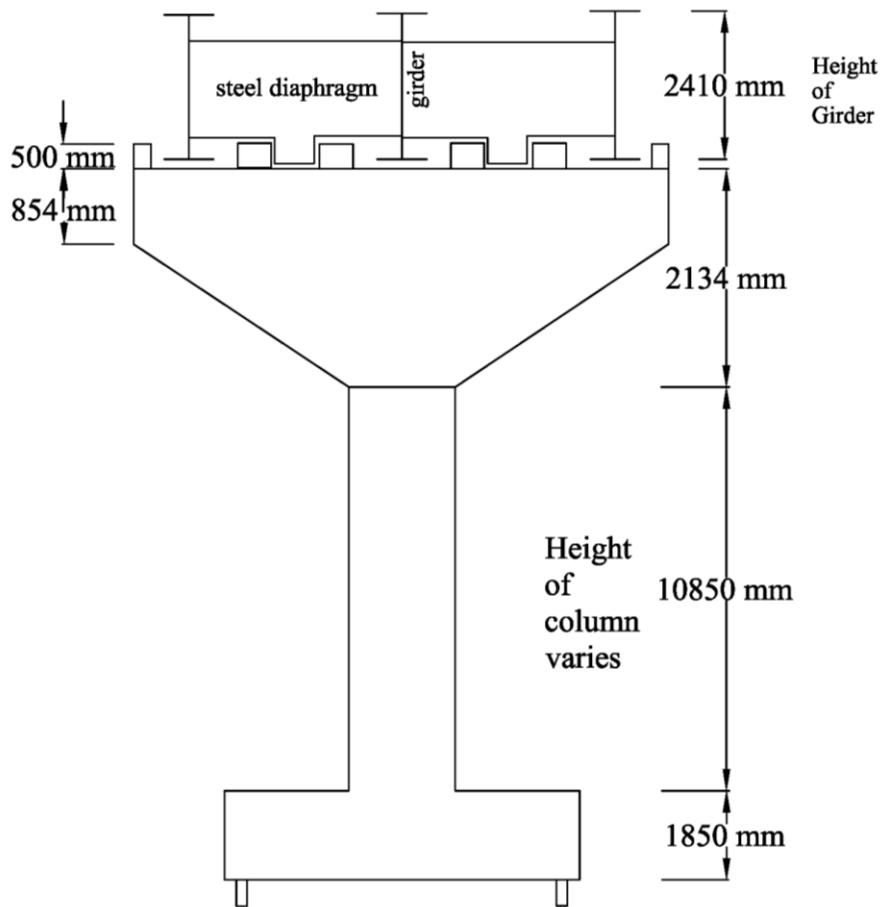
**Figure**

**Figure 2.2** Plan of bent beam 10 of curved bridge

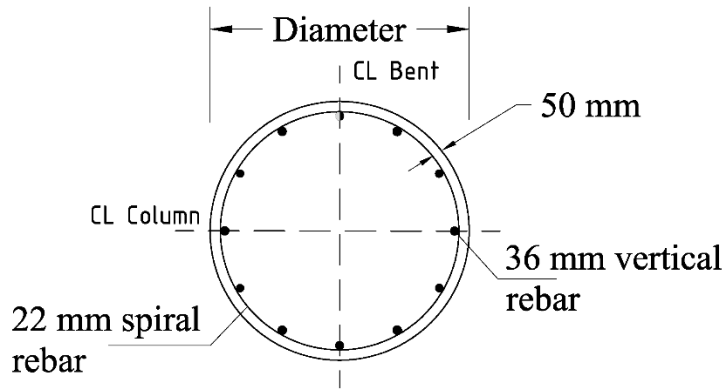
**Table 2.1** Sectional and reinforcement details for curved bridge columns

Column No.	Diameter (m)	Vertical Rebar # - bar size	Spiral Rebar @ mm
6	2.314	#36 Total 48	#22 @60
7	1.981	#36 Total 52	#22 @76
8	2.134	#36 Total 44	#22 @76
9	1.981	#36 Total 44	#22 @76
10	1.981	#36 Total 32	#22 @76
11	2.134	#36 Total 64	#22 @60
12	1.981	#36 Total 36	#22 @79
13	2.134	#36 Total 36	#22 @76
14	2.134	#36 Total 56	#22 @63

Note: Refer to Appendix B for bar sizes



(a)



(b)

**Figure 2.3** Details of bent 10 of curved bridge: (a) Elevation; (b) Typical column section details (size and number of rebar are given in Table 2.1)

The girders rest on bearings that are connected to the pier cap with grouted bolts. Except at the expansion joint and the abutments, all bearings are of the rocker type, and are restrained in translation but free in rotation about the vertical axis. The bearings at the abutment and expansion joint are “expansion type” and free to slide in the longitudinal direction of the girders. The expansion pot bearing at bent-10 is shown in Figure 2.4. Pot bearings consist of two layers, with the top layer sliding, longitudinally or rotationally, on the bottom layer. Both the layers are coated with PTFE (Poly-ethylene Tetra Fluoro Ethylene), which has a very low coefficient of friction and helps in sliding. Rotation type pot bearings have the top layer sitting in a pot type bottom layer while unidirectional expansion pot bearings have a bar attached to the top layer, sliding in a groove in the bottom layer, to direct the translation.

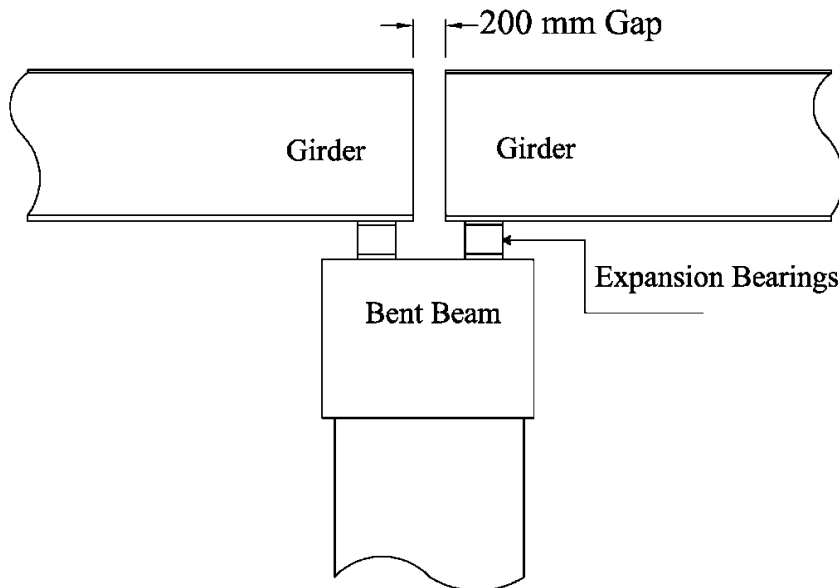


**Figure 2.4** Expansion joint detail for curved bridge.

One of the critical components of a bridge is the expansion joint, which must allow traffic to cross the bridge structure while permitting movement of the bridge deck due to thermal effects, wind, traffic loading, and seismic effects. Since the characteristics of the expansion joint have a major influence on the

seismic performance of bridge structures, they must be modeled accurately. The existence of a gap introduces non-linearity into the seismic analysis of the structure. The unidirectional pot bearing at the expansion joints increases the possibility for the girders to experience large displacements during seismic events. To restrict large displacements, steel restrainer rods with a 40 mm diameter and 3,600 mm length are deployed at this bridge; these are connected to both girders at either end with a bolted assembly. The restrainer rods improve the performance of bridges in an earthquake but may fail if the axial load is higher than the maximum allowable load. Figure 2.5 shows the restrainer rod arrangement for the bridge under investigation. The bridge bent foundations have rigid pile-caps, and pile groups vary from 24 piles to 30 piles. The pile diameter is 624 mm, and the pile-cap thickness varies from 1.050 m to 1.200 m.



**Figure 2.5** Restrainer rods at expansion joints of curved bridge

**Table 2.2** Details of pile groups and pile caps at various bents of curved bridge

<b>Bent No.</b>	<b>Length</b>	<b>Width</b>	<b>Thickness</b>	<b>No. of Piles</b>	<b>Pile Dia.</b>
	<b>mm</b>	<b>mm</b>	<b>mm</b>		<b>mm</b>
2	7920	7920	1850	24	324
3	7920	7920	1850	24	324
4	7920	7920	1850	24	324
5	7920	7920	1850	24	324
6	7920	7920	1850	24	324
7	7920	7920	1850	24	324
8	7920	7920	1850	24	324
9	10050	10050	1850	36	324
10	7920	7920	1850	26	324
11	7920	7920	1850	32	324
12	10050	10050	1850	24	324
13	10050	10050	1850	32	324
14	10050	10050	1850	42	324

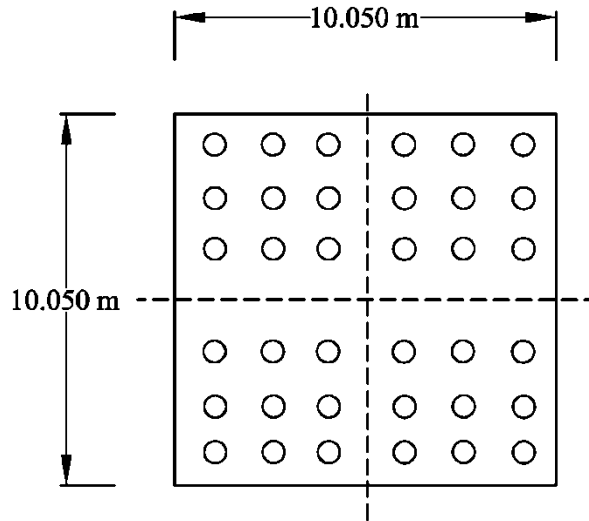


**Figure 2.6** Pile cap for bent 10 of curved bridge

## 2.2 Design of Skewed Bridge

The bridge investigated in this study is a three-span cast in-place RC box girder bridge with a total length of 127.5 m (425 ft), located in Ripon, CA (Kaviani et al., 2012). The on-site bridge has two bents and abutments skewed  $36^\circ$  with respect to the bridge longitudinal axis. Detail information of on-site bridge presents in Appendix C. Each bent has three columns, each with a diameter of 1.68 m (5.6 ft) and a height of 7.38 m (24.6 ft), as shown in Figure 2.7. The longitudinal reinforcement of the columns consists of 34 No. 14 rebars (43 mm in diameter), arranged in bundles of two rebars each, as shown in Figure 2.8a. The piers are supported on 24 HP 305  $\times$  79 steel piles per column, as seen in Figure 2.8b. The seat-type abutments have nine bearing pads and 40 piles underneath. The pinned columns were originally designed with guidelines from Caltrans (1999) and AASHTO (1998). For comparison, this  $36^\circ$  bridge is “straight” with a conservative consideration as the second individual bridge.

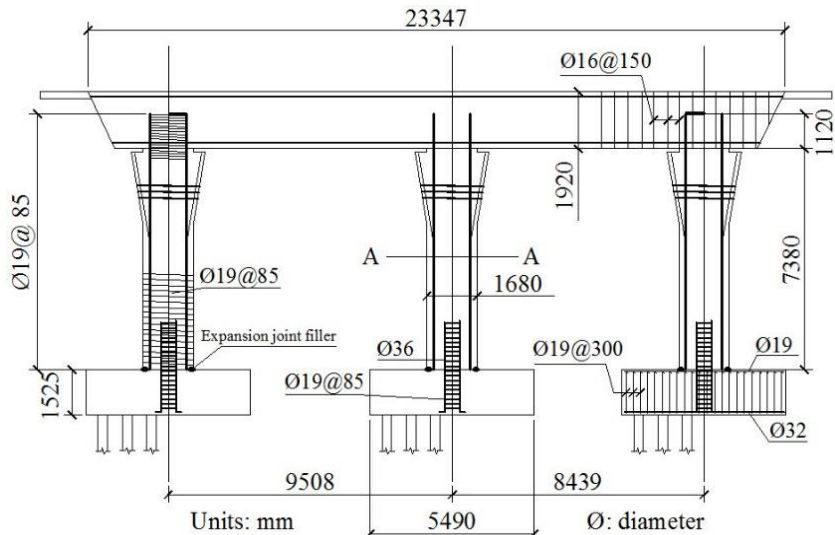


**Figure 2.7** Bent design details (adapted from Caltrans 2008)

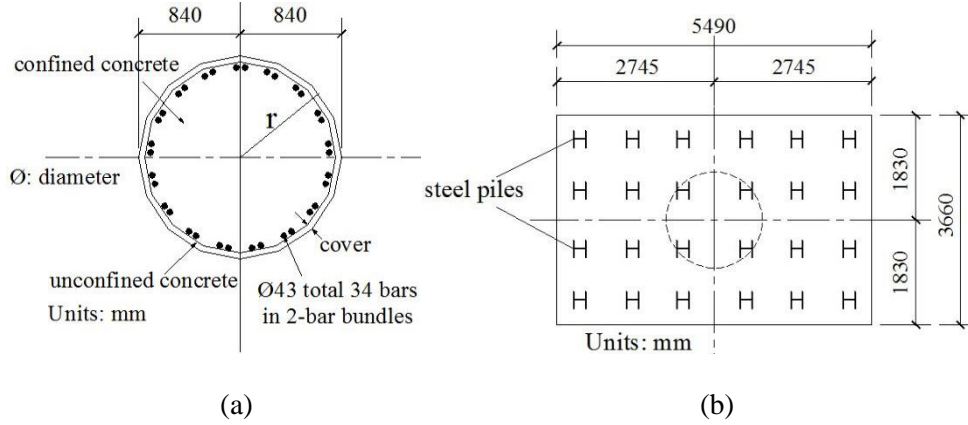


**Figure 2.8** Bent detail: (a) Column cross section; (b) Footing plan (Caltrans 2008)

The bridge is located in Seismic Zone 3, and it is classified as a multiple-column bent bridge for Operational Category (AASHTO, 2012). This classification is associated to a response modification factor  $R = 5.0$ , and an overstrength factor  $\phi = 1.3$ . The RC bent frame and the BRB form a dual system that provides lateral resistance to the bridge. The bent stiffness, as theoretically determined from pushover analysis in Section 4.2, is  $K_{\text{bent}_T} = 2.52 \times 10^5$  kN/m (1,470 k/in). As a substitute to guidelines for bridge BRB design, ASCE 7 (2010) indicates that moment frames shall be capable of resisting at least 25% of the design seismic forces in dual systems. Wang et al. (2016) evaluated several dual systems to optimize the system response by modifying the BRB core area. In the baseline dual system, 50% of the lateral resistance capacity is assigned to the BRBs (DS-50BRB). This 50% distribution of lateral resistance leads to BRB components with two core plates of 25 mm  $\times$  238 mm (1  $\times$  6.25 in.), and two connection plates of 25 mm  $\times$  325 mm (1  $\times$  13 in). The BRB axial stiffness,  $K_{\text{BRB, ax}}$ , is based on the core and connection stiffness. The BRB lateral stiffness,  $K_{\text{BRB, lat}}$ , depends on  $K_{\text{BRB, ax}}$  and the BRB angle with respect to the horizontal,  $\theta$ :

$$K_{\text{BRB, lat}} = K_{\text{BRB, ax}} \cos^2 \theta = \frac{1}{\left(\frac{1}{K_{\text{core}}} + 2\frac{1}{K_{\text{con}}}\right)} \cos^2 \theta \quad (1)$$

where  $K_{\text{core}} = EA_{\text{core}}/L_{\text{core}}$ , and  $K_{\text{con}} = EA_{\text{con}}/L_{\text{con}}$  are the stiffness of the core and connection plates, respectively, with  $E$ ,  $A$ , and  $L$  being steel modulus of elasticity, and area and length of the plates, respectively. The lateral resistance distribution is optimized by modifying the BRB contribution, as shown in Table 2.3. A reasonable BRB yield length ratio (core length-to-working point length ratio)  $L_{\text{core}}/L = 0.55$  is used in all dual systems, whereas the BRB core area is modified to obtain different BRB stiffness. The study was extended to consider systems in which BRBs can withstand 25%, 40%, 50%, 60%, and 75% of the bent's shear forces (DS-25BRB, DS-40BRB, DS-50BRB, DS-60BRB, and DS-75BRB, respectively). Note that the DS-75BRB dual system needs three times larger core plate areas than those of the baseline case, DS-50BRB.



**Table 2.3** BRB dimensions for skewed bridge

Specimen	Core Area, $A_{core}$ (mm <sup>2</sup> )	Core Configuration (mm)	Design load (kN)	Lateral stiffness (kN/m)	BRB Lateral Contribution
DS-75BRB	23,750	2 BRB of 25 x 238 (2)	5,330	379,140	75%
DS-60BRB	11,875	25 x 238 (2)	2,660	189,570	60%
DS-50BRB	7,813	25 x 157 (2)	1,760	126,380	50%
DS-40BRB	5,157	25 x 207 (1)	1,170	84,370	40%
DS-25BRB	2,500	25 x 100 (1)	595	54,290	25%

Note: All BRBs have a yield strength  $F_y = 260$  MPa (38 ksi), a core length-to-working point length ratio  $L_{core}/L = 0.55$ ,  $L_{con} = 1,350$  mm (53 in.),  $L_{core} = 6,500$  mm (256 in.)

Figure 2.9 shows the idealized pushover curves of a bare column bent, a BRB component, and a BRB retrofitted bent system. Bilinear idealizations are used to represent the bare column bent and BRB system with yield forces  $V_{Bent}$  and  $V_{BRB}$ , respectively. The  $K_{BRB}$ , as a function of the designed percentage of lateral resistance capacity, is shown in Table 2.4. To ensure BRB components yield first, the BRB yield displacement  $\Delta_{BRB}$  should be less than the yielding displacement of the frame,  $\Delta_{Bent}$ .

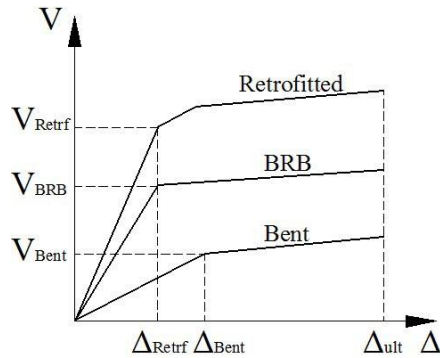


**Figure 2.9** Idealized pushover curves for column bent system with BRB

In the retrofitted structure, the ductility demand increases by decreasing yield displacement from  $\Delta_{bent}$  to  $\Delta_{Retrf}$  with additional hysteretic energy capacity provided by BRB components. Considering the energy of the whole system, the complete energy balance is given by the equation (Uang and Bertero 1990), as follows,

$$E_I = E_S + E_K + E_D + E_H \quad (2)$$

where  $E_I$  is cumulative input energy,  $E_S$  is instantaneous strain energy stored by the structure,  $E_K$  is instantaneous kinetic energy of the moving mass,  $E_D$  is cumulative viscous damping energy, and  $E_H$  is cumulative hysteretic energy. For retrofitted systems, the reduction in shear demand is mainly provided by decreasing  $E_S$  due to the BRB hysteretic energy dissipation capabilities, delaying the occurrence of plastic hinges at the column and decreasing corresponding energy dissipation to change  $E_{H,Orig}$  to  $E_{H,Retrf}$ , as follows,

$$E_{H,Orig} = E_{H,bent} + E_{H,abut} \quad (3)$$

$$E_{H,Retf} = E_{H,bent} + E_{H,BRB} + E_{H,abut} \quad (4)$$

Considering that most bridge substructures are RC components, the retrofit BRB steel component has to connect to an RC structure. Dusicka et al. (2015) proposed to use post-installed adhesive anchor rods according to ACI 318 for connecting the gusset plate to concrete elements (Figure 2.10a). Also, a steel plate jacket around outside RC column (Figure 2.10b) could be used as a connection for the gusset plate. Also, outside steel buckling restrained braces frames (BRBFs) could be constructed to resist lateral seismic forces (Figure 2.10c), as in the retrofit projects of the University of Utah Marriott Library and the Wallace F. Bennett Federal Building at Salt Lake City, Utah. This method could be used when the original column capacity and ductile characteristics are insufficient or not easily obtained.

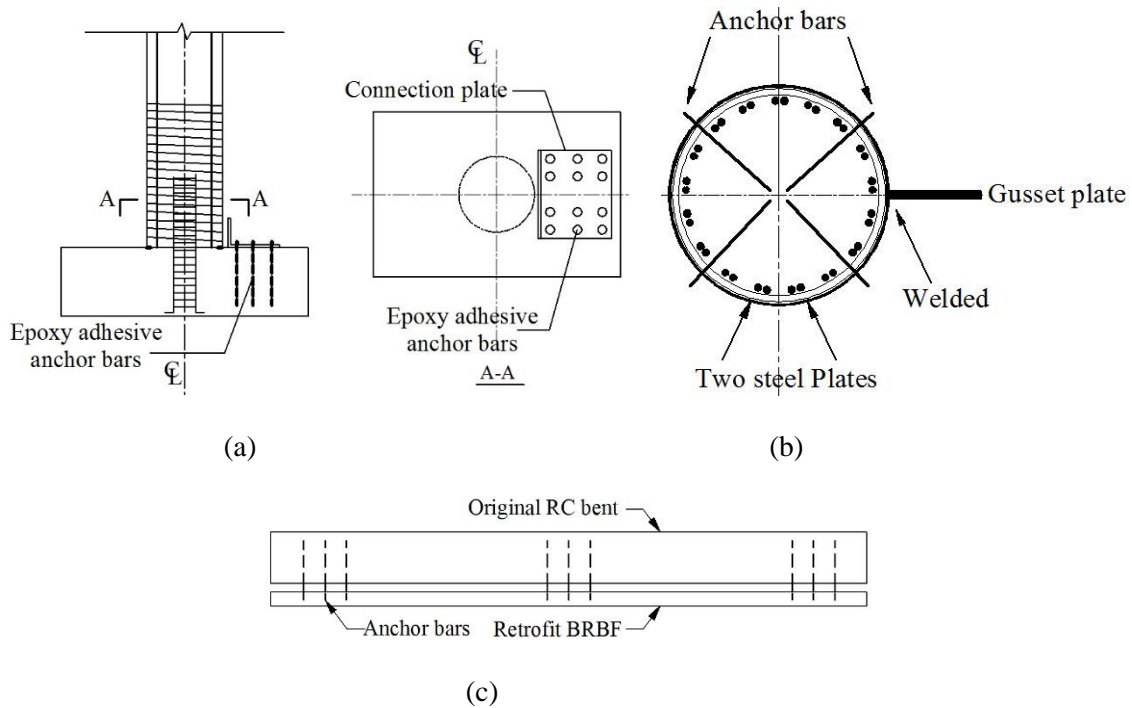


**Figure 2.10** Proposed connection: (a) Post-installed adhesive anchor rods; (b) steel plate jacket; (c) additional outside steel frame

### **3. FINITE ELEMENT MODEL**

#### **3.1 Curved Bridge**

A non-linear time history analysis has been performed taking non-linearity of bearings, restrainer rods, and soil springs into account. Two spans of the existing bridge, span 2 (from bent 5 to bent 10) and span 3 (bent 10 to abutment 15), have been modeled in SAP 2000® Nonlinear (CSI 2013), as shown in Figure 3-1. Three-dimensional beam elements, with six degrees of freedom at each node, and section properties of different elements assigned according to the construction drawings available, have been used to model the girders of the super-structure.

##### **3.1.1 Finite Element Model in SAP 2000®**

The beam-column elements used to model the columns have concrete section properties as per the design drawings. Mander's (1988) confinement model available in SAP 2000® has been used in the plastic hinge regions. All reinforcing steel complies with ASTM A706 grade 60 and the 28-day compressive strength of concrete is assumed as 25 MPa. Pier cap beams are non-prismatic; therefore, non-prismatic sections have been generated and assigned to the beam-column elements representing the beams. The connection between the pier cap and the column is considered as rigid; the joint is designed to fail only after the column develops plastic hinges at the top and bottom of the column. All bents are single column bent, which makes it unlikely to develop a plastic hinge in the beam.

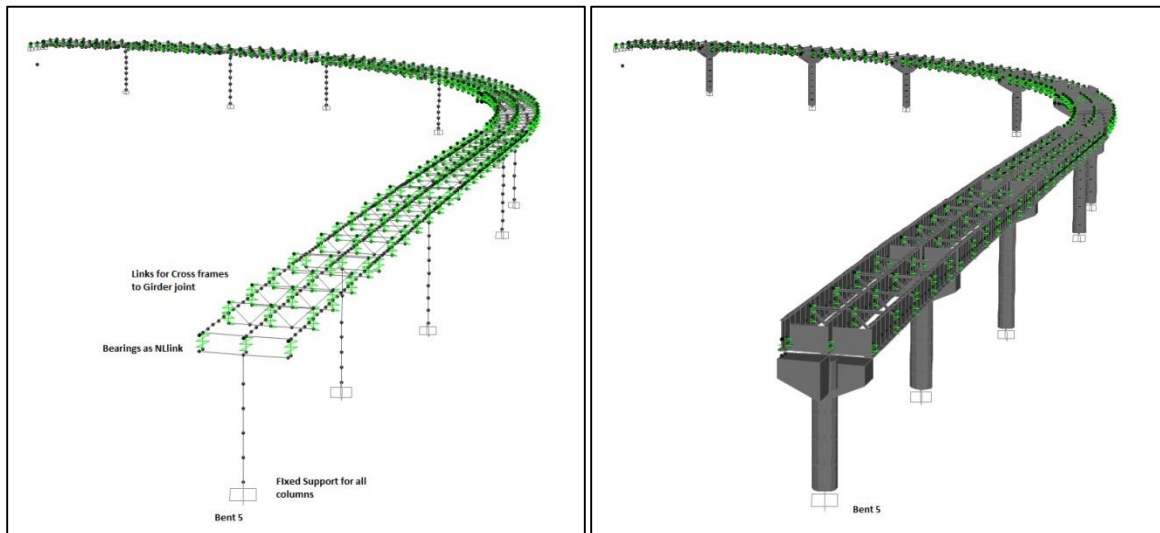
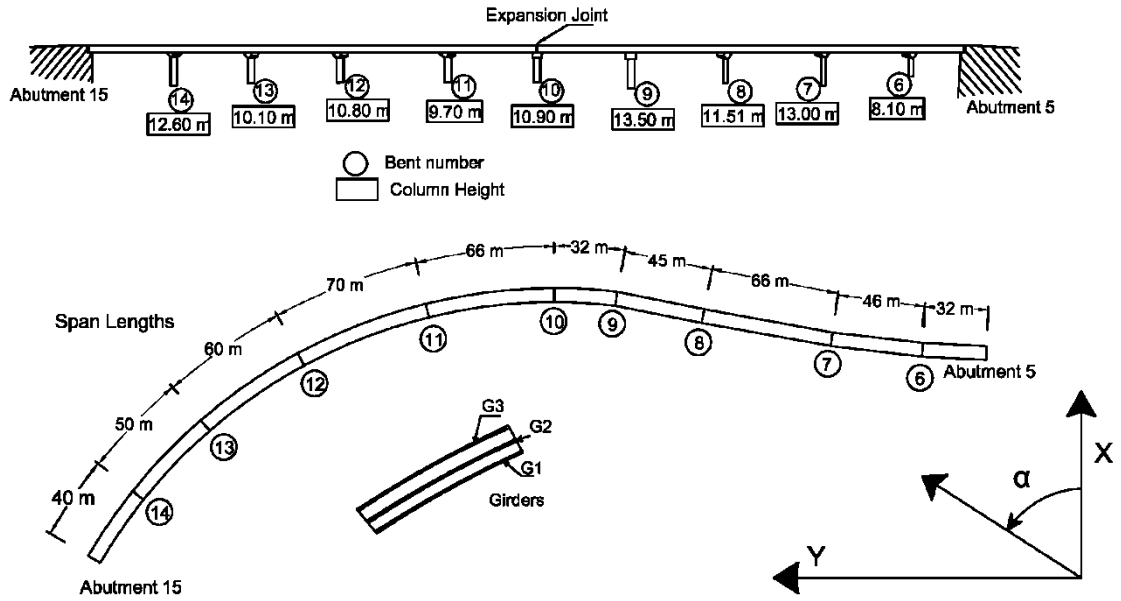


**Figure 3.1** Spans of curved bridge modeled in SAP 2000® (top) and computer model (bottom)

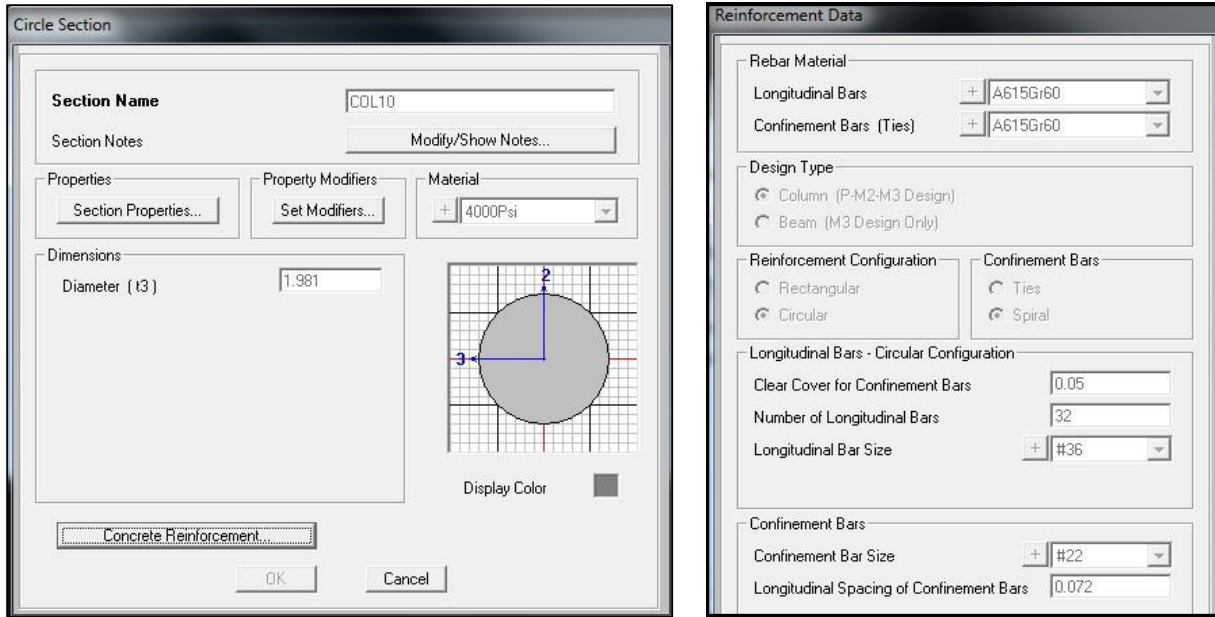


**Figure 3.2** Column section and reinforcement assignment in SAP 2000® model of curved bridge

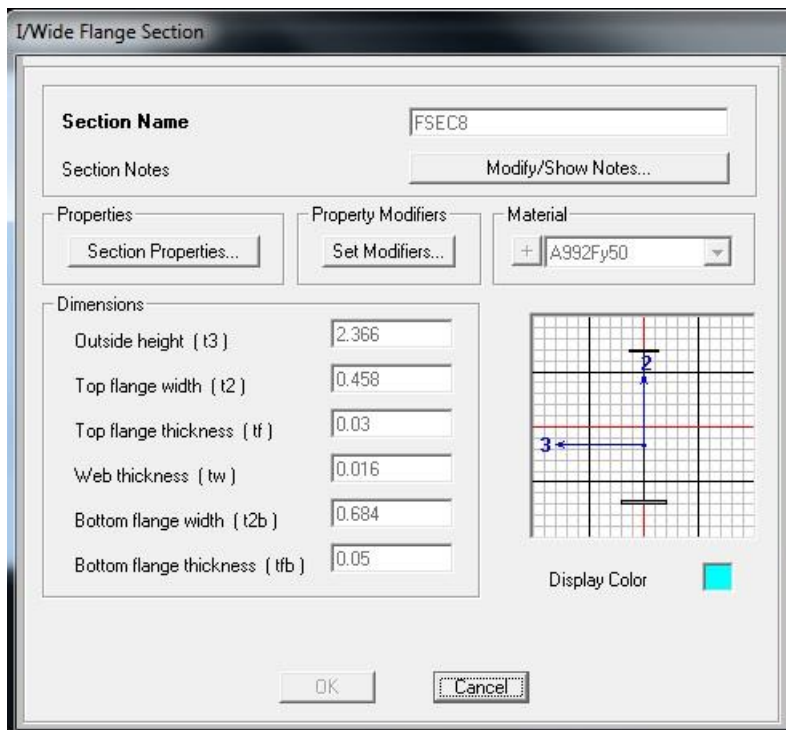


**Figure 3.3** I-section assignment for one of the girders in SAP 2000® model of curved bridge

T-sections have been used in the bridge as cross-frames between the main girders. These cross-frames make the girders work as a single assembly. For numerical analysis, the connection between cross-frames and girders has been considered as rigid and modeled using a rigid link as shown in Figures 3.4 and 3.5.

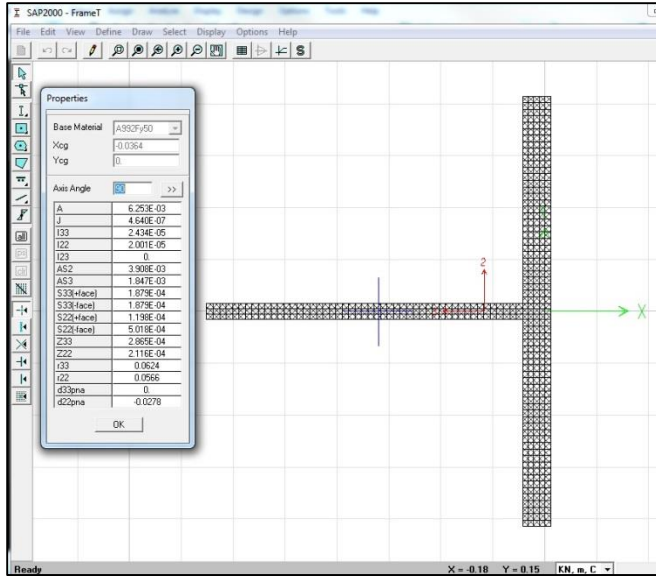


**Figure 3.4** T-section assignment using section builder in SAP 2000® model of curved bridge

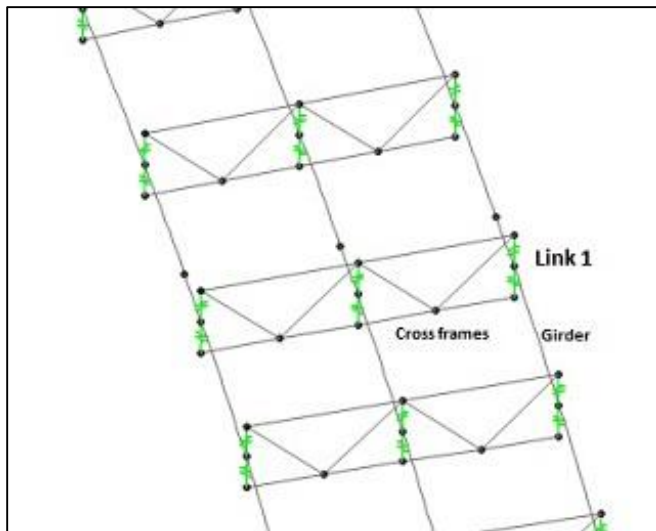


**Figure 3.5** Rigid links to model diaphragm connections in SAP 2000® model of curved bridge

The girders rest on bearings connected to the pier cap with grouted bolts. Except at the expansion joint and the abutments, all bearings are of the rocker type, and are restrained in translation but free in rotation about the vertical axis. These bearings have been modeled with linear link elements with free rotation about the vertical axis. The bearings at the abutment and expansion joint are “expansion type” and free to slide in the longitudinal direction of the girders. Expansion pot bearings are modeled using non-linear link elements. The force-displacement relationship (Figures 3.6 and 3.7) for the link elements was determined using the allowable load on the expansion bearings in the vertical and lateral direction. For the longitudinal direction, a coefficient of friction between PTFE sheets was assumed as 0.05 to 0.08.

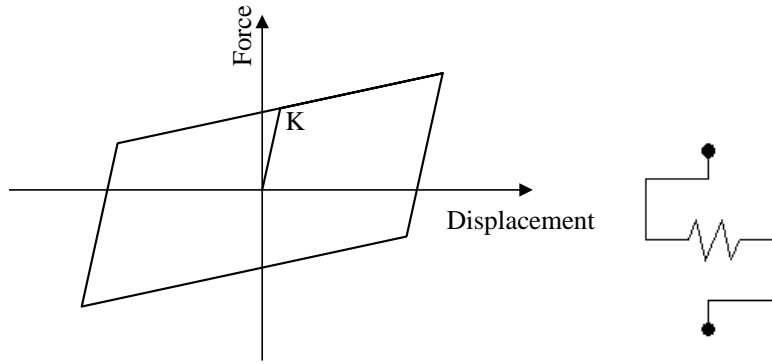


**Figure 3.6** Analysis model for transverse direction of expansion bearing for curved bridge

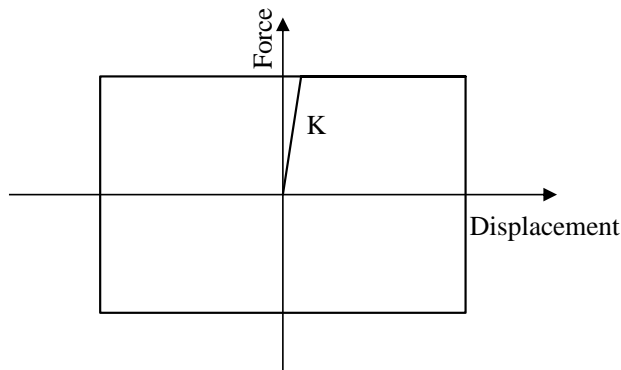


**Figure 3.7** Analysis model for friction in longitudinal direction of expansion bearing for curved bridge

Evaluation of the effects of soil-structure interaction on the behavior of the bridge is a central part of this study; the soil was modeled using non-linear link elements with a kinematic hysteretic rule. Soil-pile interaction is generally modeled with the help of P-y springs, which vary with the depth along the pile. The P-y curve for a soil spring depends on the diameter of the pile, soil unit weight and the stresses at that particular depth. Using the soil bore-hole data provided with the drawings, P-y curves at different depths for one pile at each bent have been calculated (see Appendix B). The group P-y curves were calculated by multiplying the P-y curves for a single pile with the group participation factors recommended by AASHTO LRFD (1998). The soil spring for pile-cap has been calculated following the guidelines of the FEMA 356 (2000) document. Appendix I of the thesis shows that the spring constant for the pile-cap is much higher than the spring constant for the pile-group for given soil conditions. Assuming the soil to be non-liquefiable, the soil spring for the pile-cap dominates the behavior of the foundations. Therefore, the pile-cap was modeled as a point mass with soil springs in two principal directions (Figure 3.8).

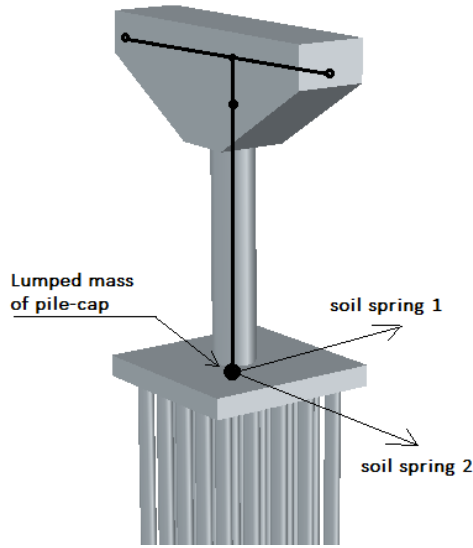


**Figure 3.8** Simplified pile-cap model for curved bridge in SAP 2000®

The California Department of Transportation (Caltrans SDC 2010) recommends a spring constant for the abutment, which includes the piles and the width and length of the abutment wall. The following equation is recommended for soil-spring constant at the abutment,

$$k_a = k_s + k_p$$

$$k_s = 115 \left( \frac{kN}{mm} \right) \cdot B \quad , \text{ and } k_p = 7 \left( \frac{kN}{m} \right) \cdot n_p$$

Here, B represents the effective abutment width and  $n_p$  is the number of piles. In the transverse direction, the effective width B is taken as the length of the wing walls multiplied by a factor for wall effectiveness ( $C_L = 2/3$ ) and participation coefficient ( $C_W = 4/3$ ) to account for differences in participation of both wing walls.

The existence of a gap at the expansion joint introduces non-linearity into the seismic analysis of the structures. As this bridge has unidirectional pot bearing at the expansion joints, there is a possibility for the girders to experience large displacements during seismic events once the restrainer rods fail (Figure 3.9). Previous studies have shown that pounding between two structural components depends on the coefficient of restitution, which is used to define damping during the impact (Anagnostopoulos and Karamaneas, 2008). Experimental studies and mathematical models to obtain load-time history during the pounding between two structures can be found in the literature (Van Mier et al. 1991; Jankowski 2005; Takabatake et al. 2014). Generally, a linear force-deformation relationship is used to define the pounding force, which can estimate elastic forces developed between the two structural components. Non-linear spring models like the Hertz model, a general non-linear model, and Jankowski model have also been used to simulate the pounding behavior more realistically (Pantelides and Ma 1998; Takabatake et al. 2014).

A linear force-deformation model is used to simulate pounding in this study. The external nodes of adjacent girders are linked using nonlinear gap elements to model the impact forces resulting from pounding between girders and between girders and abutment. The force-deformation characteristics of such elements are shown in Figure 3.10. Spring stiffness,  $K_i$ , is fixed and is equal to the axial stiffness of the neighboring structural segments. Through a sensitivity analysis of the impact element stiffness using a



nonlinear time history analysis for a wide range of impact element stiffness of this bridge model,  $K_i$  is taken equal to 1.39 GN/m. A simplified computer model for one of the bents, which has a single soil spring and four impact elements between concrete shear key and girders, is shown in Figure 3.11.

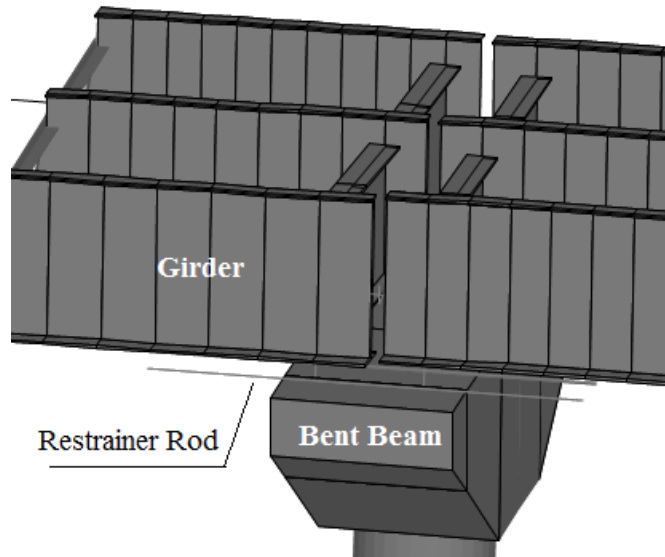


**Figure 3.9** Expansion joint with restrainer rod in SAP 2000® model of curved bridge

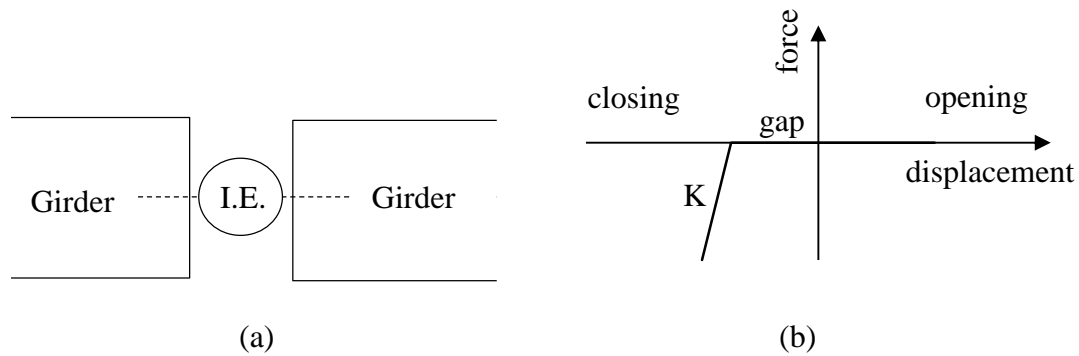


**Figure 3.10** Impact element (I.E.): (a) location; (b) analysis model for curved bridge expansion joint

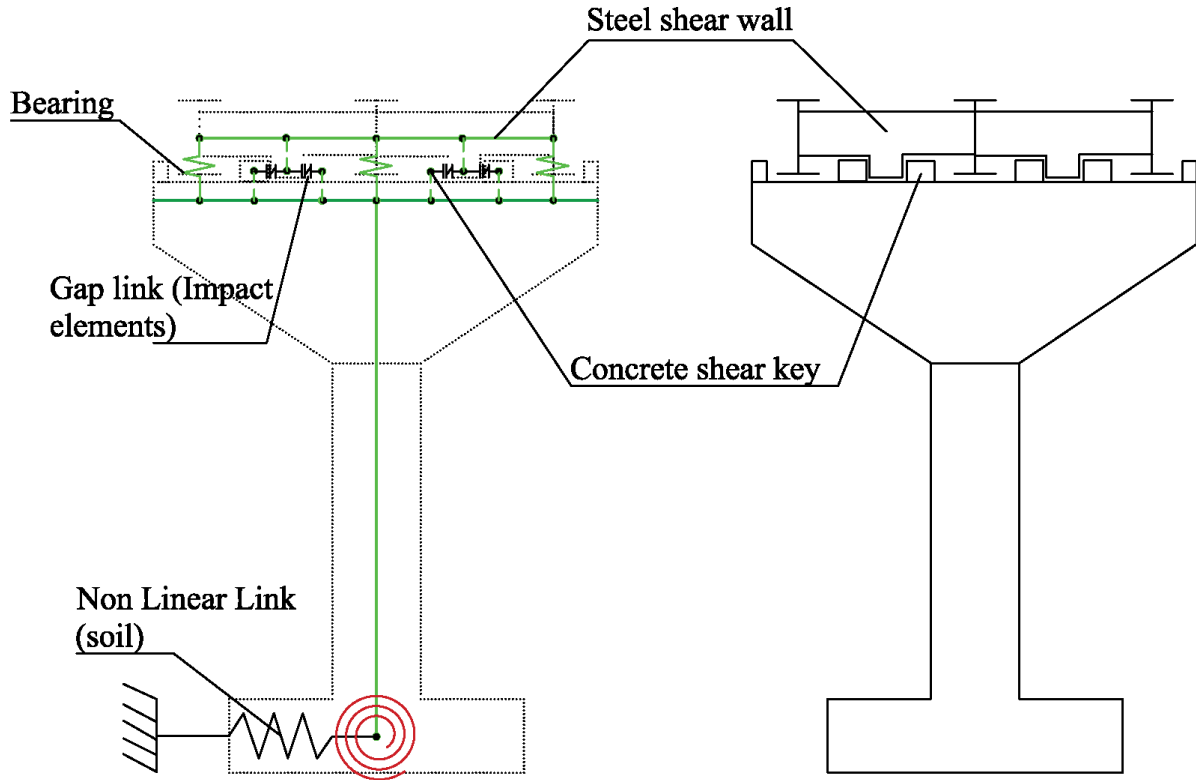


**Figure 3.11** Simplified SAP 2000<sup>®</sup> model of the curved bridge bent

This study recommends use of Buckling Restrained Braces (BRB) to mitigate the pounding forces at the abutment and expansion joint. BRBs are a widely used metallic energy dissipation device for seismic protection of buildings and other structures. BRBs provide hysteretic energy dissipation by restraining steel core plates against global buckling behavior and enabling stable yielding in both tension and compression. Nonlinear link elements with kinematic hysteretic rule have been used to model BRBs in this model. The force-deformation curve has been matched with quasi-static cyclic tests performed on full-scale BRBs by Xu (2016), as shown in Figure 3.12. Parameters for the SAP 2000<sup>®</sup> model have been adopted through sensitivity analysis by performing cyclic load simulations on a single BRB element.

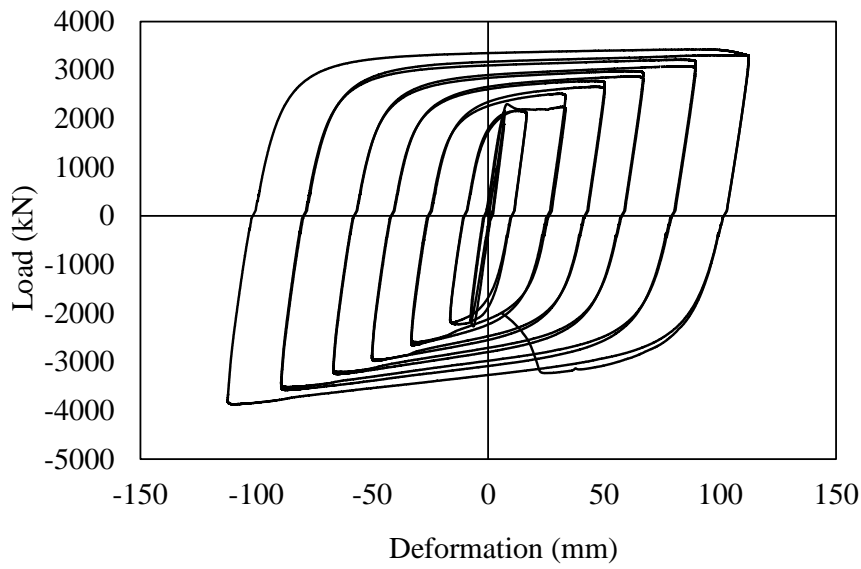


**Figure 3.12** BRB hysteresis (Xu, 2016)

In this study, it is assumed that the connection between the BRB and steel girder or abutment concrete does not fail. Thus, this study investigates the possible use of BRBs to retrofit bridges vulnerable to pounding damage. Material deterioration due to pounding and connection details of BRBs to structural members is not within the scope of the research.

### 3.1.2 Ground Motion Data

A combination of pulse type and long period earthquake ground motions is selected for time-history analysis. The Pacific Earthquake Engineering Research Center (PEER) strong motion database was searched by using a target spectrum obtained using ASCE-7 (2010) documentation; and 15 ground motions, given in Table 3.1, were selected for the study. FEMA P-752, NEHRP Recommended Provisions, Section 16.1.3, requires the use of at least three ground motions in any response history analysis. When at least seven ground motions are used, sections 16.1.4 and 16.2.4 permit the use of average response quantities for design. The objective of the response history analysis is not to evaluate the response of the structure for each record, but to determine the expected average response. This procedure helps in reducing the effort and time required to analyze the seismic response of a structure. Horizontal design response spectrum (DBE) and risk-targeted maximum considered earthquake ( $MCE_R$ ) response spectra for the Salt Lake City site of the existing bridge are developed using the USGS (2014) design maps tool (Figure 3.13). The soil data provided by Utah department of Transportation (UDOT 2014) suggest the soil to be between soft to stiff clay and hence the site to be of class D. The ground motions are matched to the target spectrum using SeismoMatch (Seismosoft® 2013) software. Figure 3.14 shows the matched 5% damping elastic spectra of the ground motions (Figure 3.15 to Figure 3.25) used in this study.

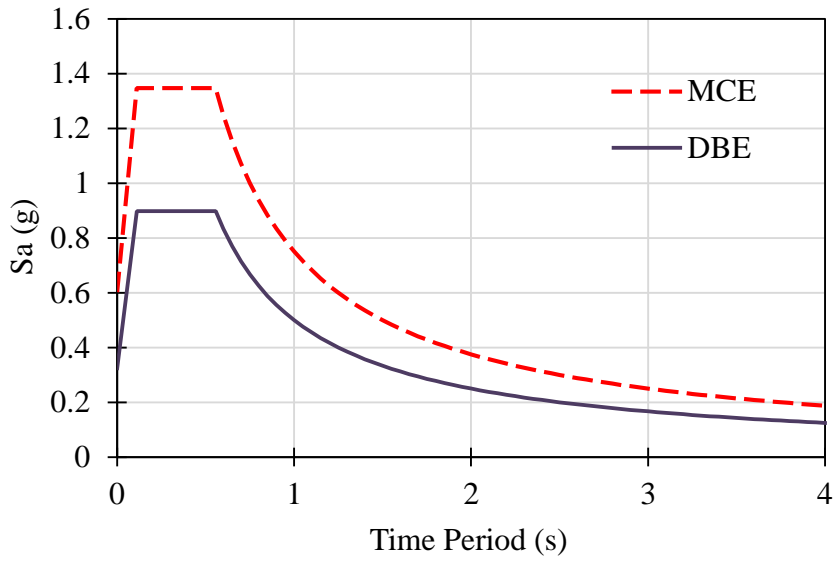


**Figure 3.13** DBE and Risk-targeted MCE for the site of curved bridge

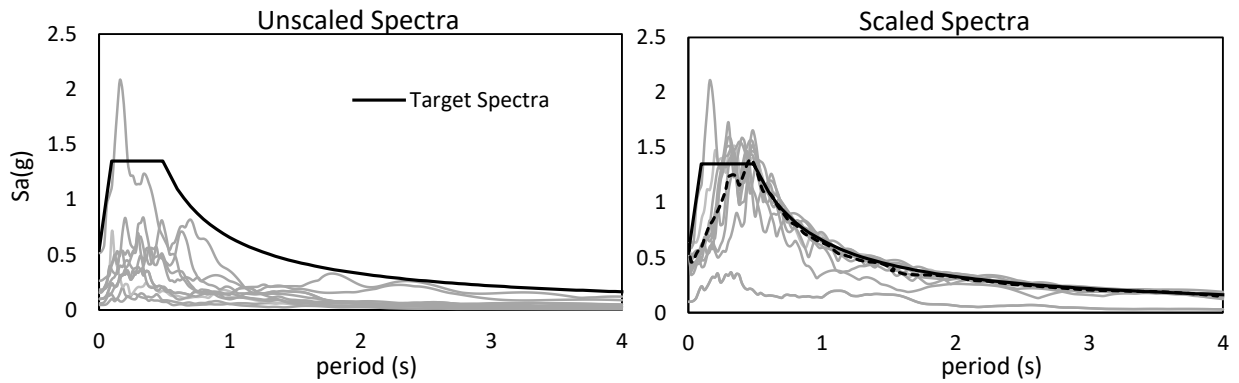


**Figure 3.14** Spectral acceleration response spectra of the ground motions for analysis of curved bridge

**Table 3.1** Ground motions used for time-history analysis of curved bridge

ID	Earthquake Name	Year	Station Name	Magnitude	Fault
1	Parkfield	1966	Cholame - Shandon Array #12	6.19	strike slip
2	San Fernando	1971	Santa Felita Dam (Outlet)	6.61	Reverse
3	Imperial Valley	1979	Cerro Prieto	6.53	strike slip
4	Irpinia Italy	1980	Rionero In Vulture	6.2	Normal
5	Chalfant Valley	1986	Bishop - Paradise Lodge	5.77	strike slip
6	Duzce Turkey	1999	Lamont 1061	7.14	strike slip
7	Manjil Iran	1990	Abbar	7.37	strike slip
8	Northridge	1994	Newhall	6.7	strike slip
9	Kobe	1995	KJMA	6.9	strike slip
10	Chi-Chi Taiwan-03	1999	TCU074	6.2	Reverse
11	Cape Mendocino	1992	Loleta Fire Station	7.01	Reverse
12	Landers	1992	North Palm Springs Fire Sta #36	7.28	strike slip
13	Chuetsu-oki Japan	2007	Ojiya City	6.8	Reverse
14	Iwate Japan	2008	Tamati Ono	6.9	Reverse
15	Iwate Japan	2008	Semine Kurihara City	6.9	Reverse

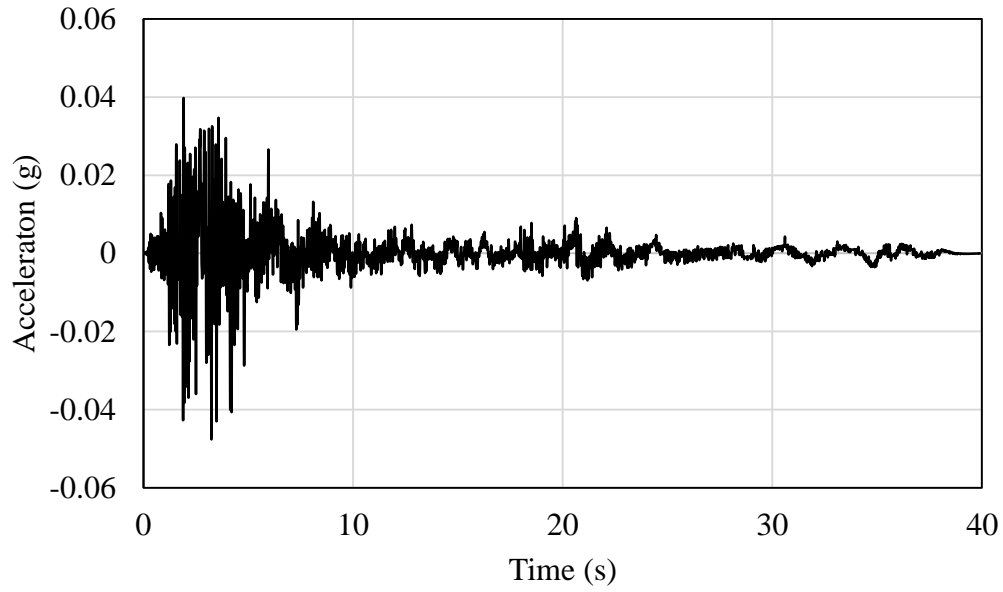


**Figure 3.15** Chalfant Valley 1986, USA (CDMG Station 54428)

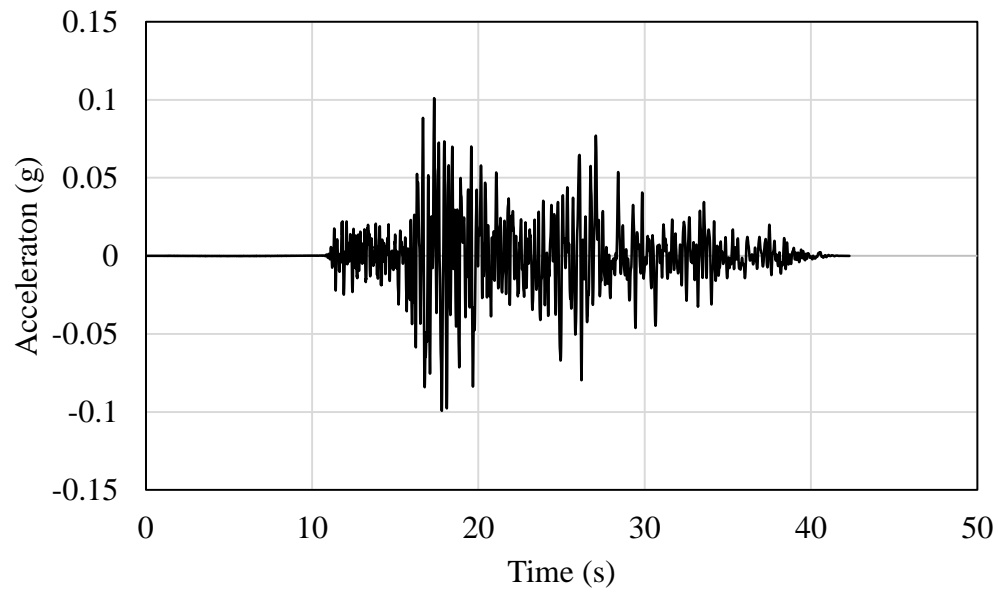


**Figure 3.16** Duzce 1999, Iran (Station - Lamont 1061)

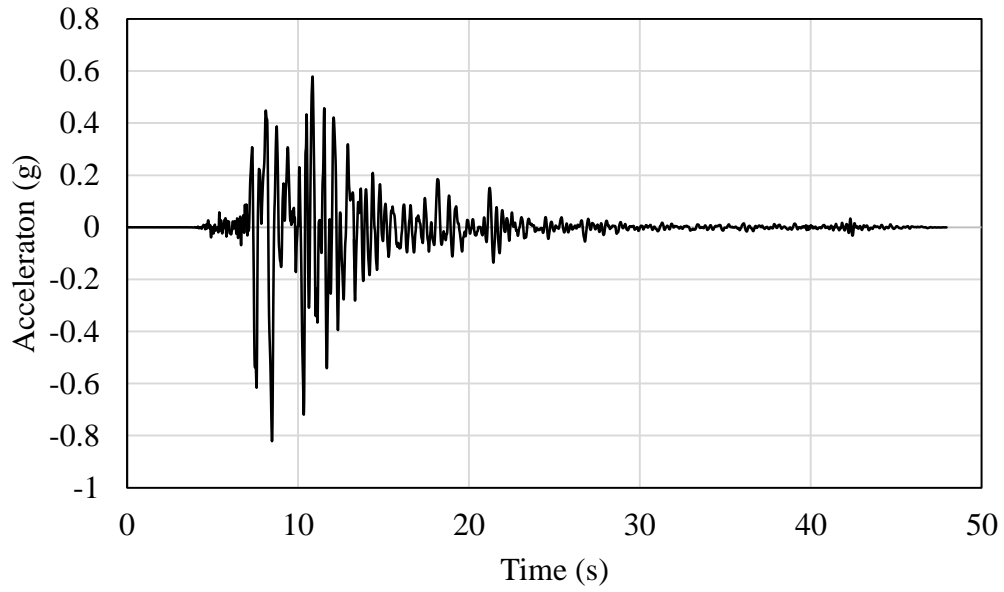


**Figure 3.17** Kobe 1995, Japan (Station - KJMA)

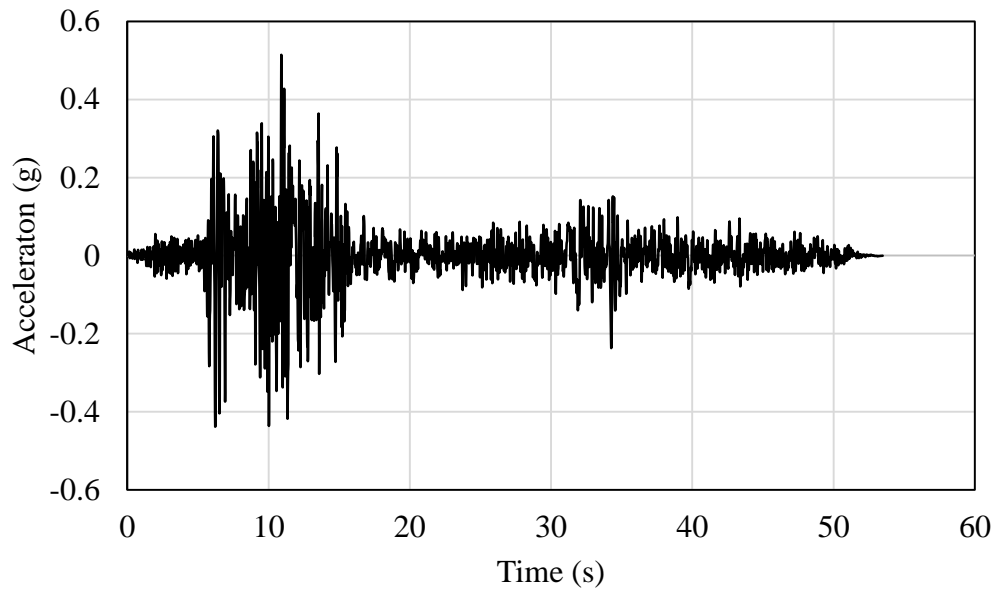


**Figure 3.18** Manjil, 1990, Iran (Station - Abbar)

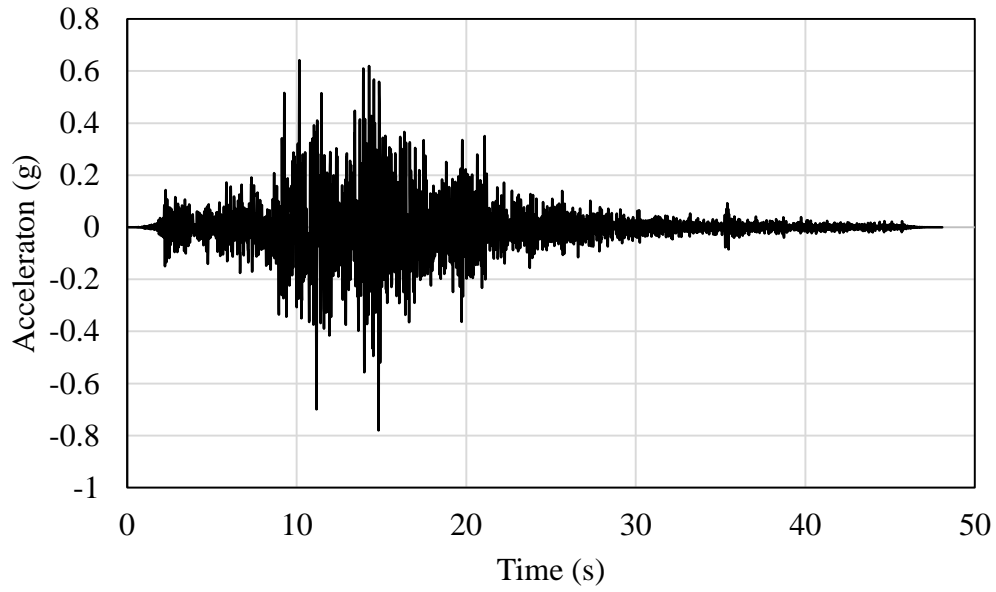


**Figure 3.19** Landers 1992, USA (Station - 000 SCE Station 24)

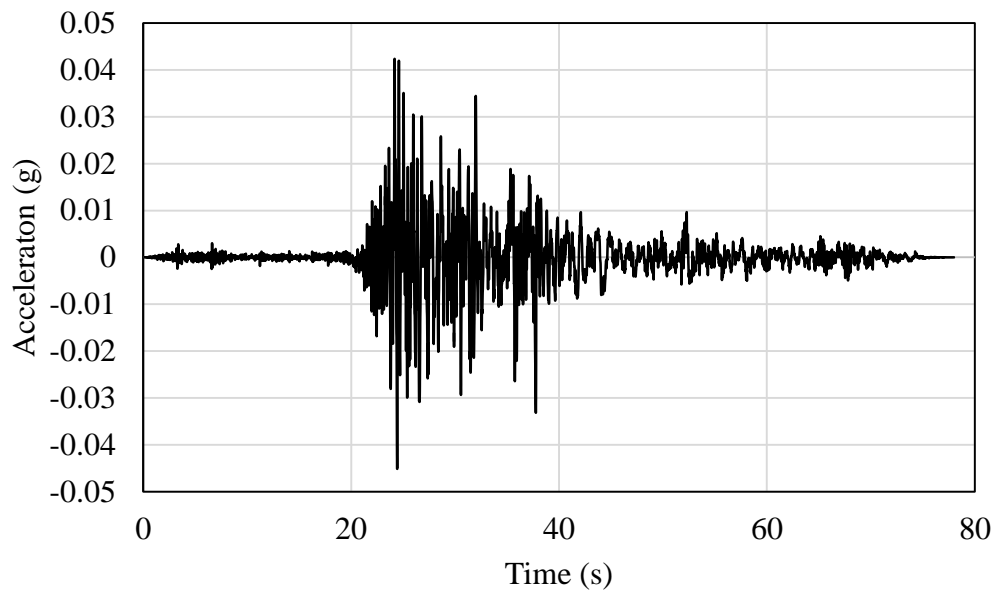


**Figure 3.20** ChiChi 1999, Taiwan (Station - TCU074)



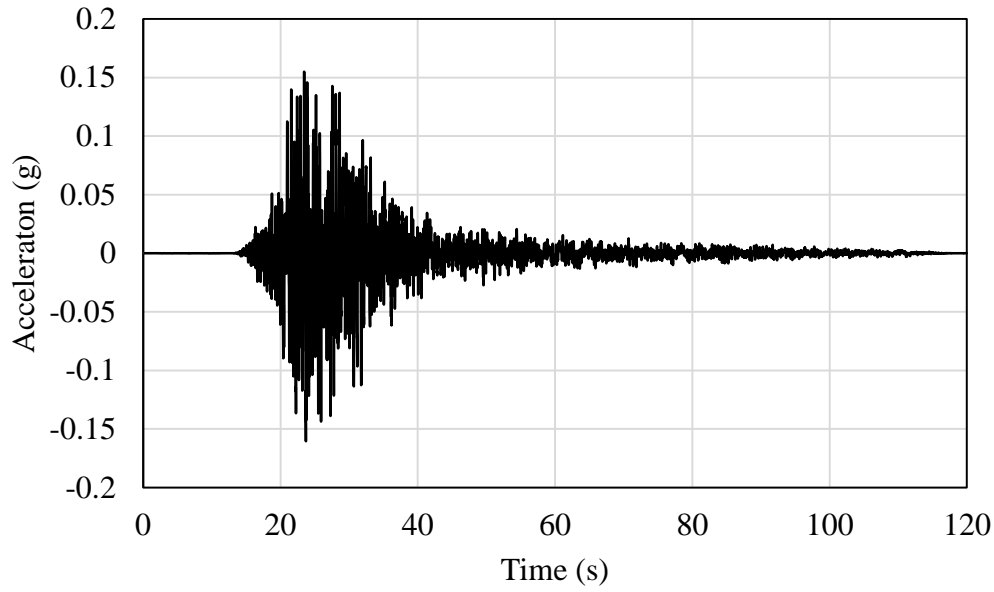


**Figure 3.21** Iwate 2008, Japan (Station – Tamati Ono)

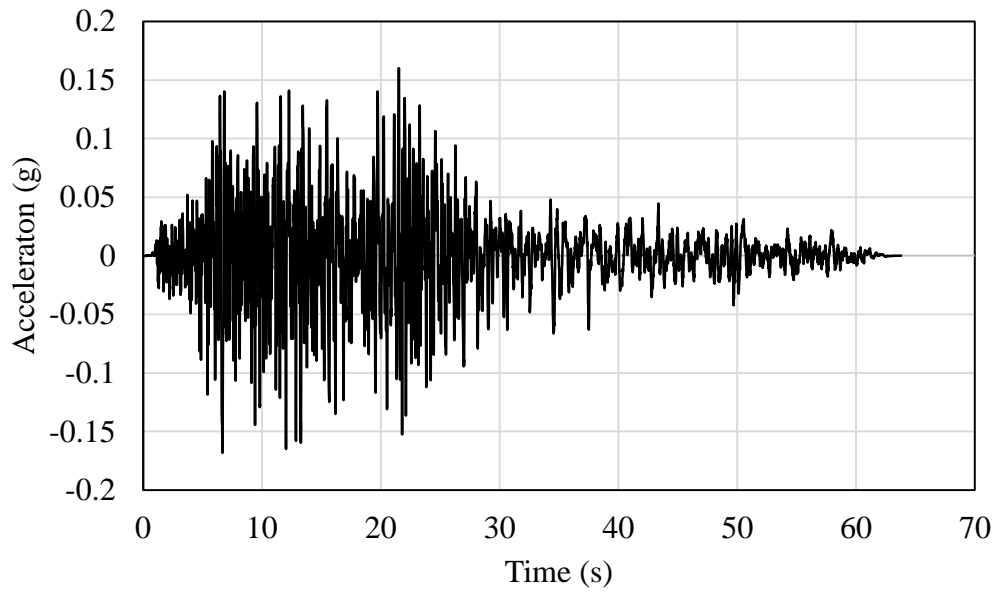


**Figure 3.22** Imperial Valley 1979, USA (Station - Cerro Prieto)

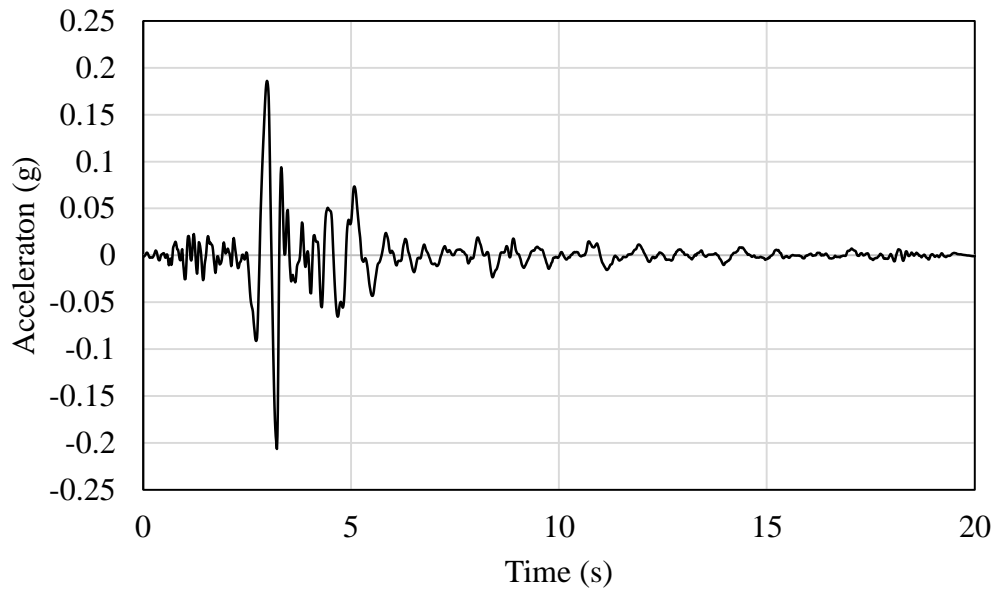


**Figure 3.23** Northridge 1994, Newhall, USA (Station - LA County Fire Station, 180)

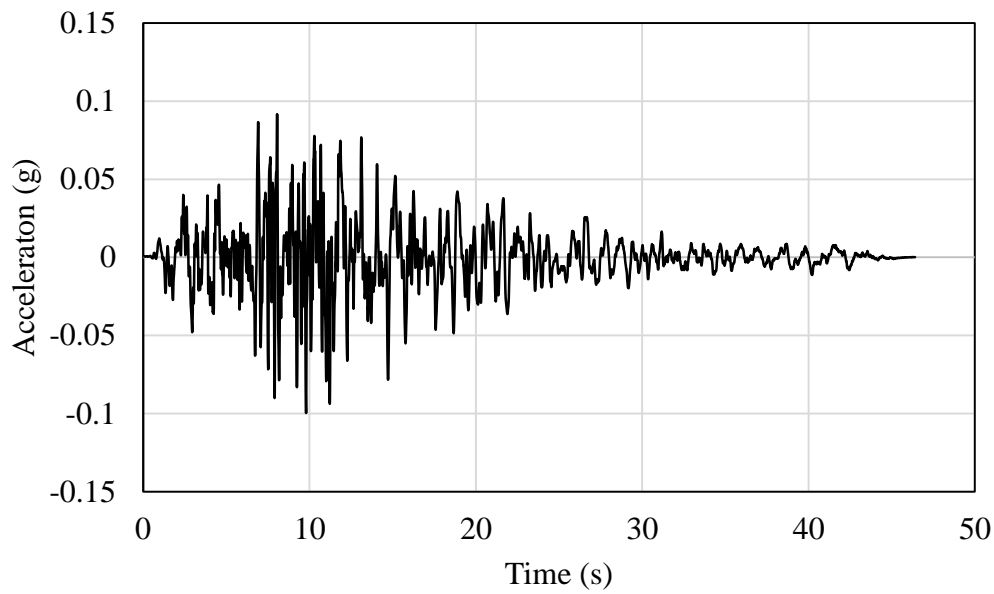


**Figure 3.24** Irpenia 1980, Italy (Station - Rionero In Vulture)

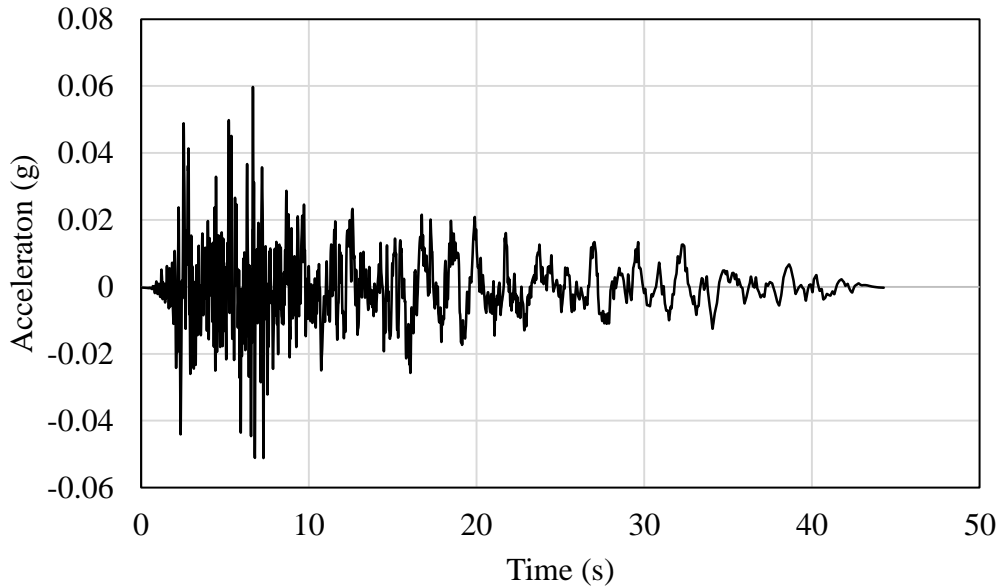


**Figure 3.25** Parkfield, 1966, USA (Cholame – Shandon Array)

## 3.2 Skewed Bridge

### 3.2.1 Skewed Bridge Characteristics

Skew configurations are commonly used for bridges requiring the best space usage in complex intersections, especially in crowded urban areas. Due to asymmetrical abutment and bent response, skew bridges have a complicated seismic response that leads, for instance, to rotation and deck unseating. Maragakis and Jennings (1987) showed that deck rigid body motions, along with the impacts between deck and abutments, are the main sources of severe damage on skew highway bridges. Wakefield et al. (1991) utilized linear and nonlinear models to analyze skewed seismic effects on Foothill Boulevard Undercrossing Bridge. The results showed the skewed dynamic responses were dominated by in-plane rigid body motion in translational and rotational directions. The analytical vulnerability was at center bent columns and transverse direction of abutment due to deck rotation, which corresponded to bridge failures in the San Fernando earthquake. Watanabe and Kawashima (2004) conducted analytical studies with a 200-m-long bridge with a skewed angle of  $50^\circ$ , showing the potential for pounding of the deck and abutment. When ground motions were set at certain directions, additional deck rotations were found to be magnified by skewed decks to the abutment pounding.

In a recent study, Amjadian and Kalantari (2012) showed the transverse displacements that are amplified by pounding at the corners of the deck are essential in asymmetric straight bridges. They concluded that pounding effects can be significant under larger values of skewness angle and smaller gap. Skewed bridges may amplify the rotational motion about the center of the superstructure, resulting in higher forces on the transverse support of the abutment. In the meantime, lower forces can be distributed to the backing soil in the longitudinal direction (Wilson et al. 2014).

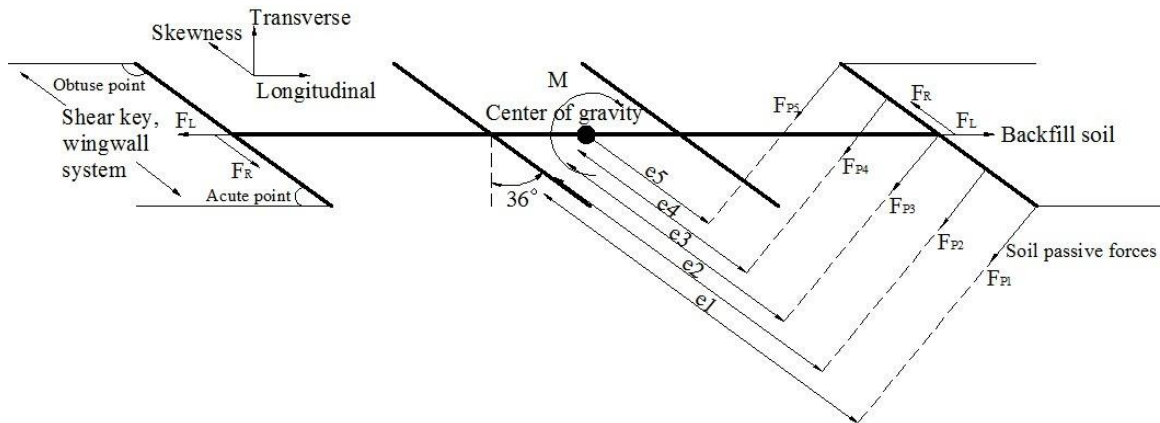


**Figure 3.26** Typical forces distribution on skewed bridge

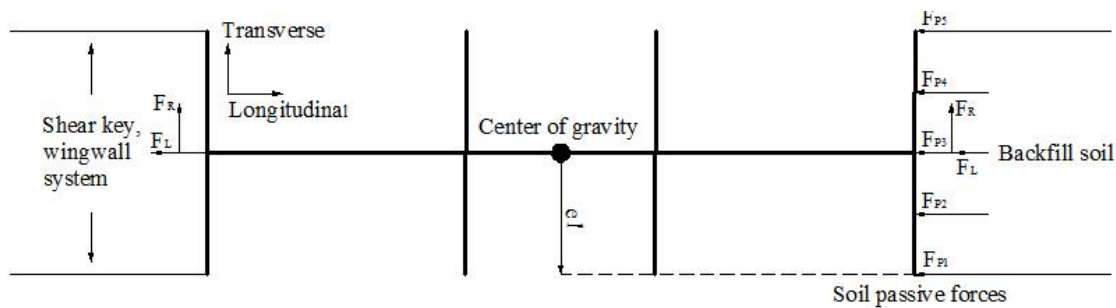


**Figure 3.27** Typical forces distribution on straight/non-skewed bridge

Typical forces and additional moment distributions of a skewed bridge and a straight bridge are presented in Figures 3.25 and 3.26. Longitudinal and transverse seismic excitations may induce longitudinal forces ( $F_L$ ) and transverse forces that must be resisted by the backfill soil passive force ( $P_p$ ) normal to the abutment wall, and the shear resistance ( $P_R$ ) on the shear key and wingwall system. However, compared with the symmetric force distribution of a straight bridge in Figure 3.26, the asymmetric forces may cause a rotational moment  $M_R$  when the deck collides with the abutment (Watanabe and Kawashima, 2004). Unlike straight bridges, skew bridge components are usually affected by the combination of longitudinal and transverse GMs because the bent and longitudinal directions of the bridge are not orthogonal.

### 3.2.2 Skewed Bridge Numerical Model

The 3D skewed bridge model originally created by Kaviani et al. (2012) in Opensees (McKenna et al. 2000) was modified to include a BRB bracing system. The deck was modeled using linear-elastic beam-column elements, and its mass and moment of inertia were calculated based on the deck's net area, in agreement with Caltrans requirements. As part of the current study, Kaviani's model was modified to include BRBs and a new transverse abutment system. Figure 3.27 presents the retrofitted bridge with the inclusion of BRBs at the bents.

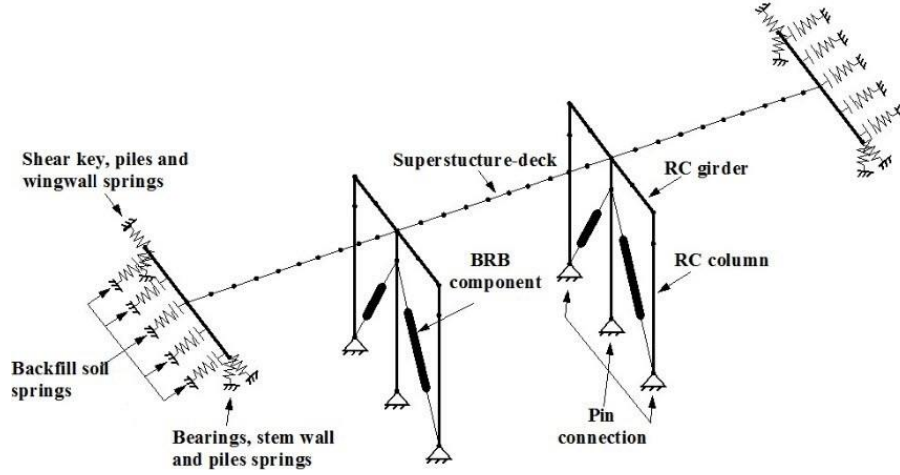


**Figure 3.28** Retrofitted bridge model in OpenSees

The passive backfill response and expansion joints were represented by five nonlinear springs, and the gap elements were simulated with the OpenSees hyperbolic gap material. Regarding the abutment longitudinal stiffness, the soil-structure interaction (SSI) properties were modified based on Caltrans SDC (2010) recommendations, as well as experimental data from Stewart et al. (2007), Rollins and Jessee (2012), and Marsh (2013). The longitudinal backfill stiffness,  $K_{abut}$ , and strength,  $P_{bw}$ , from Caltrans SDC (2010) are shown in Equations 5 and 6.

$$K_{abut} = \begin{cases} 25 \frac{\text{kip/in}}{\text{ft}} \times w \times \left(\frac{h}{5.5}\right) & (\text{ft, kip}) \\ 14.35 \frac{\text{kN/mm}}{\text{m}} \times w \times \left(\frac{h}{1.7}\right) & (\text{m, kN}) \end{cases} \quad (5)$$

$$P_{bw} \text{ or } P_{dia} = \begin{cases} A_e \times 5.0 \text{ ksf} \times \left(\frac{h_{bw} \text{ or } h_{dia}}{5.5}\right) & (\text{ft, kip}) \\ A_e \times 239 \text{ kpa} \times \left(\frac{h_{bw} \text{ or } h_{dia}}{1.7}\right) & (\text{m, kN}) \end{cases} \quad (6)$$

where  $w$  and  $h$  represent the width and height of the backwall or diagram abutments, respectively. Note that the unequal longitudinal abutment response from skewness was not considered by Stewart (2007) and Caltrans (2010). However, recently Rollins and Jessee (2012) and Marsh (2013) performed several experimental and numerical tests about soil-structure interaction for skewed abutments. The results show that, although the initial stiffness for each skew angle curve is remarkably similar, the peak passive force/strength at the center of skew abutment clearly decreases as the skew angle increases. They proposed a correction factor,  $R_{skewed}$  given by eqn.10, which describes the relationship between the peak passive force for a skewed abutment ( $P_{P-skew}$ ) and the peak passive force for a non-skew abutment ( $P_{P-no skew}$ ) as a function of the skew angle  $\theta$ .

$$R_{skew} = \frac{P_{P-skew}}{P_{P-non skew}} = 8.0 \times 10^{-5} \theta^2 - 0.018 \theta + 1.0 \quad (7)$$

Furthermore, due to the difference of backfill soil near the obtuse point (OBT) and the acute point (ACU), the spring near the OBT point could have larger stiffness and strength because of larger volume of soil.

Because of the lack of experimental data, Kaviani et al. (2012) assumed the largest variation along the abutment equals to 30% when the skewed angle is  $60^\circ$ . In this study, however, based on experimental data from Marsh (2013) the definition of largest variation along the skewed abutments is adjusted to equal 160% when the skewed angle is  $60^\circ$  as represented by Equation 8.

$$\beta = 1.6 \times \frac{\tan \alpha}{\tan 60^\circ} \quad (8)$$

Several alternatives are available to obtain the abutment transverse stiffness. For instance, Caltrans (2010) proposes, as a first order approximation in elastic models, to use 50% of the elastic transverse stiffness of the adjacent bent as abutment stiffness. For the case study,  $K_{\text{abut}} = 0.5K_b = 1.26 \times 10^5$  kN/m (710 k/in).

Caltrans (2010) also indicates the “transverse stiffness of diaphragm type abutments supported on standard piles can conservatively be estimated, ignoring the wingwalls, as 7,000 kN/m (40 kips/in) per pile.” For the evaluated bridge containing 40 piles underneath the abutment, the resulting abutment stiffness is  $K_{\text{abut}} = K_{\text{piles}} = 2.8 \times 10^5$  kN/m (1,575 k/in).

The shear key stiffness,  $K_{\text{SK}}$ , also contributes to the abutment stiffness (Goel and Chopra 2008). This stiffness was modeled with the “strut-and-tie analogous model” from Megally et al. (2002), which was calibrated experimentally to estimate the shear key force-deformation behavior. Based on the Megally et al. (2002) model, the shear key ultimate strength was estimated as 10,500 kN. The consideration of piles and shear key stiffness reduced the total abutment’s stiffness, but did not change the ultimate strength of the abutment (Goel and Chopra, 2008).

$$K_{\text{abut}} = \frac{K_{\text{SK}}K_{\text{piles}}}{K_{\text{SK}}+K_{\text{piles}}} = 1.65 \times 10^5 \text{ kN/m (926 k/in)} \quad (9)$$

The stiffness contribution of the wingwall during SSI may be incorporated using different approximations. For example, Makris and Zhang (2002) showed that the transverse stiffness of the embankment and wedge can be estimated by multiplying the dynamic stiffness of the embankment by an effective length  $L_c$ . According to Megally et al. (2002), the wingwall transverse stiffness,  $K_{\text{ww}}$ , can also be estimated by modifying the longitudinal abutment stiffness using factors corresponding to wall effectiveness ( $C_L = 2/3$ ) and participation coefficients ( $C_W = 4/3$ ):

$$K_{\text{ww}} = K_i \times L_{\text{ww}} \times \left( \frac{H}{1.7} \right) \times C_L \times C_W = 1.06 \times 10^5 \text{ kN/m (596 k/in)} \quad (10)$$

where  $K_i = 13,350 \frac{\text{kN/m}}{\text{m}}$  ( $25 \frac{\text{k/in}}{\text{ft}}$ ) is the initial embankment fill stiffness recommended by Caltrans (2010).  $L_{\text{ww}} = 7.0$  m is the wingwall length, and  $H = 5.4$  m is the abutment height. For the baseline case, the stiffness contributions from piles, shear keys, and wingwalls were included in the abutment transverse stiffness calculation, as follows.

$$K_{\text{abut}} = \frac{K_{\text{SK}}K_{\text{piles}}}{K_{\text{SK}}+K_{\text{piles}}} + K_{\text{ww}} = 2.71 \times 10^5 \text{ kN/m (1,522 k/in)} \quad (11)$$

For the case study, Caltran’s (2010) initial recommendation of only considering the piles contribution provides a close estimate of the abutment stiffness because the shear key and wingwall stiffness contributions offset each other.

For the vertical direction, a nonlinear spring with two stiffness segments working only in compression was implemented. The initial stiffness represents the stiffness flexibility of the elastomeric bearings, and a larger second stiffness represents the rigid behavior of the abutment stem wall stiffness.

The fundamental periods of the straight bridge is  $T_{1,L} = 0.66$  s. in longitudinal direction,  $T_{1,T} = 0.38$  s. in transverse direction, and  $T_{1,V} = 0.29$  s. in vertical direction (Table 3.2). For the skewed bridge, the longitudinal fundamental period is shorter while the transverse period elongates due to the tendency of the deck to rotate (Figure 3.28). However, BRB retrofit has negligible effects on straight bridge longitudinal effects, while the BRB would change the frequency response in the longitudinal direction of a skewed bridge. The additional BRB stiffness results in a larger reduction of transverse periods of vibration for straight, as compared with, skewed bridges. This is because BRB stiffness partially contributes to the longitudinal stiffness in skewed bridges. The model shapes of the original straight and skewed bridges are shown in Figure 3.29.

Because of the additional stiffness provided by the BRBs, the 4<sup>th</sup> mode of the original bridge and the 3<sup>rd</sup> mode of the skewed bridge are both rotational modes, but they have combinational mode shapes with rotational and transverse displacement.

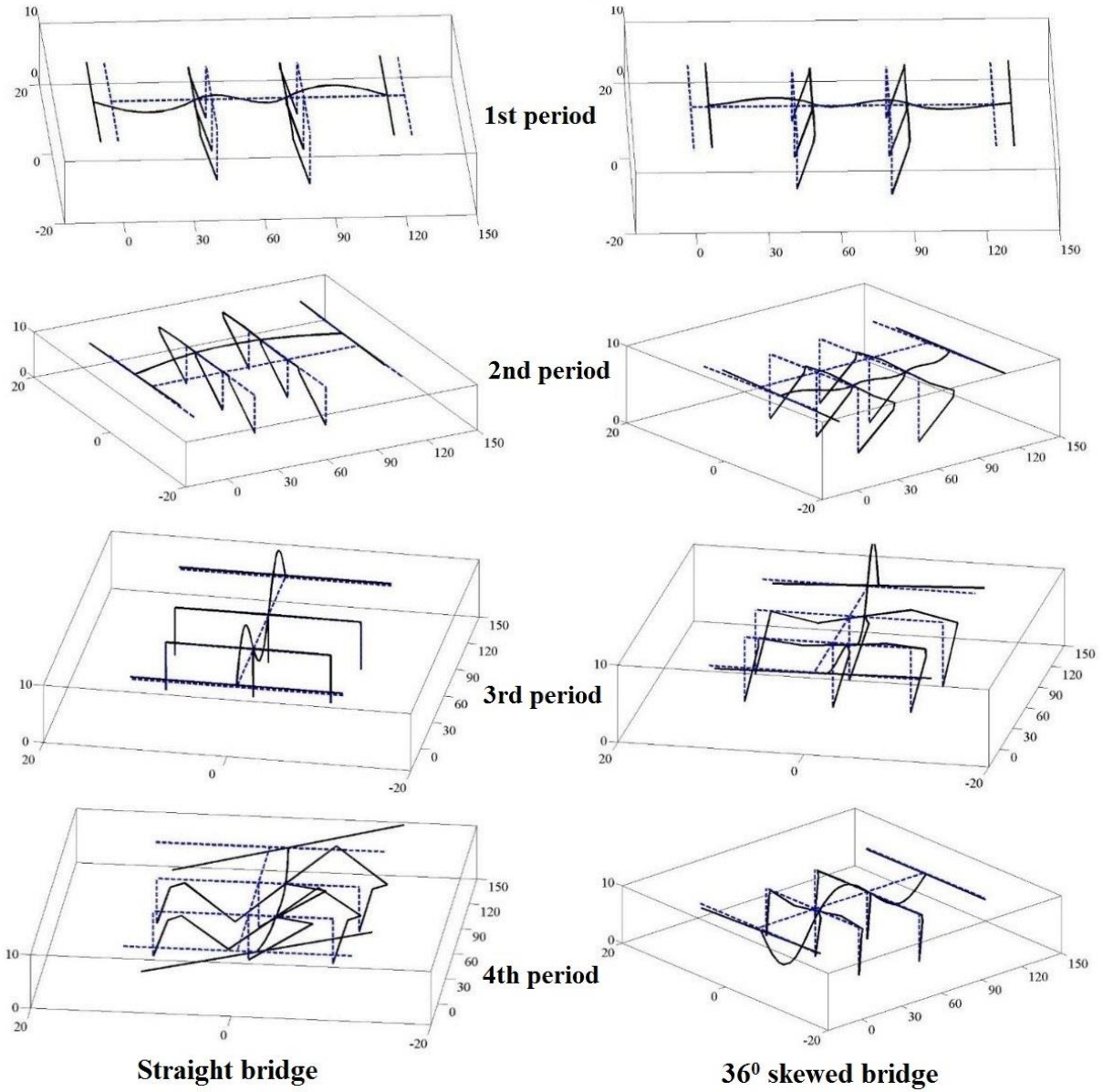


**Figure 3.29** Mode shapes of original straight bridge and 36° skewed bridge



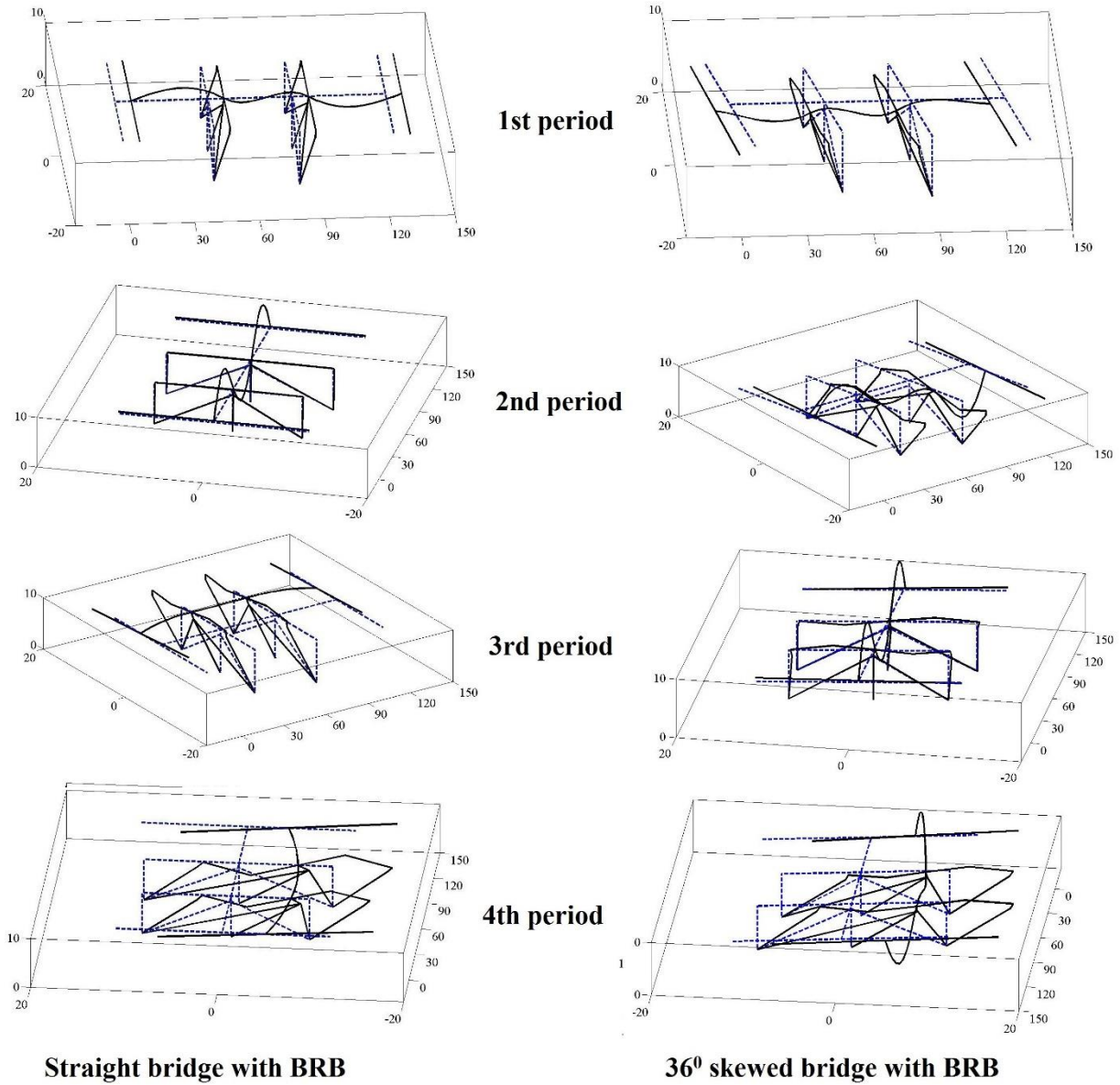


**Figure 3.30** Mode shapes of retrofit straight bridge and 36° skewed with BRB

**Table 3.2** BRB dimensions for skewed bridge

Period of vibration	Straight (s.)	Straight with BRB (s.)	36 <sup>0</sup> Skew (s.)	Skew with BRB (s.)
1 <sup>st</sup> (Longitudinal dir.)	0.66	0.66	0.65	0.58
2 <sup>nd</sup> (Transverse dir.)	0.38	0.28	0.40	0.32
3 <sup>rd</sup> (Vertical dir.)	0.29	0.29	0.30	0.29
4 <sup>th</sup>	0.26	0.26	0.29	0.29

Note: The contribution percentage of BRB to lateral resistance in this table is 50%.

### 3.2.3 Performance Limit States

Vision 2000 (OES 1995) defined four bridge performance levels: i) fully operational at 0.2% drift, ii) operational at 0.5% drift, iii) life safety at 1.5% drift, and iv) near collapse at 2.5% drift. AASHTO (2012) also suggested four limit states: i) service, ii) fatigue and fracture, iii) strength, and iv) extreme event limit states; but it did not include quantitative values for these limit states. Lu et al. (2005) proposed three performance limit states for RC columns: i) fully operational at a drift of 1.08%, ii) damage control and life safety between 0.8 and 2.16% drift, and iii) ultimate drift limit from 1.13% to 3.3%. For this study, three drift limit states are used from Vision 2000 by consolidating the fully operational and operational limits (Table 3.3).

In addition, Priestley (2000) and Kowalsky (2000) proposed two performance limits based on concrete and steel strain: i) fully operational, and ii) damage control limit states. The latter would be somewhere between the Operational and Life Safety performance limits, as shown in Table 3.3.

**Table 3.3** Limit state definition

Limit State	Priestley-Kowalsky Strain Limits		Drift limits
	Concrete compression strain	Steel tension strain	Vision 2000
Operational	0.004	0.01 (beam), 0.015 (column)	0.5%
Life Safety	0.018	0.06	1.5%
Near collapse	-	-	2.5%

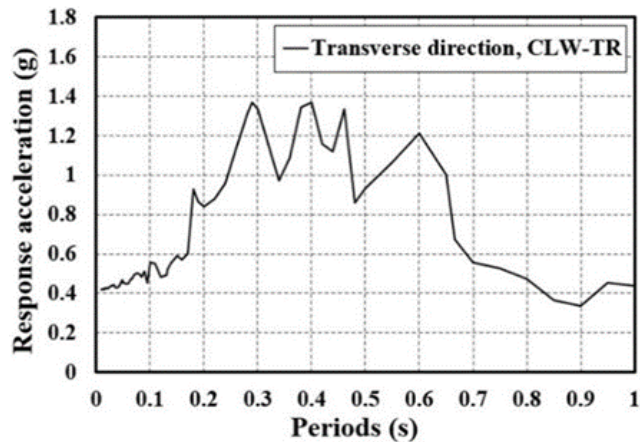


**Figure 3.31** Transverse response spectra for unscaled Landers 1992 Earthquake

### 3.2.4 Bridge Seismic Performance

The bridge was initially subjected to the three orthogonal accelerations of the unscaled Californian far-field ground motion (FFGM) Landers 1992, Coolwater station (FEMA, 2009), which has a longitudinal peak ground acceleration  $PGA = 0.283$  g, transverse  $PGA = 0.417$  g, and vertical  $PGA = 0.174$  g. The ground motion was selected to eliminate the effect of different transverse spectral accelerations for the original and retrofitted bridges. Coincidentally, the horizontal spectral acceleration  $S_a$  is approximately the same for the retrofitted straight bridge transverse fundamental period  $T_{T1, BRB} = 0.28$  s., and for the original straight and skewed bridge transverse period  $T_{T1} = 0.38$  s (0.40 s). The spectral acceleration at both transverse periods is approximately  $S_a(T_{T1, BRB}) = S_a(T_{T1}) = 1.37$  g (Figure 3.31).

### 3.2.5 Optimization of BRB Core in Straight Bridge Under ASCE 41-13 Scaled Method

The BRBs redistribute seismic energy from the abutments to the retrofitted bents. For the DS-BRB50 system, the bent stiffness-to-abutment stiffness ratio ( $K_b/K_{abut}$ ) increased from 0.97 to 1.43, leading to larger bent column shear demands. For this reason, the study was extended to consider systems in which BRBs can withstand 25%, 40%, 50%, 60%, and 75% of the bent's shear forces (again DS-25BRB, DS-40BRB, DS-50BRB, DS-60BRB, and DS-75BRB, respectively).

### 3.2.6 Principal Direction of Skewed Bridge Under ASCE 41-06 Scaled Method

Seismic demands applied to bridge structures are dependent on ground motion type and direction. Penzien and Watabe (1975) determined that the major principal axis of a ground motion points to the epicenter in general, which is normal to the fault. Principal directions are often used because they have zero covariance with respect to each other. Maleki and Bisadi (2006) conducted linear seismic analysis on skewed bridges with orthogonal ground motions to determine the critical response for varying ground motion incidence angles. They were not able to determine the critical input angle that produced the maximum response for the evaluated bridge. Bisadi and Head (2011) performed a parametric study with 100 paired ground motions, 100 different bridge configurations, and ground motion incidence angles varying from  $0^0$  to  $180^0$  with increments of  $10^0$ . The results showed that the critical angle of incidence that caused maximum response was dependent on the characteristic of the ground motions and bridge characteristics. Basu and Shinozuka (2011) analyzed the effect of seismic ground motion incidence angle on the seismic performance of straight bridges, concluding that straight bridges were most sensitive to

ground motions when their incident angle was between  $30^{\circ}$  and  $60^{\circ}$  with respect to longitudinal direction of the bridge.

Torbol and Shinozuka (2012) examined the effect of ground motion incidence angle on the fragility curves of straight bridges with fault normal/fault parallel (FN/FP) ground motions. The results showed that although the bridges were regular and symmetric, neither longitudinal nor transverse was consistently the weakest direction. Bhatnagar (2013) modeled the skewed Painter Street Bridge to compare the effects of various incident angles with a suite of orthogonal ground motions. The results proved that variation of the maximum response of skew bridges could be observed with respect to change in angle of incidence, change in skew angle, and a combination of both. However, the uncertainty in the response spectrum shape may bias the analyses results.

A parametric study with the BRB base case, DS-50BRB, was performed for straight and skewed bridges using 21 acceleration ground motions from the FEMA P-695 far-field record set (FEMA 2009). To reduce the influence of epicenter uncertainty and record-to-record (RTR) variability, the ground motions are first rotated to minimize the correlation in the orthogonal directions. Similar to the method proposed in ASCE 41-06 (2006), each set of rotated response spectra was then scaled in such a way that the average of the square root of the sum of the squares (SRSS) spectrum in the interval  $0.2T_{1,T} \approx 0.1$  s to  $1.5T_{1,L} \approx 1.0$  s was equal to 1.3 times the average  $S_a$  of the MCE spectrum in this interval ( $1.3S_{avg} = 0.933$  g). As observed in Figure 3.32, the dispersion of response accelerations ( $S_a$ ) in the range of target periods is greatly reduced. After ground motions are scaled, each set was input to both straight and skewed bridges with different incidence angles. The FN component with small PGA is applied first in the longitudinal direction of the bridge; whereas, the FP component with larger PGA is applied in the orthogonal direction. Then the orthogonal GM sets are rotated counterclockwise from  $0^{\circ}$  to  $180^{\circ}$  (Figure 3.33).

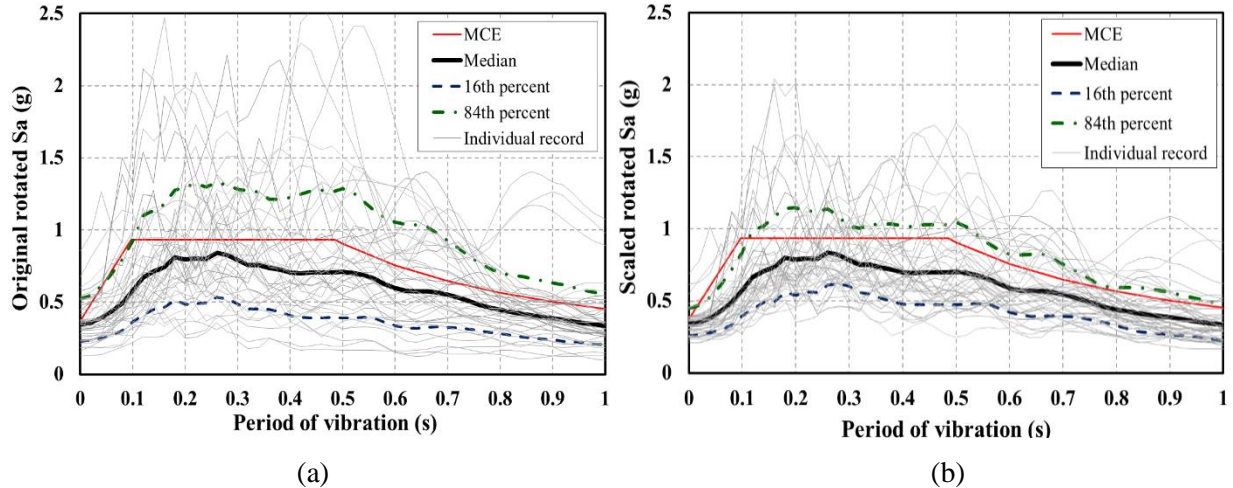


**Figure 3.32** Response spectrum for far-field FEMA: (2009) set (a) original spectrum; (b) scaled spectrum

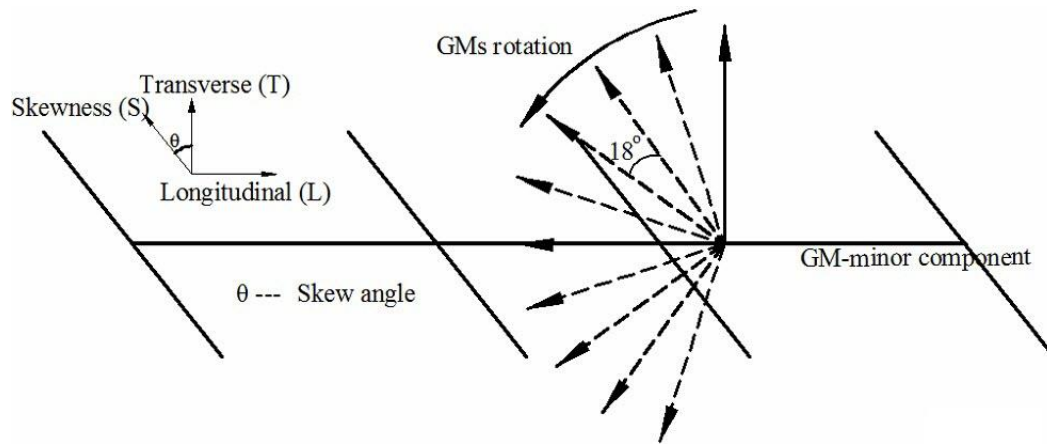


**Figure 3.33** GM set rotation direction

Scatter curves were developed for several output parameters by fitting a lognormal distribution to the data (Ibarra and Krawinkler, 2005). The curves in the plots below are based on a median response parameter and the dispersion parameter that corresponds to the standard deviation of the natural logarithm of the random variable  $x$  (FEMA-351 2001).

$$\beta = \sigma_{\ln x} = \sqrt{\frac{\sum_{i=1}^n (\ln x_i - \mu_{\ln x})^2}{n-1}} \quad (15)$$

Where “ $n$ ” is the number of data points, and  $\mu_{\ln x}$  is the mean of the natural logarithm of parameter  $x$ . In this study, the dispersion in the response is entirely caused by RTR variability.

## 4. ANALYSIS RESULTS

### 4.1 Analysis Results of the Curved Bridge

#### 4.1.1 Moment Curvature Analysis

Moment curvature analysis for column 10 is presented here. M-c analysis was performed using an SAP 2000 fiber section assignment.

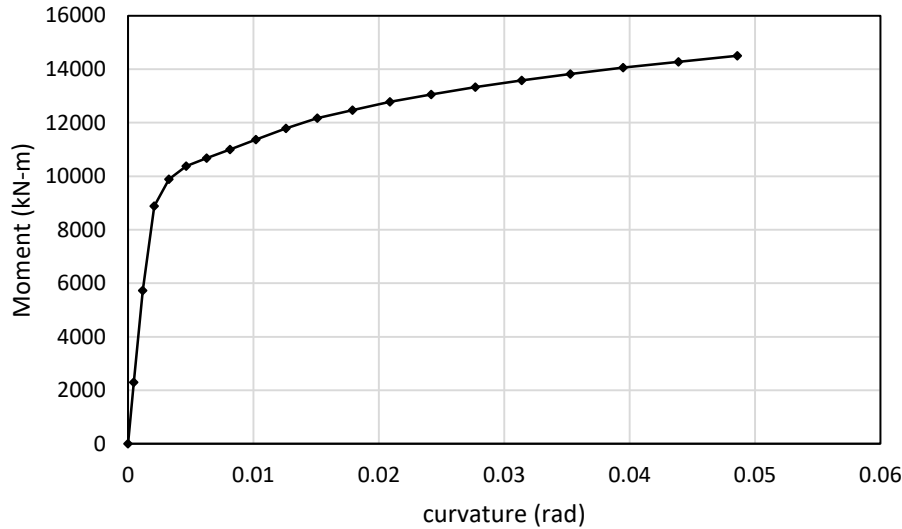


**Figure 4.1** Moment-curvature analysis for column 10 of curved bridge

Output: For Column 10

$M_Y = 6910.93$  kN-m,  $\Phi_Y = 0.001511$

$M_U = 14501.97$  kN-m,  $\Phi_U = 0.04885$

$I_C = 0.56I_g$  (SDC 2010)

Displacement Capacity:

$L_P = 0.882$  m, Column dia. = 1.981 m

$H = 10.9$  m

$\Theta_P = (\Phi_U - \Phi_Y)L_P = 0.0417$  rad

$\Delta_y = H^2 \Phi_U/3 = 0.059$  m,  $\Delta_P = \Phi_P(H - L_P/2) = 0.436$  m,

Displacement ductility  $\mu = 8.389$

#### 4.1.2 Static Pushover Analysis

Nonlinearity of the column was modeled using fiber PMM hinges in SAP 2000. These plastic hinges were engaged in the analysis while performing pushover analysis. Properties of plastic hinges were adopted using M-c analysis presented in section 3.1.1. Static pushover analysis was performed on individual columns with the axial load calculated by static dead load analysis in SAP 2000. Figure 4.2 shows pushover curves for individual columns.

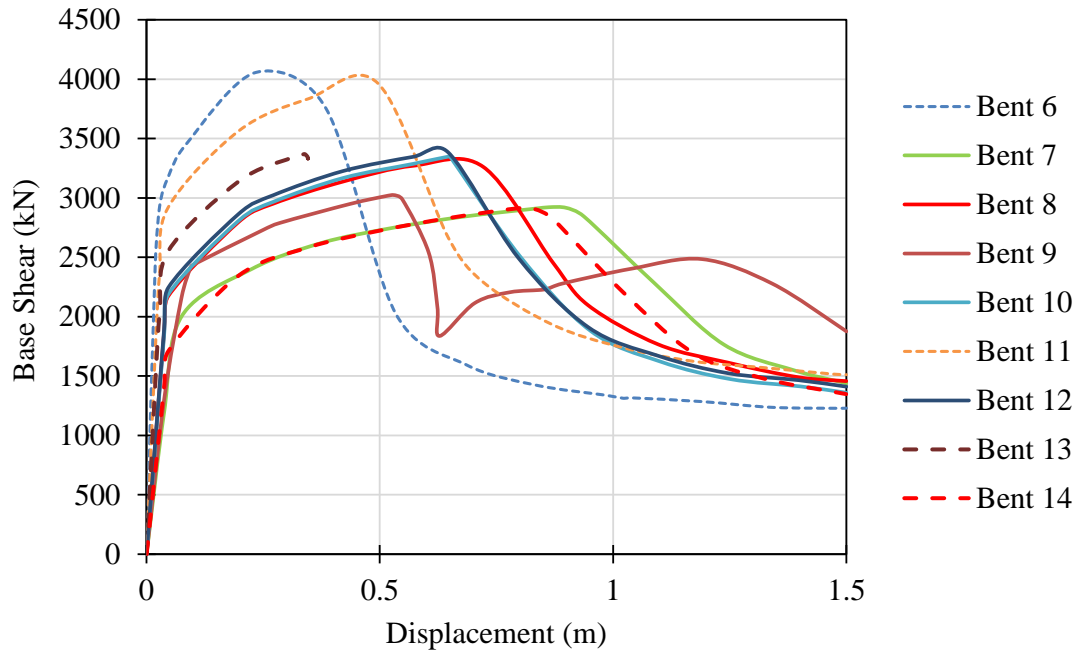


**Figure 4.2** Pushover curves for various columns of curved bridge

### 4.1.3 Results of Non-linear Analysis

#### 4.1.3.1 Modal Analysis

Table 4.1 shows the mass participation ratio of the first 30 modes of the bridge after including soil-structure interaction. The first mode participation is the maximum and is dominant as compared with the rest of the modes. The first six modes are shown in Figure 4.3.

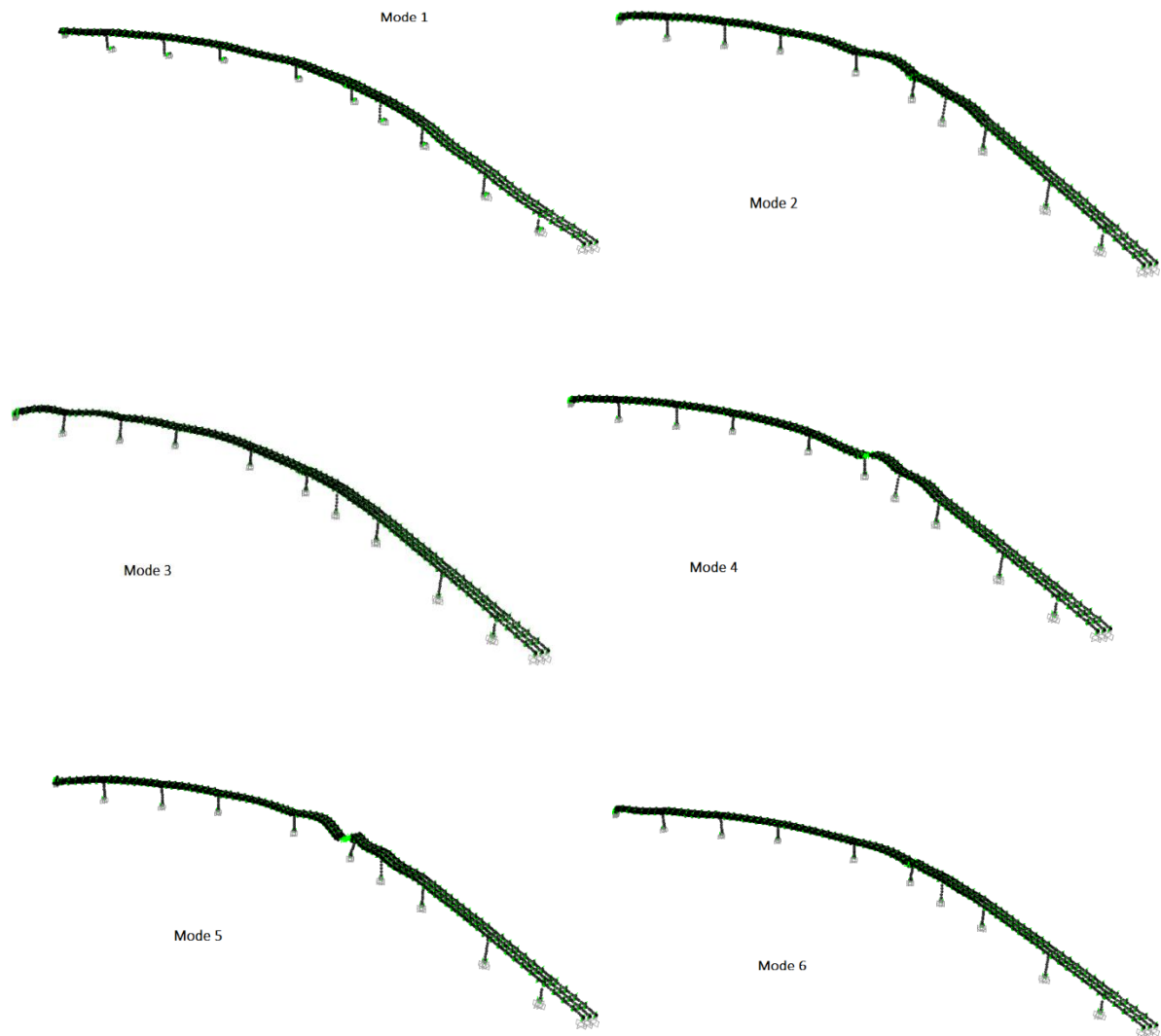


**Figure 4.3** First six mode shapes of curved bridge



**Table 4.1** Periods and mass participation ratios of first 30 modes of curved bridge

Mode Number	Period (S)	Horizontal-X	Horizontal-Y	Vertical
1	2.724	0.07614	8.0800E-03	6.968E-08
2	2.223	0.00293	1.1400E-03	5.667E-06
3	2.029	0.03452	7.7000E-04	2.901E-07
4	1.837	0.05688	5.6670E-02	1.112E-05
5	1.736	0.00171	4.7800E-03	8.484E-07
6	1.647	0.13812	6.9900E-03	7.165E-08
7	1.538	0.19357	5.2500E-03	1.059E-07
8	1.458	0.03472	1.5000E-04	6.398E-06
9	1.453	0.0166	1.7970E-02	3.067E-08
10	1.277	0.00104	9.5360E-05	4.185E-07
11	1.140	0.01586	1.7900E-03	3.370E-07
12	1.121	0.00519	9.4330E-10	9.716E-06
13	1.101	0.00955	3.4500E-03	1.886E-05
14	1.006	0.01744	3.8040E-05	1.600E-04
15	0.982	0.00359	1.5000E-04	3.614E-05
16	0.925	0.00411	4.9089E-01	8.838E-05
17	0.912	0.007	2.5100E-02	7.155E-05
18	0.882	0.00037	1.5780E-02	2.500E-04
19	0.825	0.01375	6.5000E-04	1.570E-03
20	0.798	0.00392	1.8300E-03	1.720E-03
21	0.753	0.00881	2.7360E-02	6.180E-03
22	0.731	0.0039	2.5800E-03	2.300E-04
23	0.691	0.000009649	7.3000E-04	1.932E-05
24	0.681	0.0072	1.8010E-02	9.279E-05
25	0.631	0.00006959	2.6800E-03	1.140E-03
26	0.616	0.00011	7.7770E-06	1.837E-02
27	0.590	0.00445	2.3330E-05	1.182E-05
28	0.583	0.0058	1.3980E-02	1.491E-02
29	0.580	0.00059	1.5890E-02	3.540E-03
30	0.563	0.00547	8.4100E-03	6.200E-04

#### 4.1.4 Time History Analysis

Soil-Structure Interaction (SSI) increased the fundamental period of vibration to a large extent by eliminating the fixity at the foundation level. The time period of the fundamental mode of vibration was 2.3 seconds when SSI was not considered, while it increased to 2.72 seconds when SSI was taken into account. A series of non-linear time history analyses were carried out on this bridge using the ground motions presented in section 3.1.2. The deck displacement, deck accelerations, pounding force, and bent

top displacement time histories were monitored. The motion recorded at the Irpenia, Italy, site was used for Figure 4.4 and Chalfant Valley site (1986) was used for Figure 4.6.

#### 4.1.4.1 Neglecting Soil-Structure Interaction

First, the bridge was analyzed under a set of ground motions without taking soil-structure interaction into consideration. This analysis was necessary to show the impact of SSI on the behavior of the structure. The results obtained in this section will be compared with those of section 4.2.2. Response acceleration of the girders at the abutments for the Irpenia ground motion is presented in Figure 4.4, which shows that SSI increases the number of peaks in response acceleration of the structures. The gap between the girders and abutment wall is 75 mm and girder displacement should be at least 75 mm toward the abutment to generate any pounding. From Figure 4.5, it can be observed that the maximum girder displacement is less than 75 mm and hence no pounding was observed when SSI was neglected in the analysis. An incremental dynamic analysis (IDA) was performed on the bridge model using Chalfant Valley (1986) and Kobe (1995) ground motion data without considering SSI. Figure 4.6 shows that the axial force in the restrainer rods increased with the peak ground acceleration. However, the axial force in the restrainer rod remained less than the yield force value, 519 kN, when SSI was neglected in the analysis. The structure was further analyzed by modeling soil springs to understand the effect of SSI.

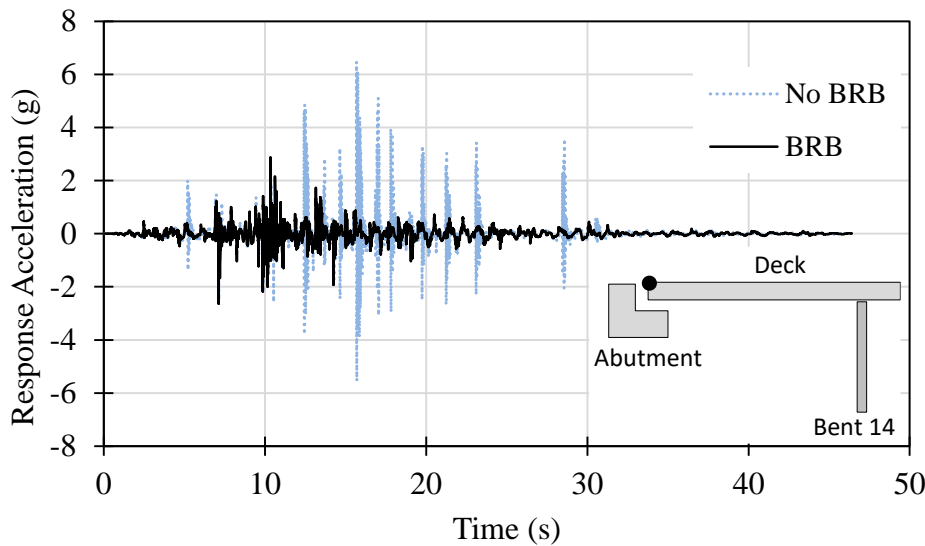


**Figure 4.4** Response acceleration of girder G1 relative to abutment for Irpenia, Italy, ground motion

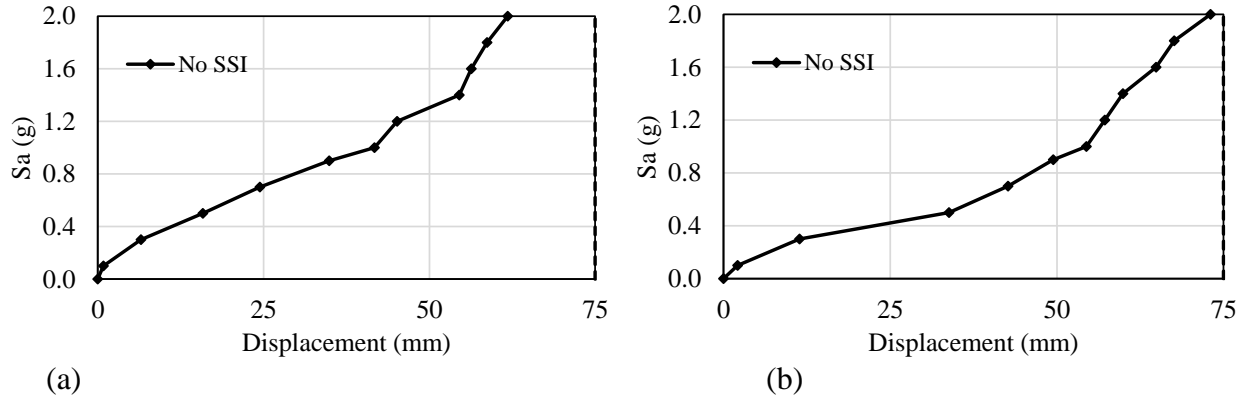


**Figure 4.5** Maximum displacement of girder G1 toward the abutment without considering SSI: (a) Chalfant Valley; (b) Kobe ground motion

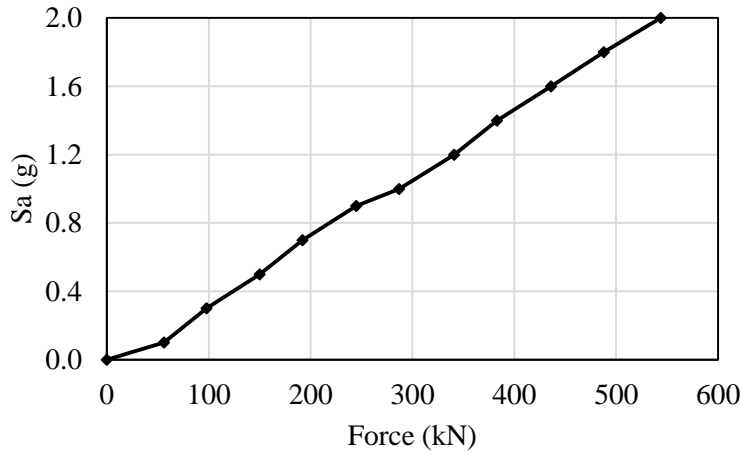


**Figure 4.6** Axial force in restrainer rod; from IDA using Chalfant Valley ground acceleration ignoring SSI

#### 4.1.4.2 Effect of Soil Structure Interaction

The soil borehole data show that the bridge was constructed on soft soil, and it is important to understand the effects of SSI on the structure's performance. SSI increased the fundamental period from 2.3 seconds to 2.7 seconds, hence shifting it to the displacement-based region of the design spectrum. Table 4.2 shows the effect of SSI on the first three modes of vibration. The peak girder displacement, which was 21 mm before inclusion of SSI, was observed to be more than 75 mm for all the ground motions listed in section 2.2. As the construction gap between the girder and abutment was 75 mm, pounding between them was expected. An IDA using Kobe ground acceleration data was performed for the bridge, and the results with and without SSI are shown in Figure 4.7. It is evident that SSI played an important role and increased the likelihood of pounding.

To calculate the pounding forces on girders and abutment, gap type compression only elements were introduced between girder nodes and abutment nodes as described in section 2. Figure 4.8 shows the girder displacement relative to the abutment and pounding force time-histories for Kobe (1995). Negative relative displacement values in Figure 4.8 represent movement of the girder toward the abutment. After pounding, the girder was displaced away from the abutment as a reaction, which in turn caused further pounding occurrences. Two conclusions can be reached from Figure 4.8: (i) to prevent pounding it is

required to limit the peak girder displacements toward the abutment below 75 mm, and (ii) in order to reduce the number of pounding events it is necessary to damp the oscillations of the girders. Using buckling restrained braces between the three girders and the abutment could be a solution to this problem. The pounding force time-histories for Kobe (1995) ground motion for girders G1, G2, and G3 of the curved bridge are compared in Figure 4.9, which shows that the force was highest for the exterior girder and lowest for the interior girder. Figures 4.10 to 4.15 show the pounding force time-histories of girder G1 for various earthquakes.

**Table 4.2** Effect of SSI on first three modes of curved bridge

	1 <sup>st</sup> Mode Period (s)	2 <sup>nd</sup> Mode Period (s)	3 <sup>rd</sup> mode Period (s)
Without SSI	2.31	2.16	2.08
With SSI	2.72	2.22	2.02

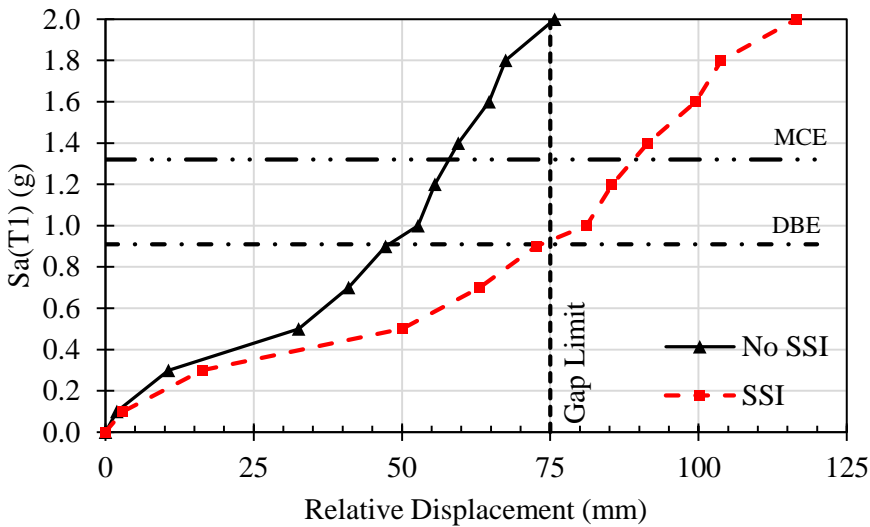


**Figure 4.7** Effect of SSI on relative displacement between girder G1 and abutment

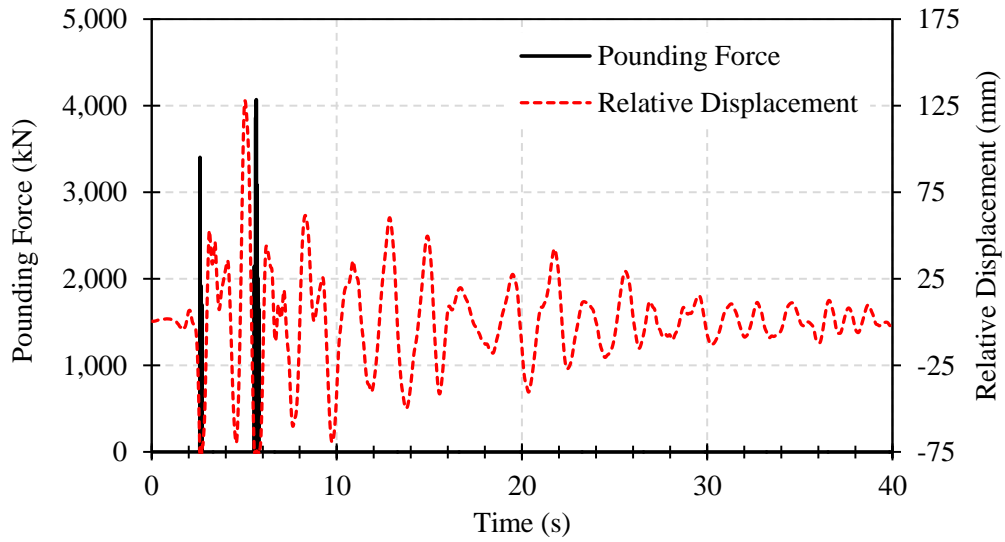


**Figure 4.8** Relative displacement and pounding force for girder G1 at abutment for scaled Kobe ground motion for as-built bridge

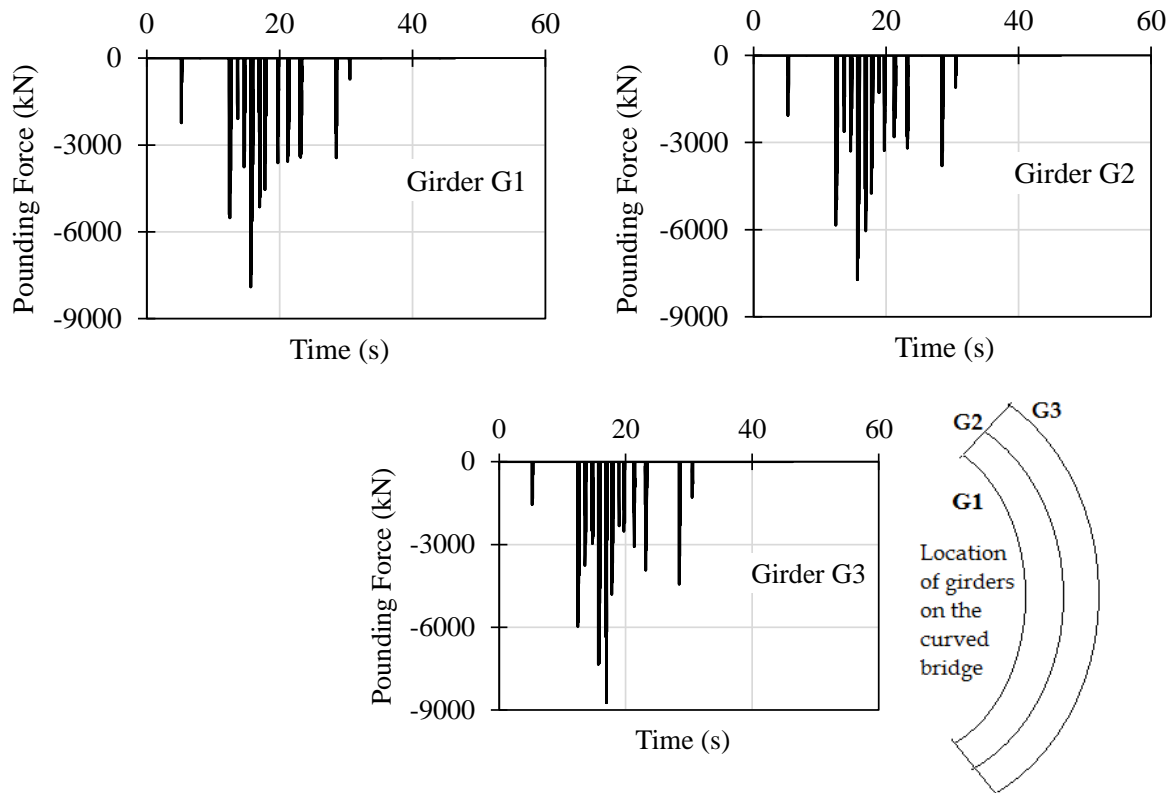


**Figure 4.9** Pounding between abutment and girders for Kobe ground motion

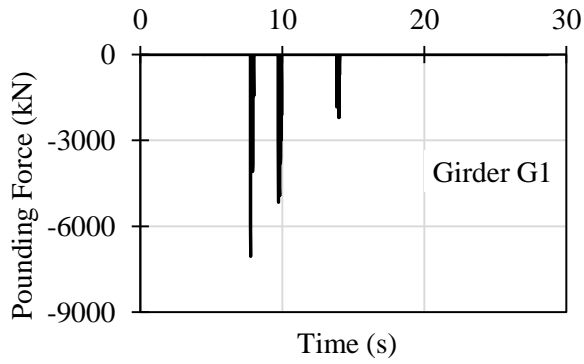


**Figure 4.10** Pounding between abutment and girder for Cape-Mendocino ground motion

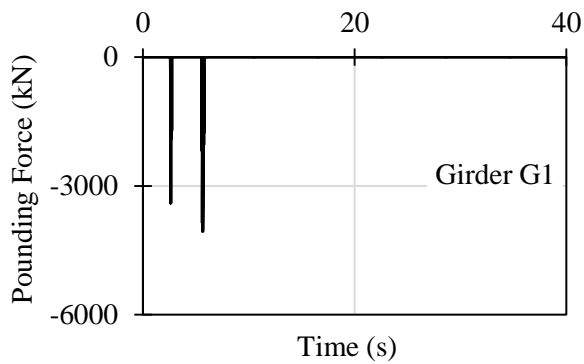


**Figure 4.11** Pounding between abutment and girder for Chalfant Valley ground motion

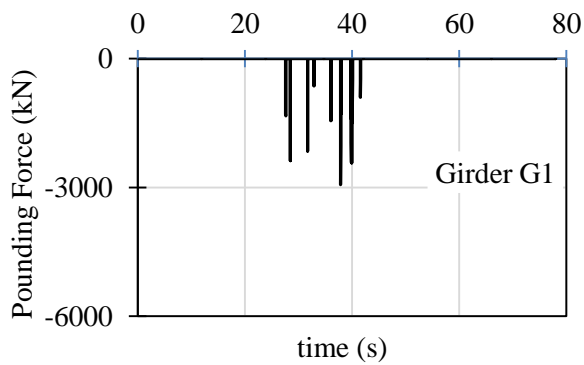


**Figure 4.12** Pounding between abutment and girder for ChiChi, Tiwan, ground motion

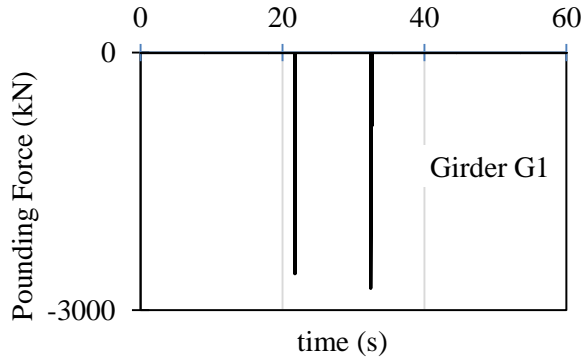


**Figure 4.13** Pounding between abutment and girder for Chuetsu-oki, Japan, ground motion

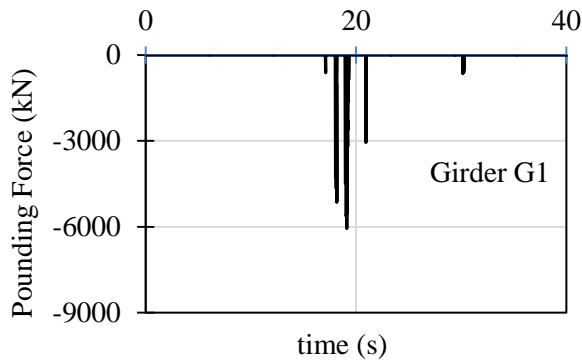


**Figure 4.14** Pounding between abutment and girder for Duzce, Turkey, ground motion

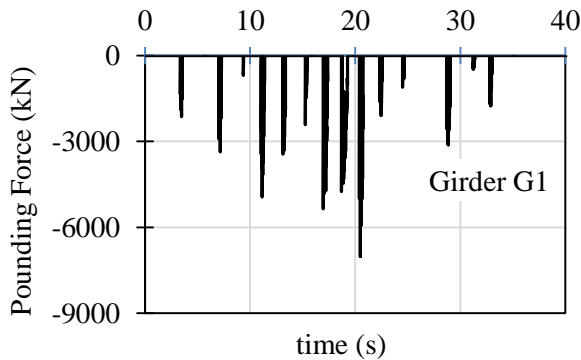


**Figure 4.15** Pounding between abutment and girder for Parkfield ground motion

Earthquake restrainer rods were used at the expansion joints of the curved bridge to prevent excessive relative displacement of the girders and potential unseating and fallout. These rods were 40 mm in diameter and had a nominal yielding force of 519 kN each. However, it is well known that the ultimate stress of the steel rods can be as much as 1.8 times the yield stress; therefore, the rods can be assumed to be working up to an axial force of 934 kN. Analyses showed that the peak axial forces generated in the rods were greater than 1000 kN, and these axial forces crossed the yield capacity many times during an earthquake event as shown in Figure 4.16. Based on this information, it was assumed that the restrainer rods suffered complete tensile failure, and pounding between the girders at the expansion joint was expected. A further analysis was done by removing the steel restrainer rods from the bridge model.

Yield force calculation for restrainer rods

Rod diameter = 40 mm

Area of cross-section of the rod = 1259 mm<sup>2</sup>

Yield stress of steel = 412 MPa

Yield force = Yield Stress x Area  
= 519 kN

Ultimate force = 1.8 x Yield force  
= 1.8 x 519 kN  
= 935 kN

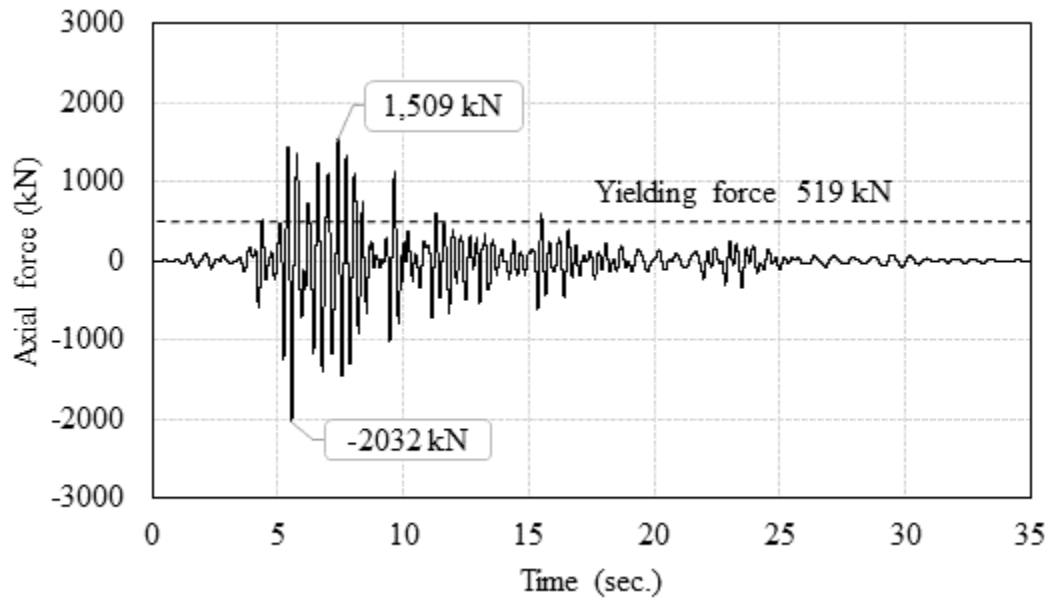


**Figure 4.16** Axial force time-history in one of the restrainer rods at expansion joint for scaled Kobe ground motion



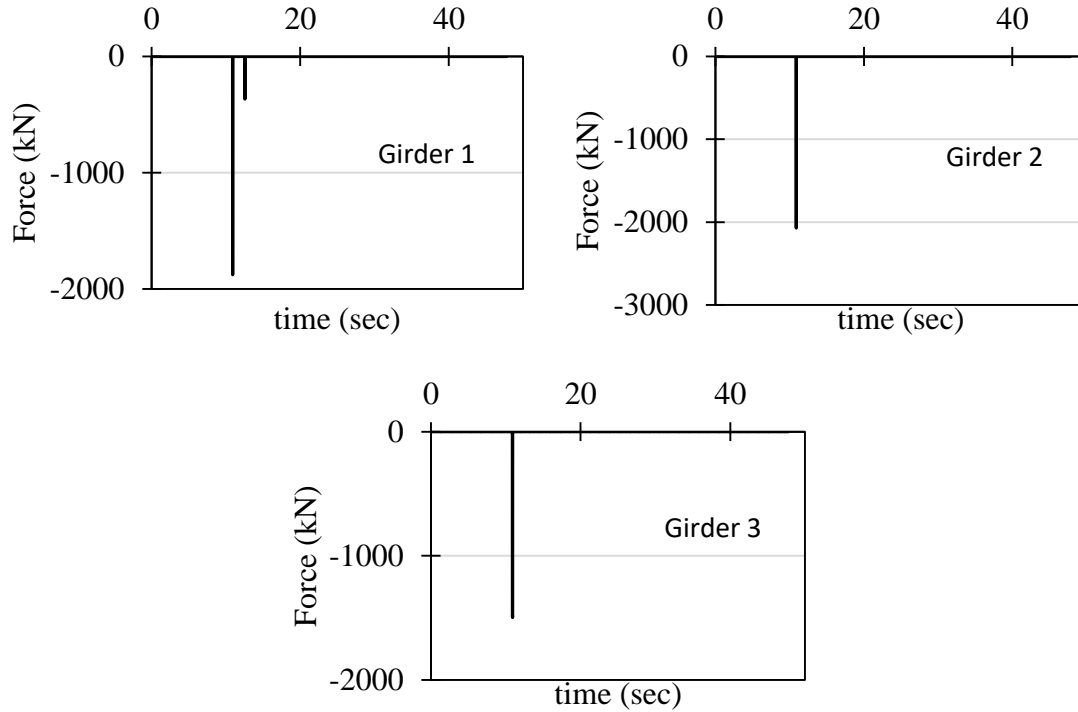


**Figure 4.17** Pounding between girders at expansion joint for scaled Kobe ground motion

Analysis of the bridge after removing the restrainer rods showed pounding between the girders at the expansion joints. However, the pounding was not repetitive and there were only a few spikes in the time history analysis, as shown in Figure 4.17, but the pounding force was up to 2000 kN. This high pounding force can cause severe damage to the deck. Along with the longitudinal movement of the girders, lateral (to the axis of the bridge) movement of the girders was also observed, and pounding between the concrete shear key and the steel girders was expected. To calculate this pounding force, compression-only gap type link elements were included in the model pounding between the concrete shear key and steel girder. Figure 4.18 and Figure 4.19 show the location of concrete shear keys and gap type link elements in the numerical model, respectively. The pounding occurred for several ground motions, and the time-history of the pounding force, at girder G1, for Kobe ground motion (1995) is shown in Figure 4.20. The pounding force at all three girders was high, which is a risk for the concrete shear keys.

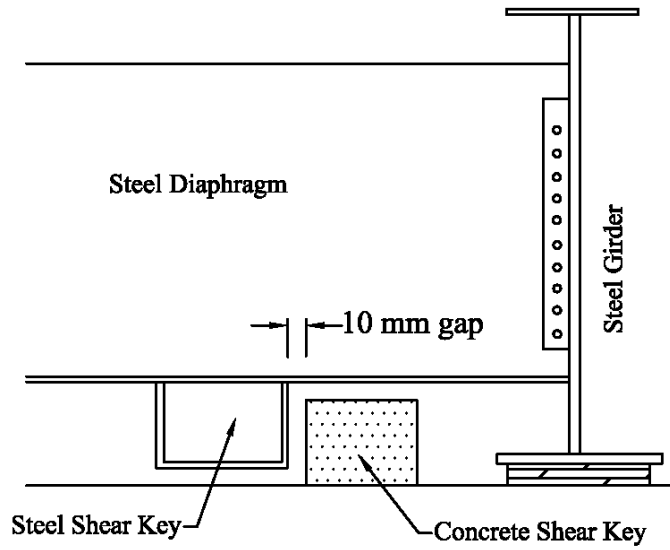


**Figure 4.18** Location of concrete shear key of curved bridge



**Figure 4.19** Shear keys on curved bridge bent

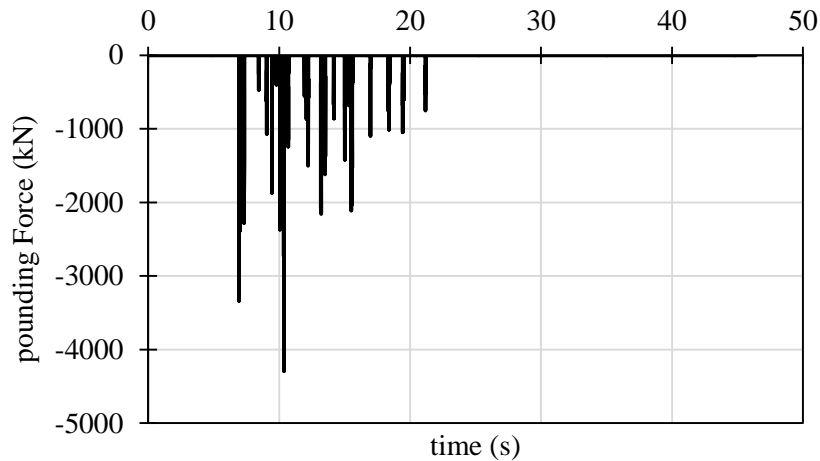


**Figure 4.20** Pounding force time-history between concrete shear keys and steel girder G1 of curved bridge for Kobe ground motion

The peak pounding force was less than the ultimate capacity of the connection between the steel shear key and the diaphragm; however, the force exceeded the concrete shear key capacity. Usually the concrete shear keys in a bridge are sacrificial, and their function is to dissipate energy by getting damaged, thus preventing damage from occurring to the superstructure. Although the damage mechanism is good for energy dissipation, there might be a probability of unseating of the girders. Repairing the girders after an earthquake is time consuming, and the strength of the repaired shear keys is less than the original.

#### 4.1.5 Application of Buckling Restrained Braces

The bridge model was retrofitted by installing one BRB on each girder in the longitudinal direction, as shown in Figures 4.21 and 4.22. The BRBs were designed following the procedure given by ASCE-07 (2014) for lateral stiffness of multi-column bridge bents. It is recommended that 70% of the seismic weight should be resisted by the BRBs and 30% should be resisted by the columns. But for this retrofit, it is assumed that 100% of the seismic weight is resisted by the BRBs. This assumption was made on the basis that the pounding at the abutment was due to abutment excitation, which is a result of soil-structure interaction. Hence, the movement of the abutment and foundations played a major role in the displacement of the girders relative to the abutment, and hence BRBs were supposed to provide sufficient stiffness to reduce that. The adopted backbone curve for longitudinal BRBs is shown in Figure 4.23. An incremental dynamic analysis was performed on the retrofitted bridge, and Figure 4.24 shows the relative displacement of girder G1 for various earthquakes. It is evident that BRBs were successful in preventing the pounding completely.

After the IDA computations, a series of scaled earthquake ground motions were used at various angles from the x-axis to analyze the performance of the longitudinal BRBs. As shown in Figure 4.25, the longitudinal BRBs performed well for all the scaled earthquakes. Response acceleration time history of girder G1 at the abutment is shown in Figure 4.26, and it is clear that BRBs provided additional stiffness between girders and the abutments; this resulted in reduced response acceleration. The hysteresis of the BRBs for various earthquakes, Figure 4.27, shows that BRBs performed well and dissipated earthquake energy to prevent the structure. Although BRBs prevented the pounding between abutment and girders, permanent deformation in the BRBs was observed at the end of seismic event. The permanent deformation of BRBs is shown in Figure 4.28.

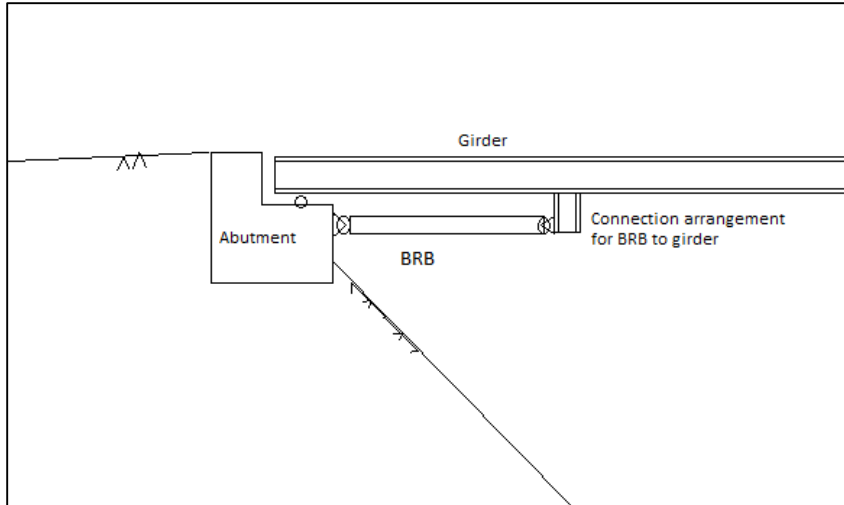


**Figure 4.21** Application of longitudinal BRB at the abutment of curved bridge

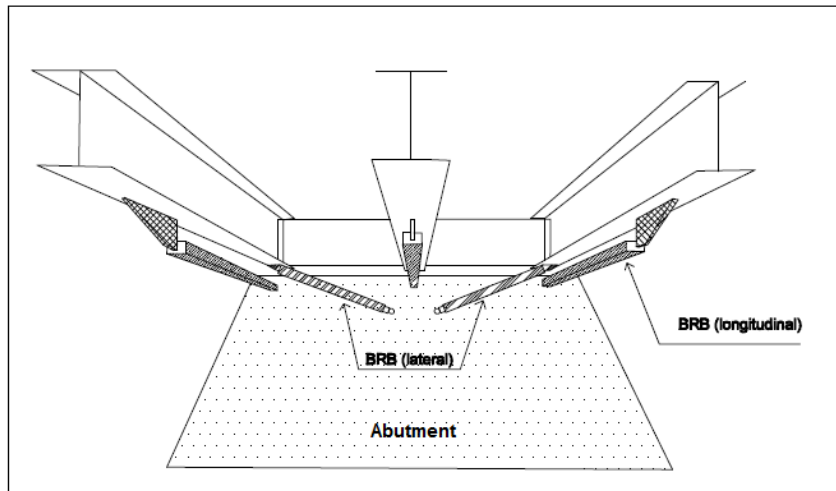


**Figure 4.22** Retrofit scheme using BRBs at abutment of curved bridge

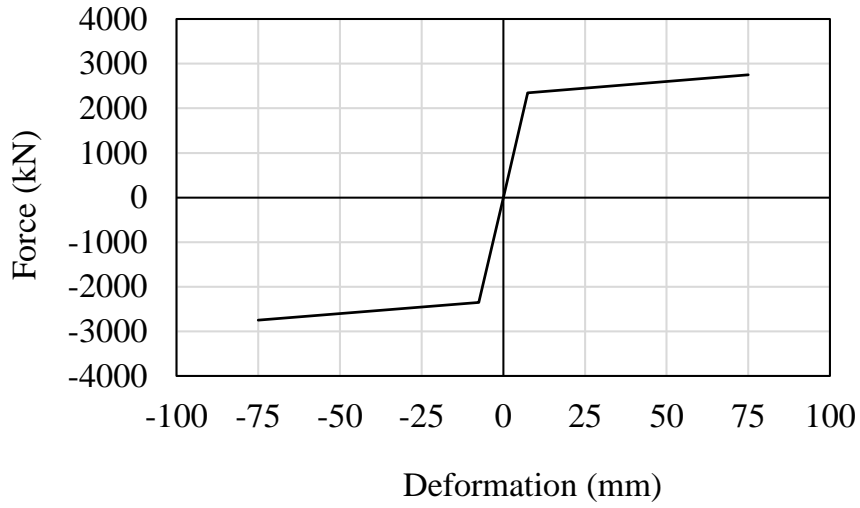


**Figure 4.23** Bilinear backbone curve used for longitudinal BRB

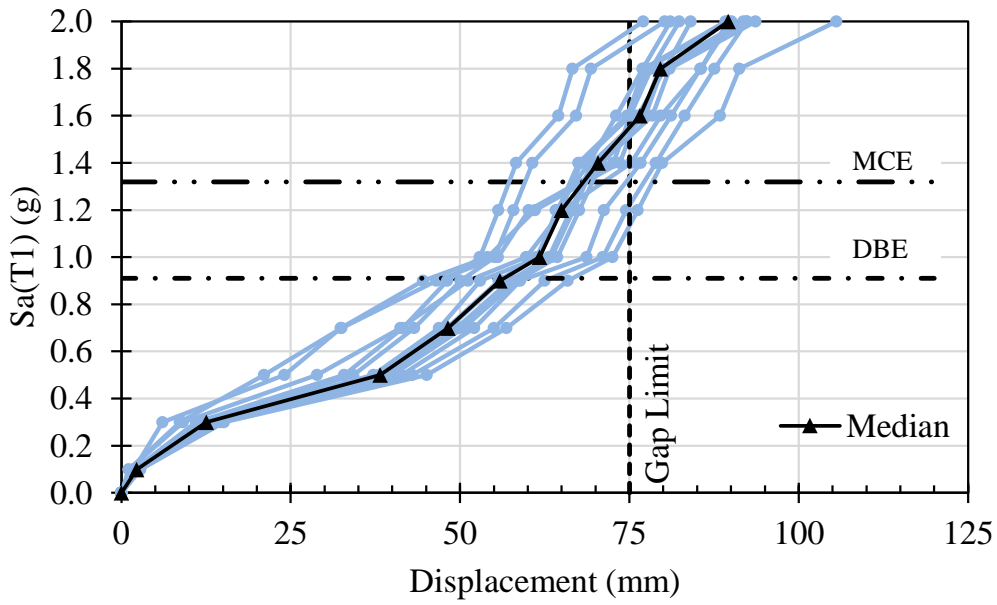


**Figure 4.24** IDA results of retrofitted curved bridge abutment

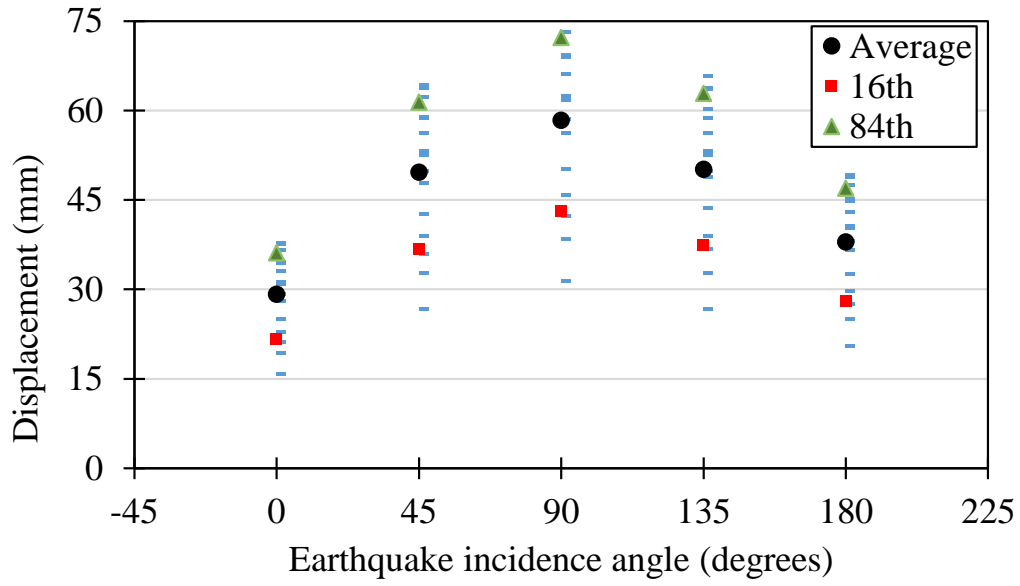


**Figure 4.25** Peak relative displacements of girder (G1) of curved bridge for ground motions at various angles of incidence

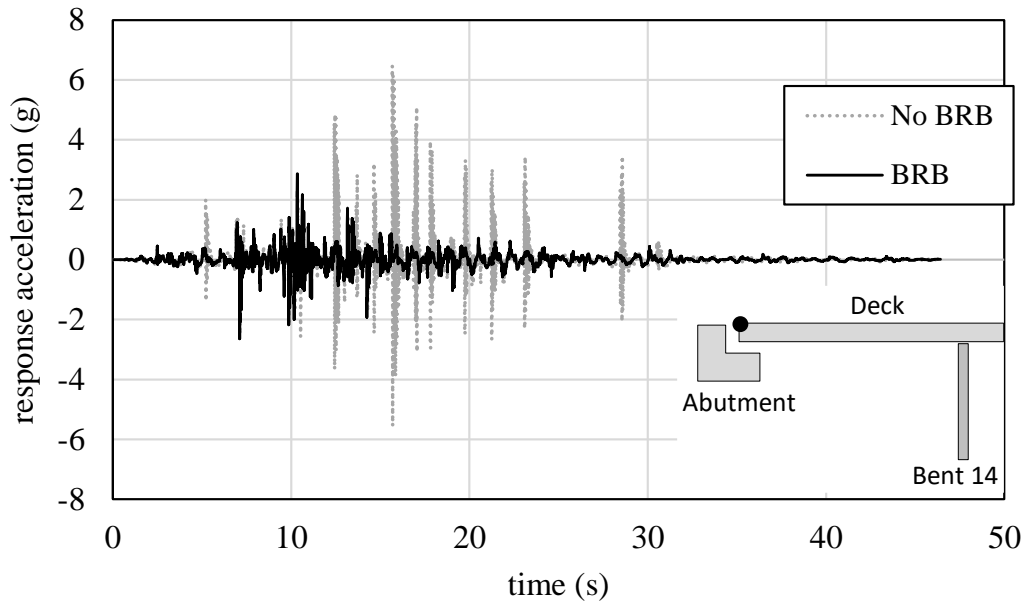


**Figure 4.26** Response acceleration time history of end of girder G1 of curved bridge for Irpenia, Italy, ground motion

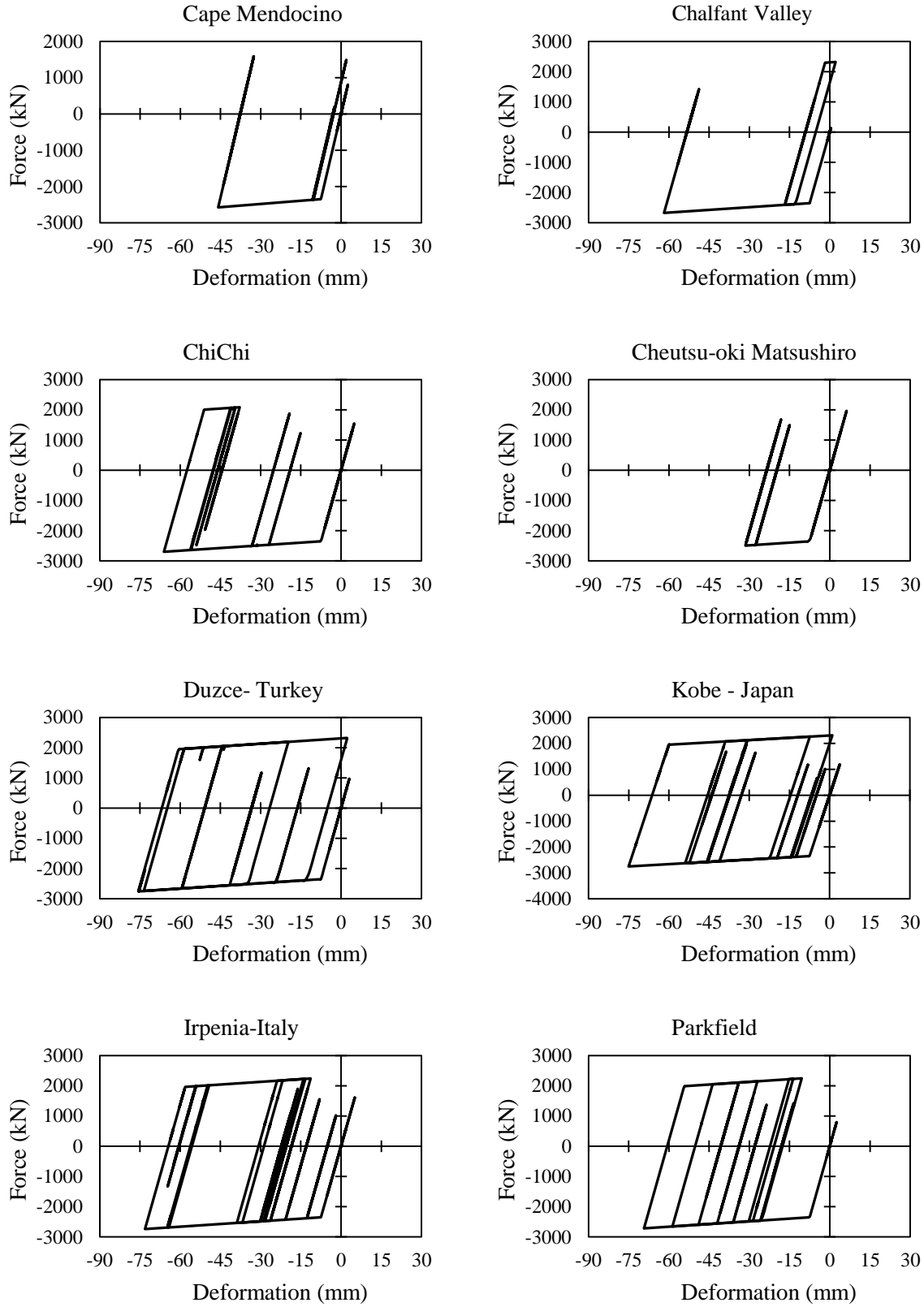


**Figure 4.27** Performance of longitudinal BRB at curved bridge abutment for scaled ground motions

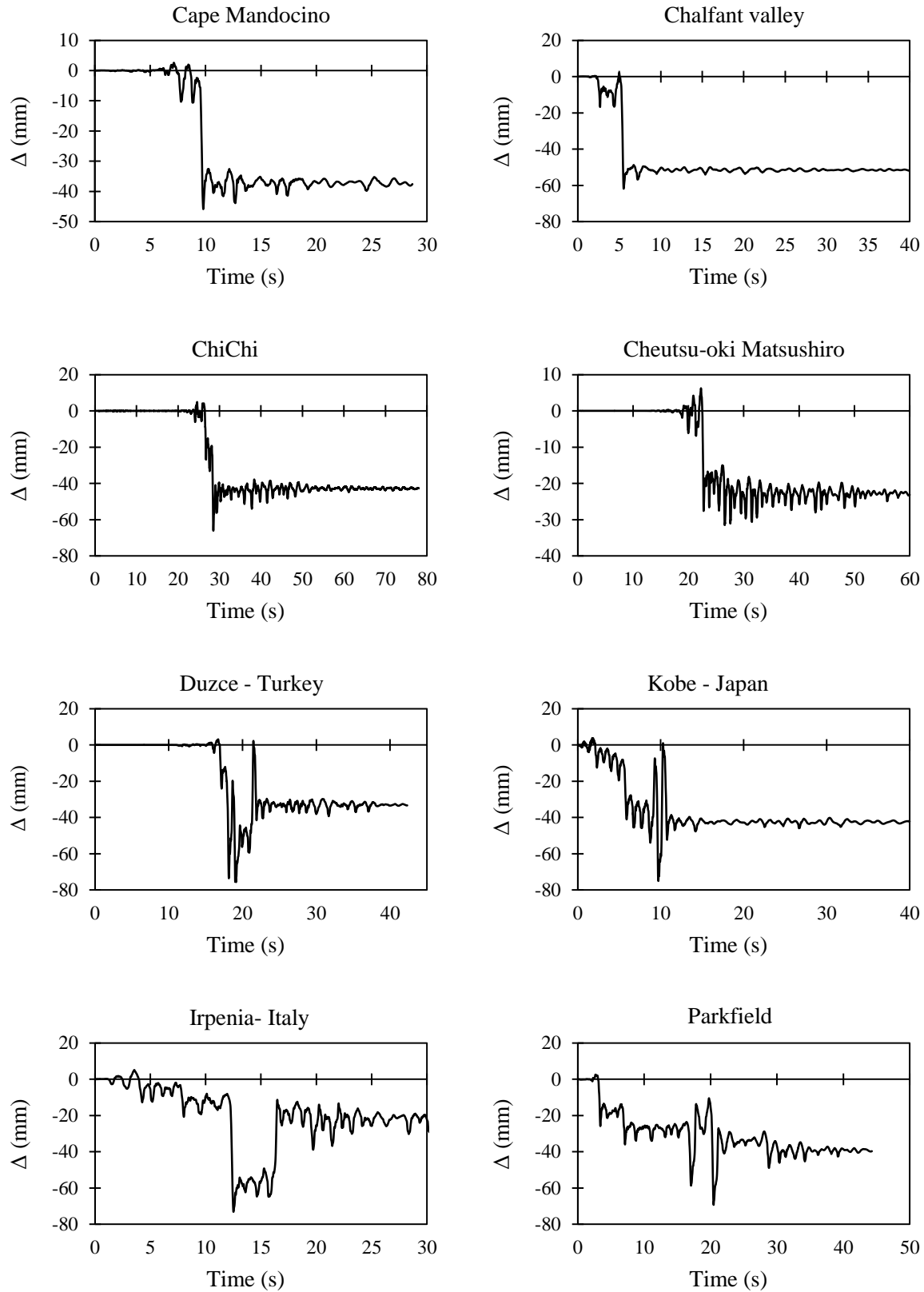


**Figure 4.28** Displacement time-history of longitudinal BRB at curved bridge abutment for scaled ground motions



To prevent pounding between concrete shear keys and steel shear keys attached to the diaphragm, additional BRBs were used in the lateral direction. As shown in Figure 4.22, lateral BRBs were connected to the bottom of the outer girders at one end and to the abutment wall at the other end. As it is not feasible to put lateral BRBs in a horizontal plane because of the girder in the middle (G2), it was decided to put these BRBs at some angle. To utilize most of the capacity of the BRBs, the angle should be low and hence an angle of  $30^\circ$  was selected. The adopted BRB backbone curve is shown in Figure 4.29. Analysis showed that low strength BRBs of a load capacity of 1350 kN and ultimate deformation capacity of 55 mm successfully prevented pounding between the shear keys. An incremental dynamic analysis (IDA) was performed with Kobe ground acceleration data (1980) to analyze the performance of lateral BRBs with increasing peak ground acceleration. Results of the IDA are presented in Figure 4.30.

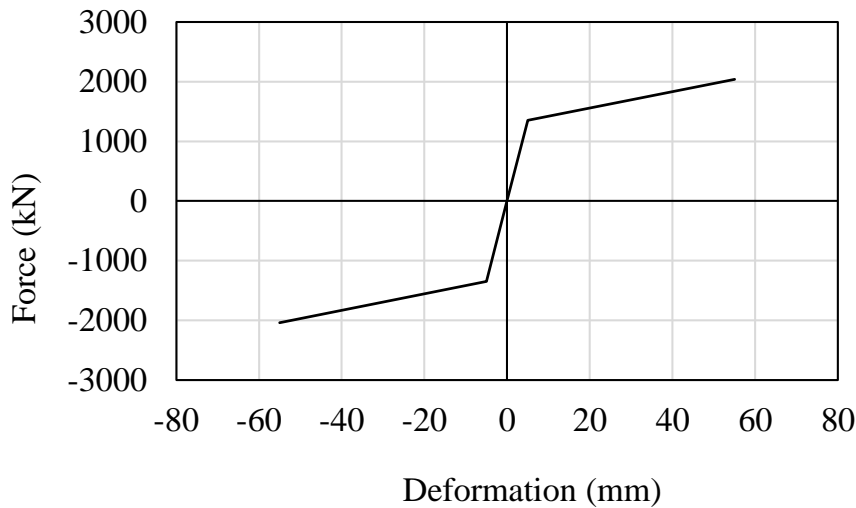


**Figure 4.29** Backbone curve for lateral BRBs for curved bridge retrofit

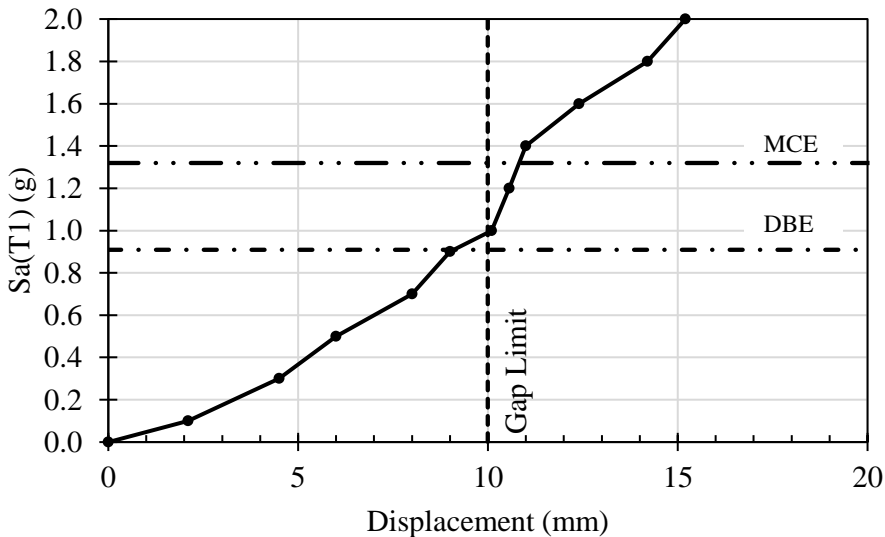


**Figure 4.30** Peak displacement of girder relative to concrete shear key for IDA of curved bridge using Kobe ground motion

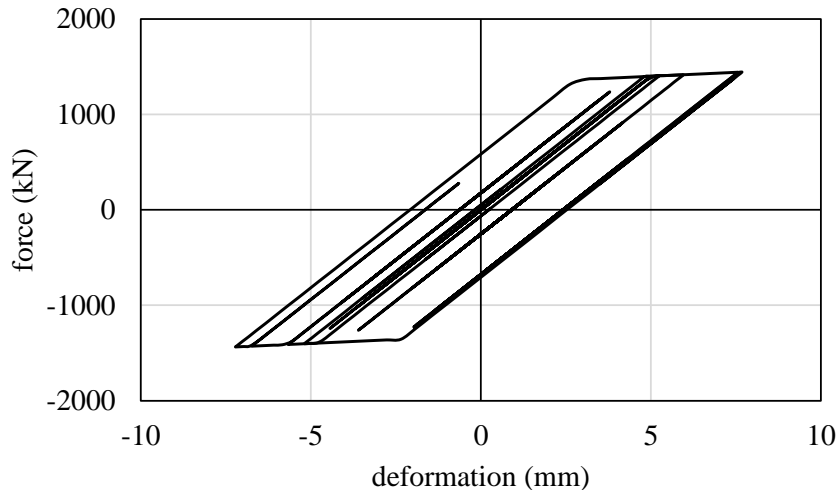


**Figure 4.31** Hysteresis of one of the lateral BRBs at curved bridge abutment for scaled Kobe ground motion

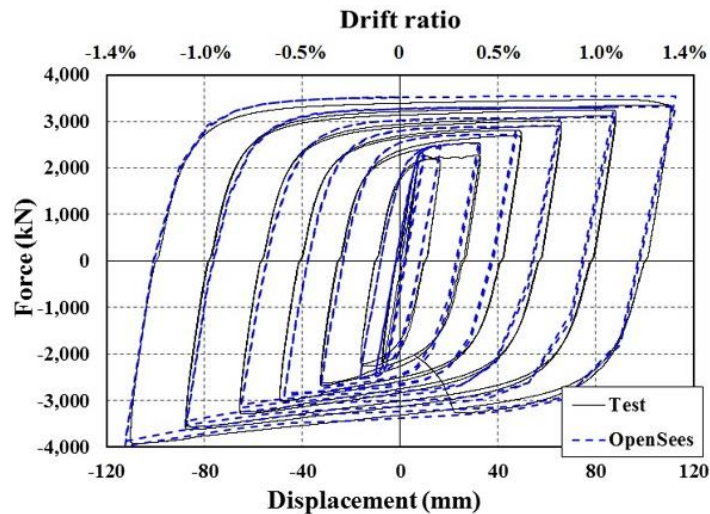
The negative deformation of lateral BRBs in the hysteresis curves is a measure of the relative displacement of the girder toward the concrete shear key. The hysteresis curves of one lateral BRB for the scaled Kobe ground motion (Figure 4.31) show that the peak deformation was 7.5 mm in compression and 7.7 mm in tension, which is less than the gap between concrete and steel shear keys (10 mm). This performance was consistent for all selected ground motions.

## 4.2 Analysis Results of the Skewed Bridge

### 4.2.1 Static Pushover Analysis

The three-dimensional (3D) column bent model was created in the structural analysis software OpenSees (McKenna 2014) to perform pushover analysis. The BRBs were assumed to be connected from the bottom column edge to the top of the middle column in each bent with a jacketing connection similar to that of Figure 2.10b. This connection design between the steel gusset plates and the concrete components may require the implementation of steel rings around the columns.

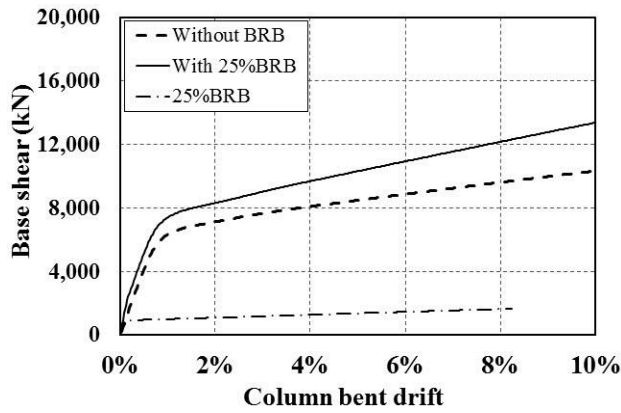
The bent columns were modeled as nonlinear force-based beam elements with fiber sections to capture the component's non-deteriorating inelastic response. The confined stress-strain concrete curve is based on Mander's model (Mander et al. 1988). This model does not include the cracking and crushing of concrete that eventually leads to material failure. Steel rebars were modeled using Steel02 material without consideration of softening, fracture, or compression buckling characteristics. Shear and torsional stiffness were also included using the section aggregator command in OpenSees. The column segment inserted into the cap beam was assumed to be a rigid link. The BRB brace system was modeled using a two-node link element. The BRB components were modeled utilizing the Menegotto-Pinto (Steel02) material in OpenSees (McKenna 2014). This model includes isotropic and kinematic hardening when using Pinching4 material, and was calibrated using experimental test results from similar BRB components (Xu 2016), as seen in Figure 4.32.



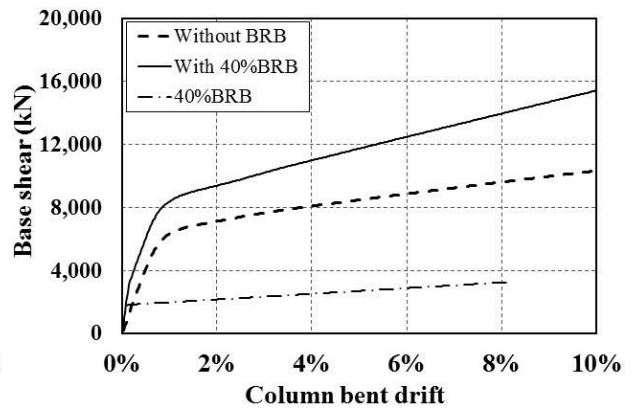
**Figure 4.32** Calibration of BRB model using experimental results from Xu (2016)

Figure 4.33 shows the effect of adding BRBs to column bents on the seismic performance of the bent. The BRB are designed as structural fuses; consequently, the yield displacements in all types of BRBs are smaller than those of column bents, which guarantees BRBs will yield prior to major bent damage. Early yielding may lead to a higher BRB hysteretic behavior, dissipating more seismic energy. However, a BRB with low capacity could result in earlier failure, causing unreparable damages to the bent structure (e.g., occurrence of plastic hinge, yielding of column reinforcement).

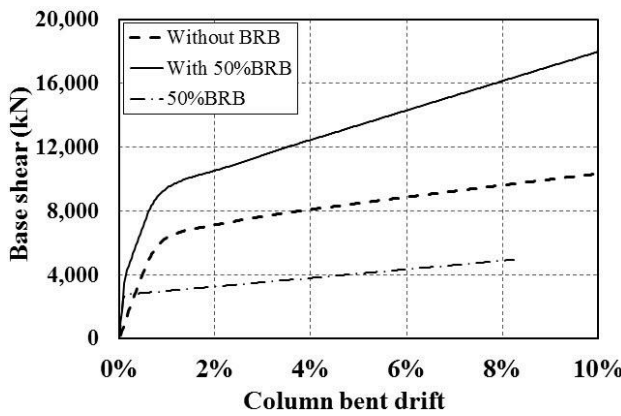
For the optimized BRB designs (i.e., 50% and 60% of the design seismic forces, Figures 4.33c and 4.33d), the BRB capacity is close to that of the retrofitted bents. Retrofit failure is postponed, and the additional BRB stiffness improves with respect to that of DS-25BRB and DS-40BRB cases. But too much stiffness from the retrofit BRB could make BRB nonlinearity hardly develop and most of the seismic energy is dissipated by the RC bent structure instead of BRBs (Figures 4.33e and 4.34).



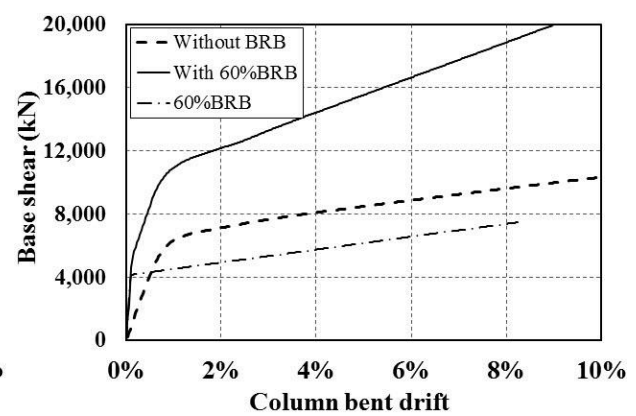
(a)



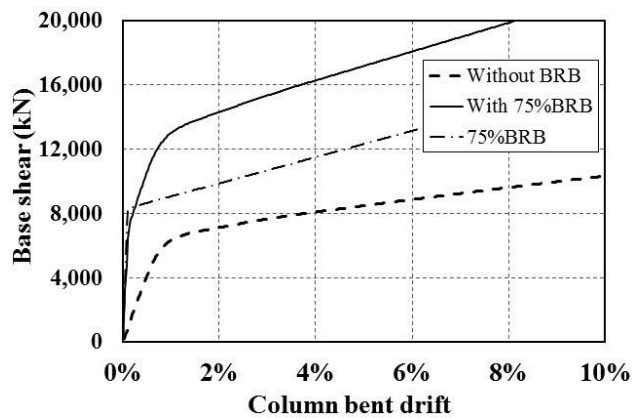
(b)



(c)



(d)



(e)

**Figure 4.33** Pushover curves of columns bents retrofitted with BRBs: (a) DS-25BRB; (b) DS-40BRB; (c) DS-50BRB; (d) DS-60BRB; (e) DS-75BRB

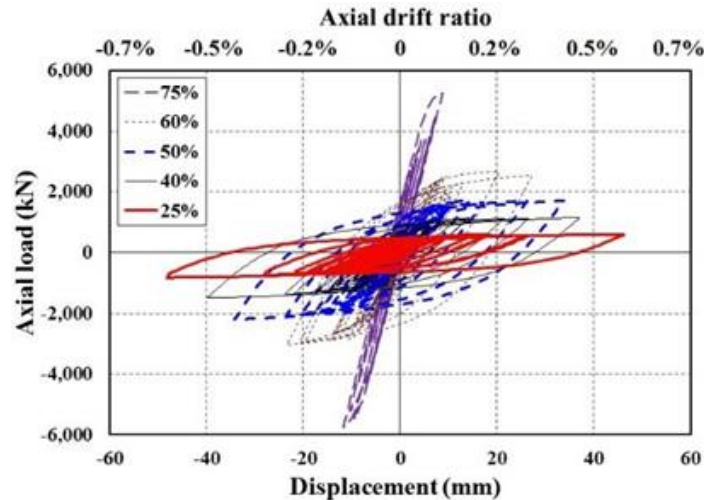


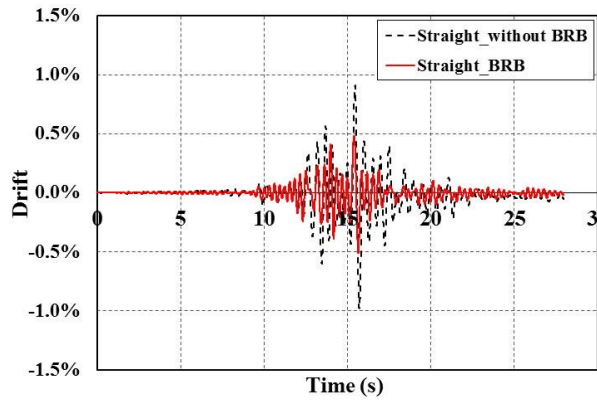
Figure 4.34 BRB hysteretic response for the three dual systems

## 4.2.2 Results of Skewed Bridge Performance Analysis

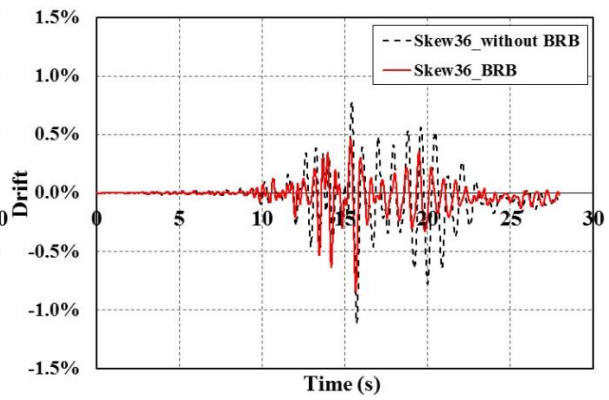
Figure 4.35a shows the transverse drift at the top of the bent column for the original, retrofitted straight bridge, and skewed bridge. As observed, the addition of BRBs reduces the bent drift about 50% in both straight and skewed cases (Figure 4.34). Also, although the original skewed bridge has lower demand in the transverse direction than the straight one, it reaches a drift 30% larger because of skewness effects, such as deck rotation. The combined ground motion effects from longitudinal and transverse direction change the frequency content in the skewed bridge's response (Figure 4.35a2).

Moreover, BRB bent drifts are reduced in spite of the increased stiffness of the bent, redistributing forces between the bents and the abutment systems. For instance, the total shear transverse demand in the original straight bridge was 34,450 kN (7,760 kips) under Landers earthquake, subdivided into 21,220 kN (4,780 kips) on the shear keys and 13,230 kN (2,980 kips) on the column bents. After the retrofit, the total shear demand decreased to 26,360 kN (5,940 kips), indicating BRB components dissipated about 23% energy of total shear demand, but this reduction was not evenly distributed between the shear keys and column bents. The shear demands decreased in the shear keys to 9,210 kN (2,070 kips), while the shear demand of the column bents actually increased by 1,120 kN (250 kips), or about 4%. The combination of ground motion effects in the skew direction increases the seismic demand at abutments and bents. As expected, seismic demands in the abutment and bent increase about 10% (Figures 4.35b and 4.35c). Regarding the abutment shear keys, Figure 4.35c shows these components are at the brink of failure in the original bridge under the evaluated seismic event. If the shear keys fail, the deck translational displacements in the transverse direction may cause the bridge deck to unseat. The shear keys' performance of the retrofitted bridge, on the other hand, is almost linear, due to a reduction in the maximum force of almost 60%. Therefore, the skew key could survive by implementing BRBs in the bridge, avoiding deck unseating.

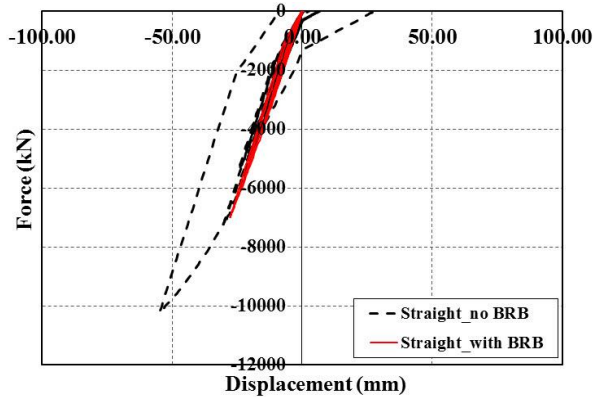
The benefits of the BRB retrofit are also present in other output parameters. Figures 4.35d and 4.35e indicate that concrete and steel strains at the top of the central column are also reduced in the retrofitted schemes. However, because of the increase in the bent stiffness, the shear forces in the edge columns increase 1.5 times (Figure 4.35c). If these shear forces are excessive, the design may be changed, and the gusset plate separated from the column to transfer the lateral forces directly to the foundation (Dusicka et al. 2015).



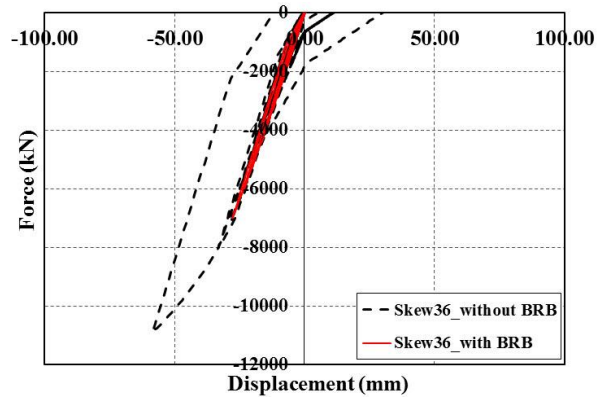
(a1)



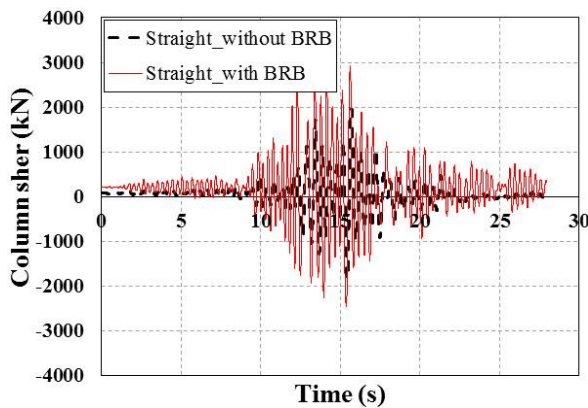
(a2)



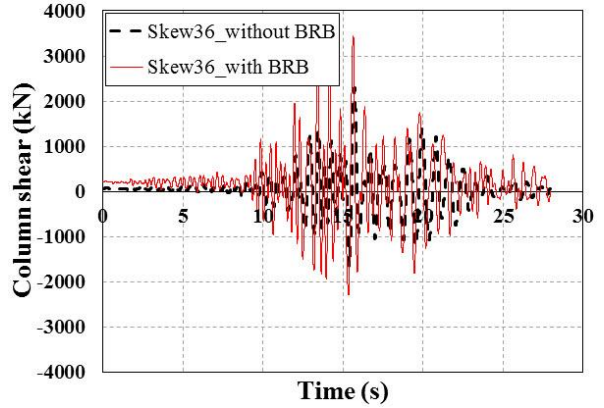
(b1)



(b2)



(c1)



(c2)

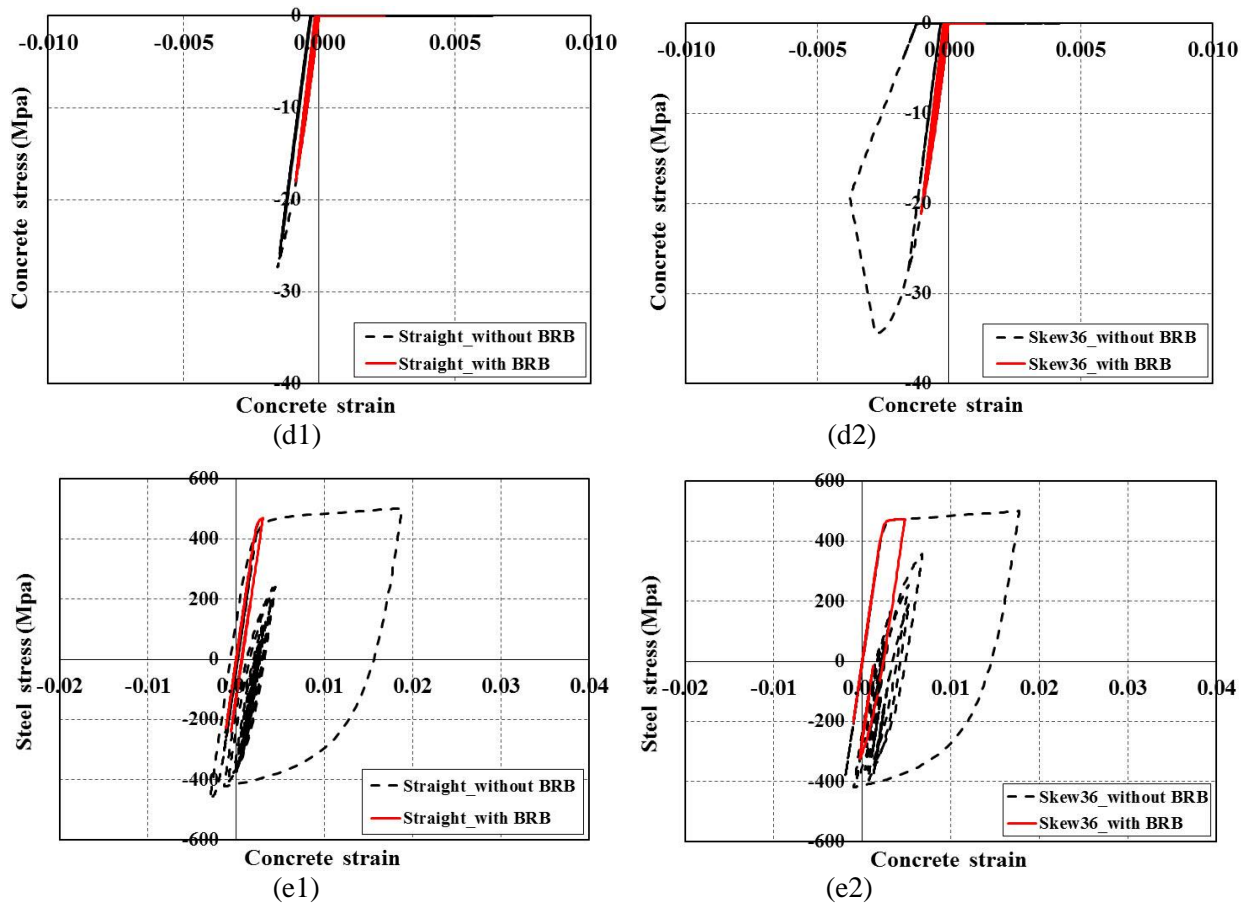


**Figure 4.35** Responses of straight bridge under Landers 1992 Earthquake, 23 Coolwater Station: (a1, a2) Column bent drift; (b1, b2) Abutment transverse direction force-displacement; (c1, c2) Column shear force; (d1, d2) Column concrete stress-strain; (e1, e2) Column steel stress-strain

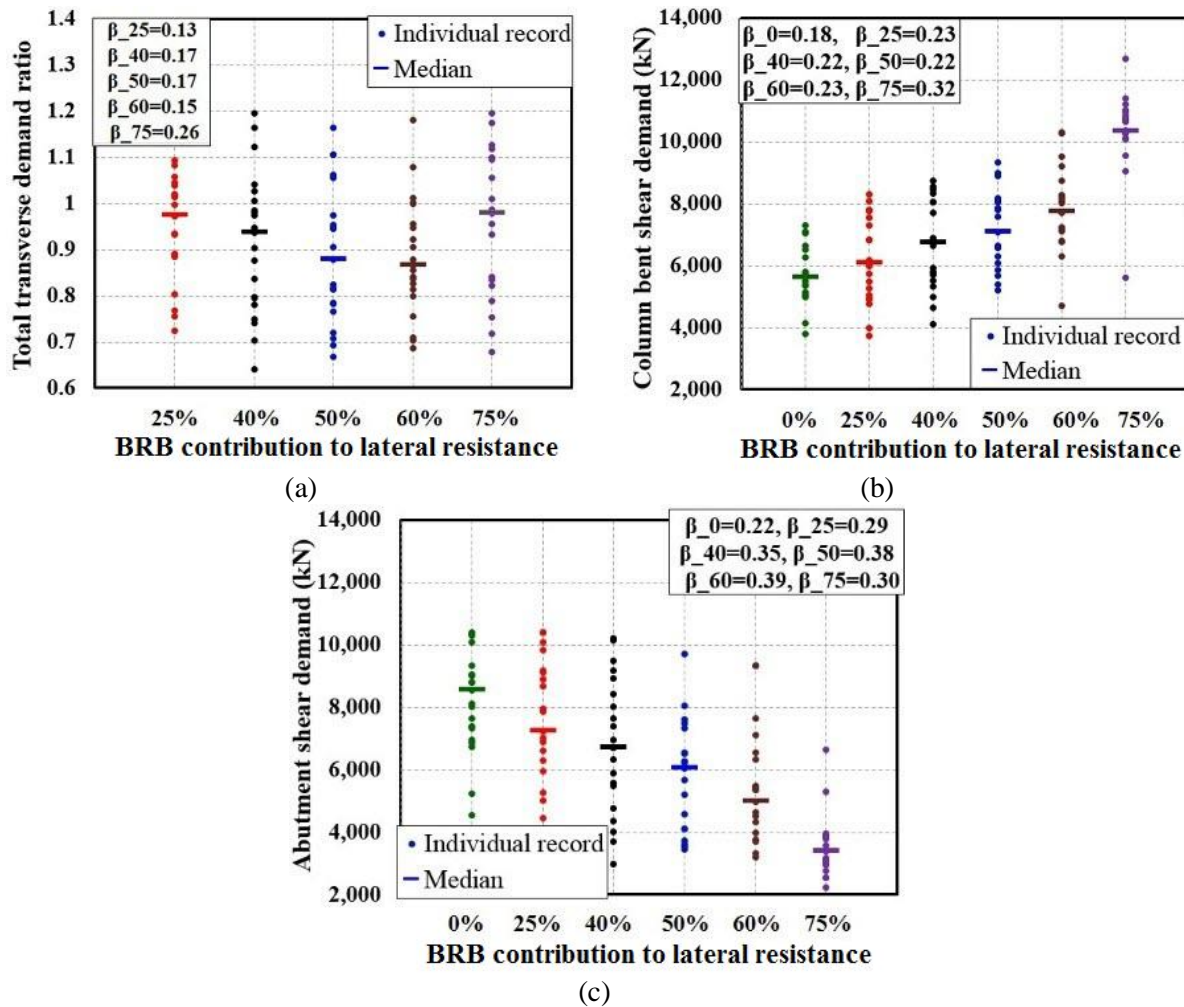
### 4.2.3 Results of BRB Core Optimization Under ASCE 41-13 Method

Figure 4.34 shows the hysteretic response of the five dual straight bridge systems with different BRB characteristics under the MCE level for Landers 1992 ground motion. As observed, the reduction in the BRB core area reduces the stiffness and strength of BRB dual systems. Also, all BRBs have drift demands significantly smaller than the minimum 2% axial drift ratio used in BRB qualification tests. The smaller axial drifts, observed in the DS-75BRB system in Figure 4.34, are due to the large core plate area inhibiting BRB nonlinear behavior.

Figure 4.36a shows the ratio of total demand of the retrofitted system to the total demand of the original straight bridge for the five evaluated dual systems for the 21 far-field FEMA P695 records. The DS-50BRB has the largest demand reduction, indicating that this system optimizes the increase in BRB hysteretic energy  $E_{H, BRB}$  with respect to the bent's energy increase. In this case, about 11% of the demand in the original system is dissipated through nonlinear hysteretic behavior of BRBs. However, this decrease in lateral demands is not uniform. For example, Figure 4.36b shows the total shear demands of bent columns for the original bridge (i.e., 0% BRB capacity), and the five dual systems. As observed, the shear loads in the bents increase as the core area of the BRBs increases, because the bent-to-abutment stiffness ratio becomes larger. For DS-75BRB, the increase on the median shear demand is about 87% with respect to that of the original bridge. Moreover, for the DS-75BRB system, the shear demand on the

exterior columns exceeds the component's shear strength capacity. Conversely, in the case of the abutment system (i.e., shear keys, piles, and wingwalls), the shear demands decrease for larger BRB sections (Figure 4.36c).

The retrofit with BRBs decreases the drift of the bent due to the additional stiffness. Figure 4.37a shows the bent inter-story drifts for the original and retrofitted bridges. Note that the median drifts of the original bridge are more than 50% larger than the operational drift limit. The system with the smallest BRB core area that meets the median drift operational limit is DS-50BRB. The retrofit also prevents the occurrence of plastic hinges at the top of the central column by increasing the moment capacity-to-demand ratios. As shown in Figure 4.37b, this median moment capacity to demand ratio was practically 1.0 for the original bridge, and increased almost 70% for the DS-60BRB bridge because part of the energy that was being dissipated in the plastic hinge ( $E_{H,Bent}$ ) was transferred to the BRBs ( $E_{H,BRB}$ ).



**Figure 4.36** Comparison of different BRB designs for transverse global responses: (a) Ratio of total demand of retrofitted system to total demand of original system; (b) Column bent shear demand; (c) Abutment shear demand



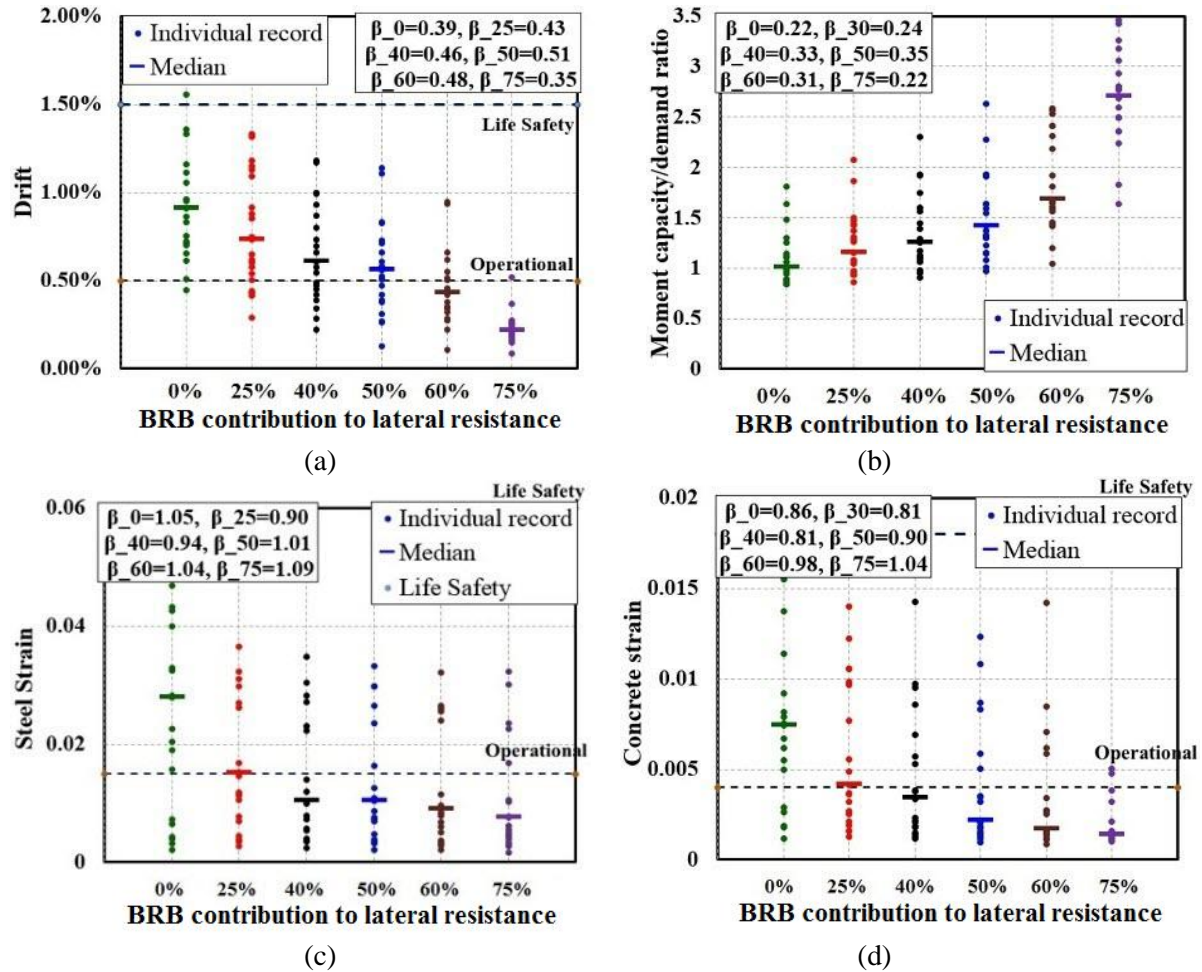


**Figure 3.47** Comparison of different BRB designs for column bent responses: (a) Drift; (b) Moment capacity-to-demand ratio; (c) Concrete strain; and (d) Steel strain

Regarding the strains at the top of the RC column, the concrete compressive strain decreased up to 50% when the bents were retrofitted with BRBs (Figure 4.37c). On the other hand, the median steel reinforcement strain marginally improved for the retrofitted bridges (Figure 4.37d). Because of the orthogonality of the longitudinal deck and bent axis in straight bridges, BRBs had a negligible effect at the abutment longitudinal direction. According to the above results, the DS-50BRB and DS-60BRB systems optimize the structural response parameters, reducing drifts, steel, and concrete strains, with respect to those of the original system. At the same time, these dual systems do not lead to a large increase on column shear demands.

#### 4.2.4 Results of Parametric Analysis under ASCE 41-06 Method

Figure 4.38 shows the total shear demand of the straight and 36° skewed bridges for 11 GMs incidence angles (0°, 18°, 36°, 54°, 72°, 90°, 108°, 126°, 144°, 162°, and 180°) in transverse/skew directions. The 90° incidence angle creates minimum demands in each case, because under such conditions the minor GM component is closest to the transverse/skew direction of bridges. Data in each column show the total shear demands of individual records for certain incidence angle (vertical left axis), while the standard deviation of log results ( $\beta$ ) for each incidence angle is shown with triangle marks (see right vertical axis in Figure 4.38). The variation of critical excitation angles mentioned by Bisadi and Head (2011) is restricted to

some extent since the RTR variability is constrained in such a way that both elastic and inelastic behavior in transverse and longitudinal directions were included in the scaled method.

A comparison of Figures 4.38a to 4.38c shows that the median demand of skewed bridges is increased by 8% to 10% under different incidence angles. After being retrofitted with BRBs, the seismic energy is partly dissipated through BRB hysteretic behavior, decreasing the structural damage. When the GMs are input under high demand angles (i.e., 0° and 18°), BRBs can dissipate more seismic energy by having larger inelastic excursions. Considering both straight and skewed bridges, the use of BRBs dissipates 20% to 25% seismic shear demands through hysteretic behavior, independently of the GM incidence angle.

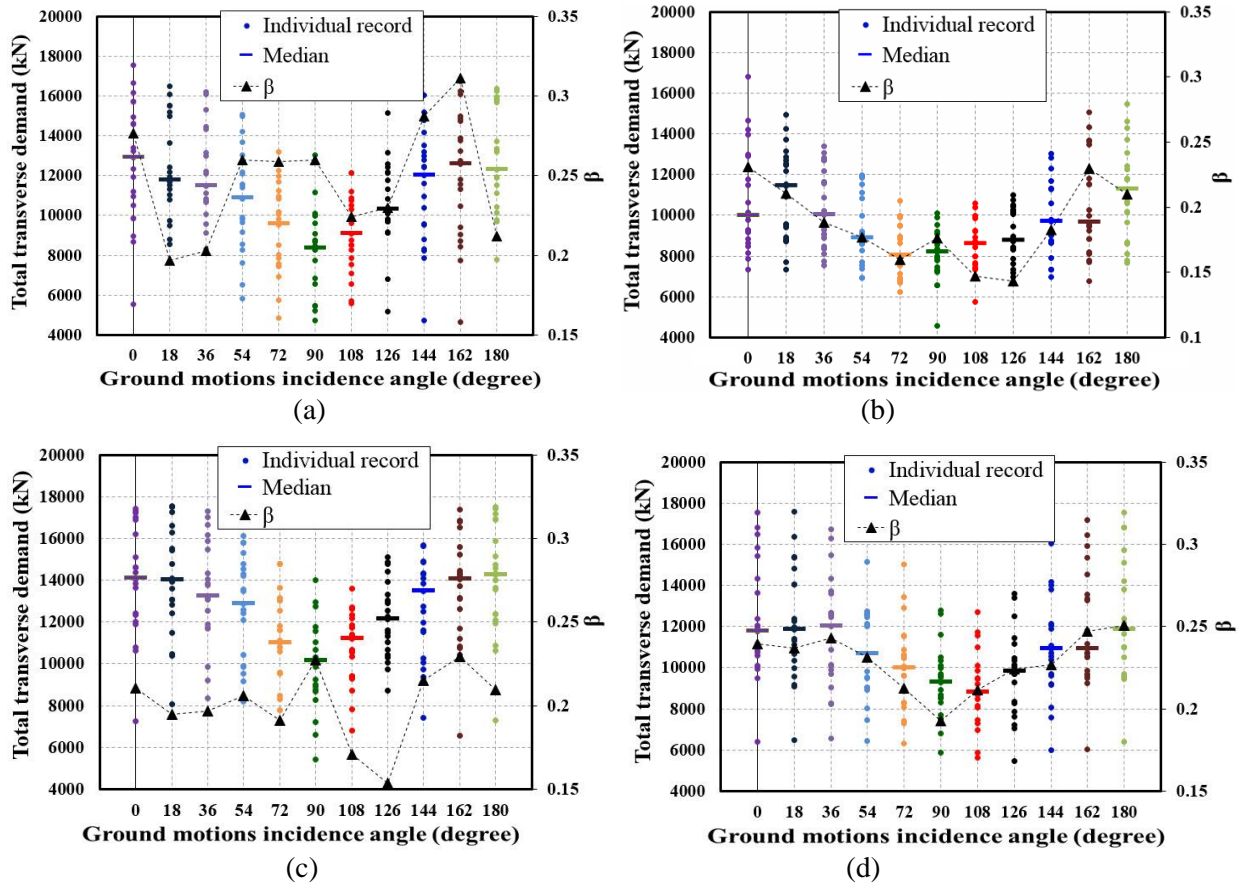


**Figure 4.38** Comparison of total demand of straight and skewed bridges under 10 incidence angles: (a) Original straight bridge; (b) straight bridge retrofitted with BRB; (c) Original 36° skewed bridge; (d) 36° skewed bridge retrofitted with BRB

As mentioned by Wang et al. (2016), the implementation of BRBs leads to more seismic energy being redirected to column bents. The skew effect will create greater demands at column bents due to rotational effects. The additional stiffness from BRB can also decrease the difference in the response caused by the ground motion incidence angle (Figure 3.32).

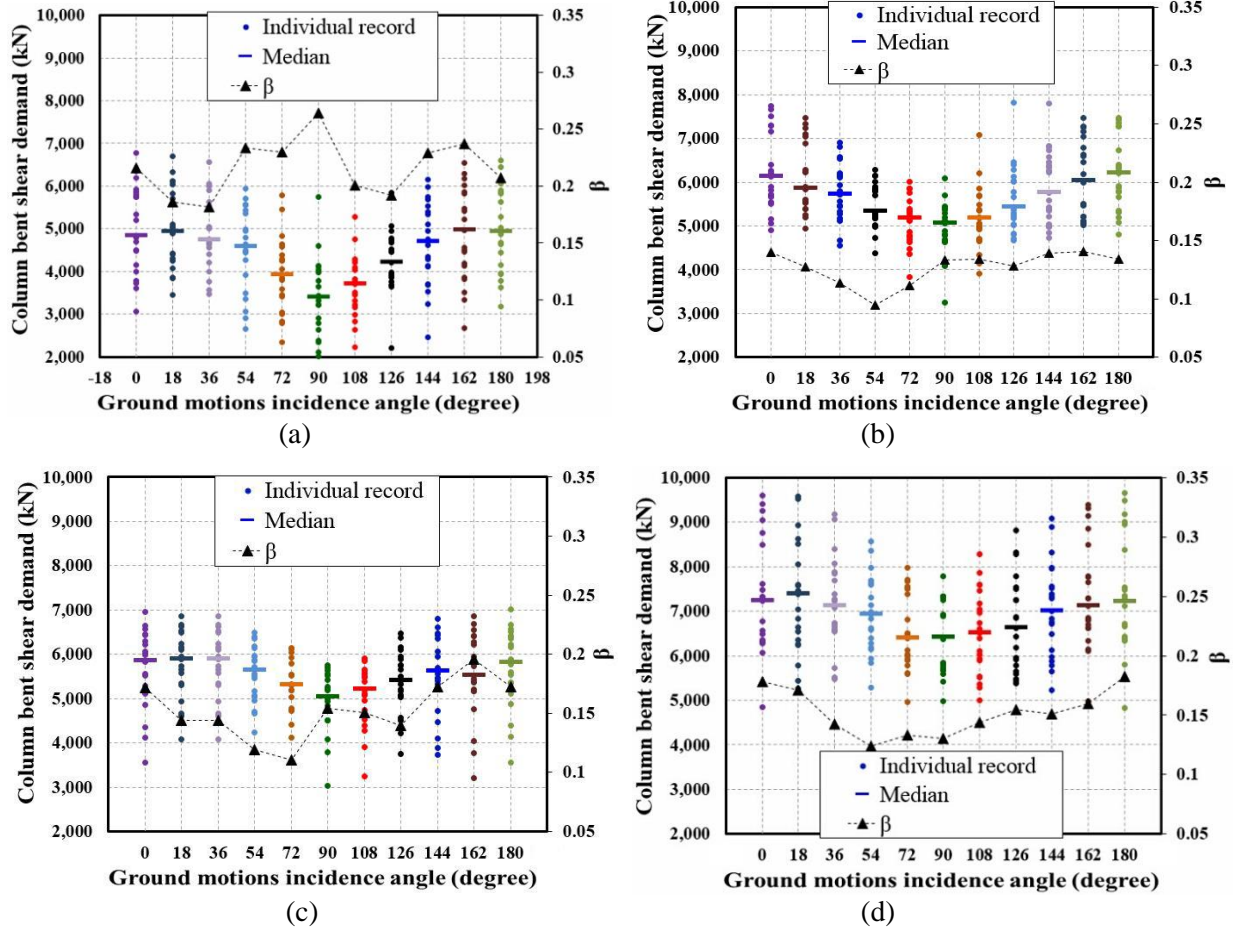


**Figure 4.39** Comparison of bent shear of straight and skewed bridges under 10 incidence angles: (a) Original straight bridge; (b) straight bridge retrofitted with BRB; (c) Original 36° skewed bridge; (d) 36° skewed bridge retrofitted with BRB

As noticed, transverse shear demands of straight bridges show a ‘V’ shape with incidence angle varying from 0° to 180°, while the shear demands in skew bridges are flatter (Figure 4.39a). This phenomenon can be traced from the input seismic demand represented by the combination of PGAs in skew and Y direction, as GMs rotate (Figure 4.40). In Figure 4.40, input PGAs also exhibit a ‘V’ shape on the response seismic shear demand under various incidence angles. This phenomenon may be attributed to the scaling of the SRSS spectrum of both horizontal directions. Although the maximum input seismic energy is the same for skew and transverse Y direction, the latter one could have larger response shear demand due to the combined effects

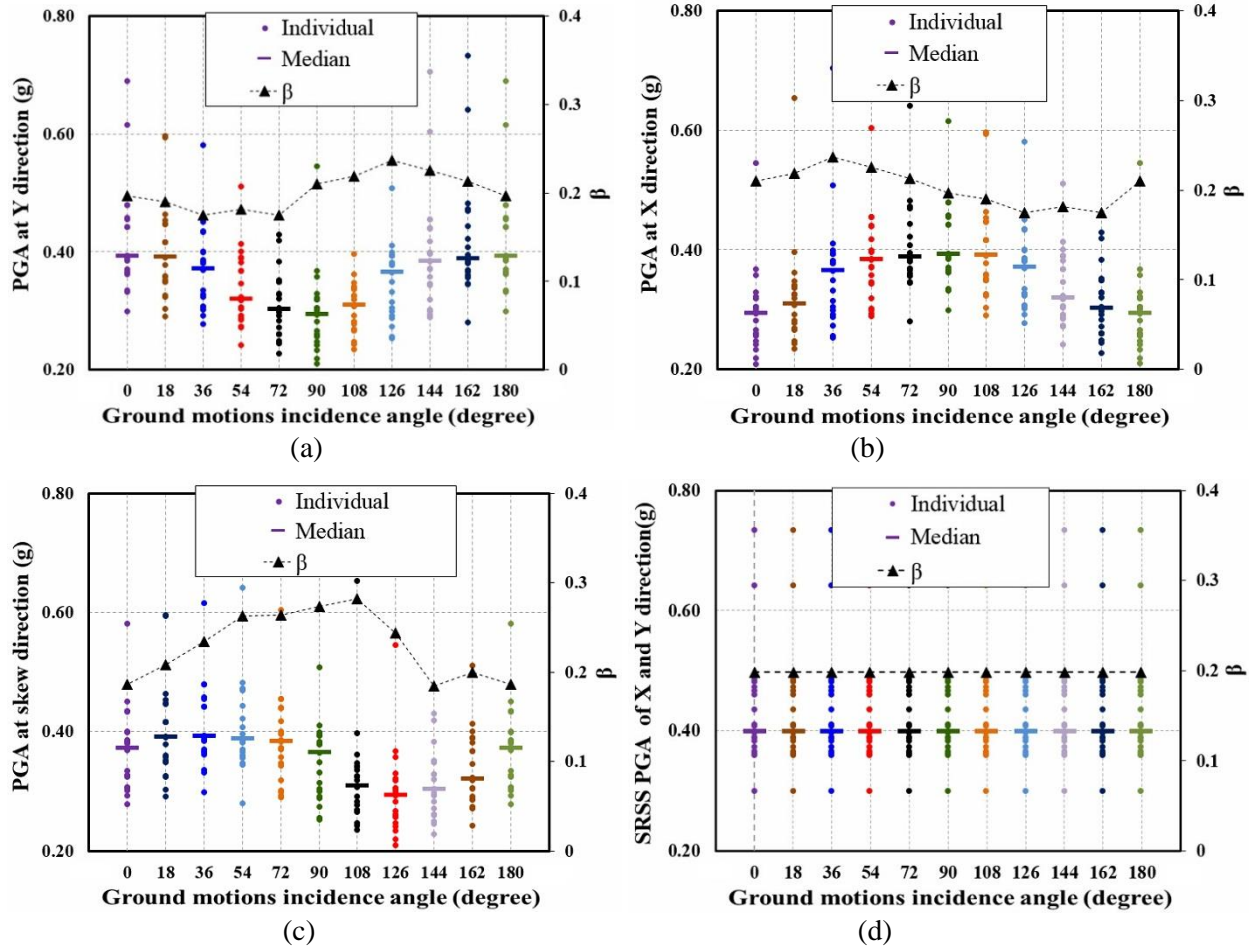


**Figure 4.40** Combinational PGA: (a) at transverse Y direction; (b) at longitudinal X direction; (c) at skew direction; (d) SRSS PGA of both longitudinal and transverse direction referring to Figure 3.32

The input PGA was kept constant in the Y direction, while GMs were rotated in Figure 4.40b. The critical direction of input in Y direction is close to  $18^\circ$  and  $144^\circ$  while either major principal GM component or the minor one close to the skewed angle. The PGA values in the skew direction indicate that the GM incidence has less influence on the skew bridge than on straight bridge response. This may be attributed to the skewed direction being close to the SRSS values of X and Y direction that have constant distribution pattern regardless of different incidence angles (Figure 4.40d).

The shear keys are weak in most of the damaged skewed bridges because the entire deck twisted or rotated about a vertical axis representing the center of stiffness, as seen in Figure 3.32 (Yashinsky et al. 2010). The rotation creates additional seismic demands for skewed bridges. A comparison of Figures 4.41a and 4.41c indicates that this effect is independent of the GM direction. Higher demands could lead to deck unseating if the shear key is heavily damaged. At the same time, uneven passive soil forces and potential pounding forces may create rotational effects increasing shear key forces. Parts of seismic energy may be transferred to the column bent due to the additional BRB stiffness and its corresponding hysteretic behavior.

BRBs have negligible effects on the longitudinal abutment responses in straight bridge cases. In the case of the longitudinal response, incidence angles around  $90^\circ$  have larger effects because the major GM's component is close to the longitudinal direction under these cases (Figure 4.42). The potential deck rotations could induce the energy transition from longitudinal direction to transverse direction, increasing the vulnerability of the shear key. Finally, the unequal longitudinal response forces occur as measured in previous experimental tests (Rollins and Jessee 2012).

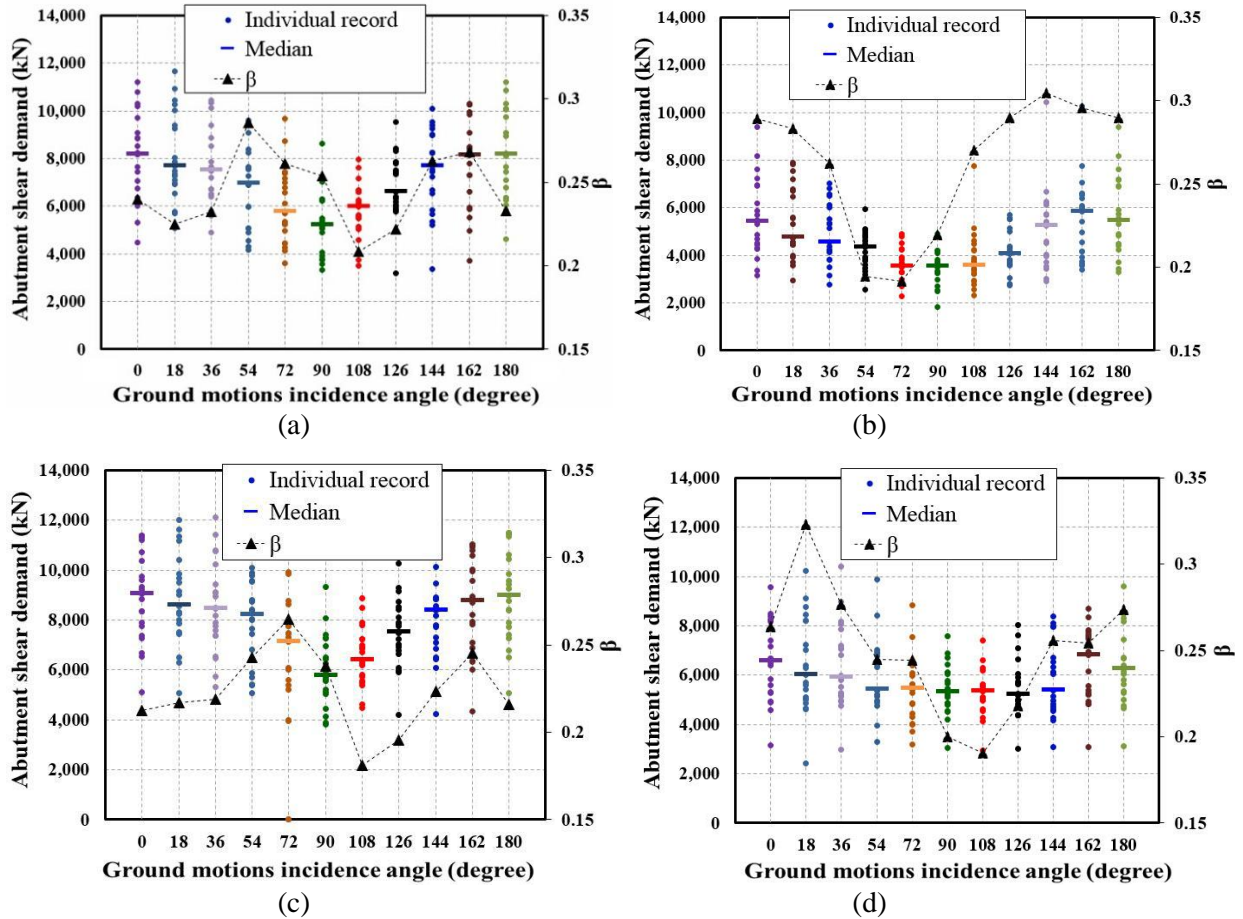


**Figure 4.41** Comparison of abutment transverse shear of straight and skewed bridges under 10 incidence angles: (a) Original straight bridge; (b) straight bridge retrofitted with BRB; (c) Original  $36^\circ$  skewed bridge; (d)  $36^\circ$  skewed bridge retrofitted with BRB

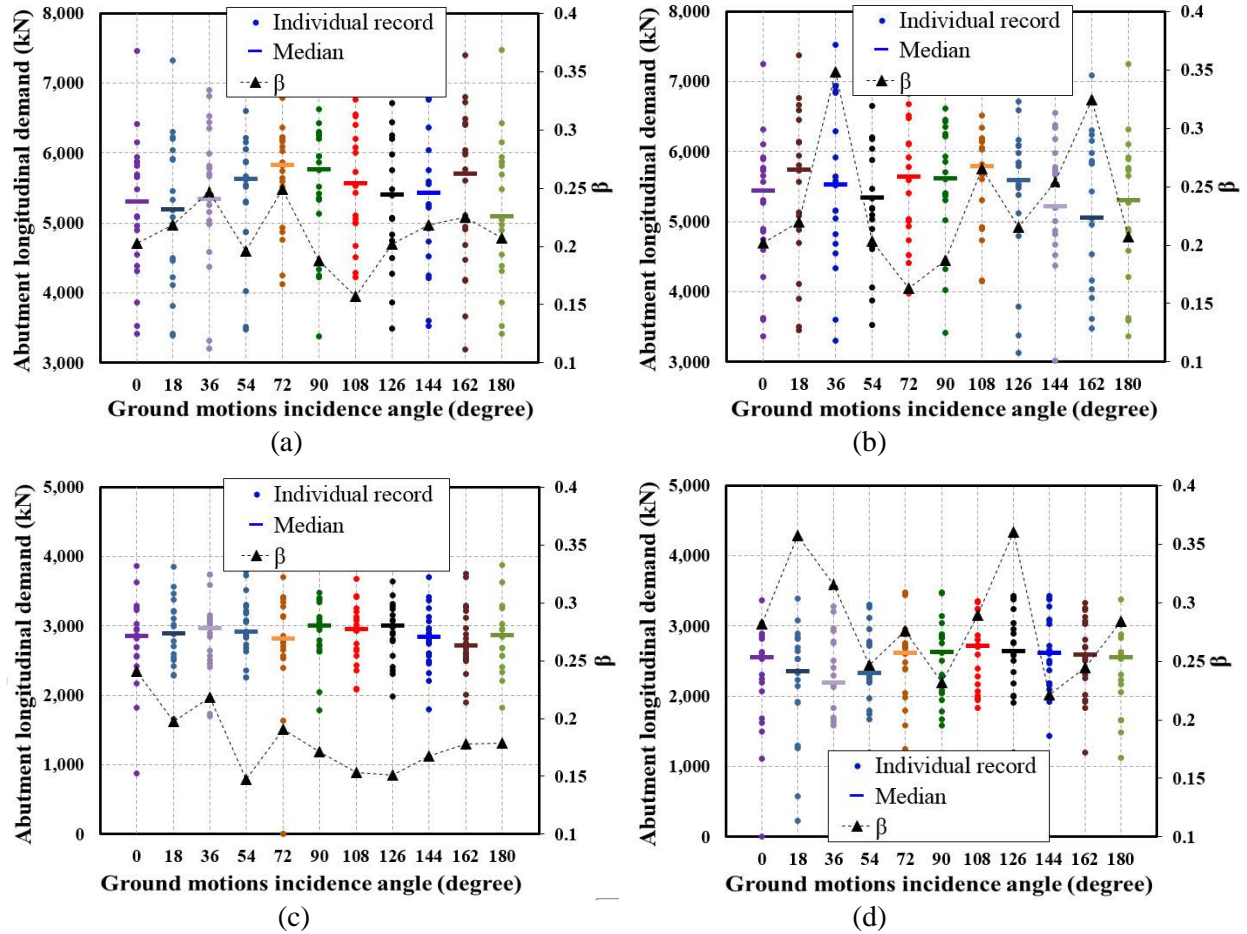


**Figure 4.42** Comparison of abutment longitudinal pounding force of straight and skewed bridges under 10 incidence angles: (a) Original straight bridge; (b) straight bridge retrofitted with BRB; (c) Original  $36^\circ$  skewed bridge; (d)  $36^\circ$  skewed bridge retrofitted with BRB

Significant rotation is observed in the absence of larger bent drifts for skewed bridges (Figure 4.43). The median drifts of the skewed bridges are more than 50% larger than the operational drift limit, and some cases are even above the life safety limit. Drifts in transverse Y direction of the straight bridge reflect the input energy in Y direction (Figure 4.43b), while the skew direction can capture the combined PGAs at Figure 4.43c with a “flat” distribution for different incidence angles. The retrofitted skewed and straight bridges show drifts below or at least close to the operational limit, with maximum drifts decreasing by 50%. The difference in responses for different GMs’ incidence angles is smaller for retrofitted bridges because part of the seismic energy is absorbed by the BRB components.

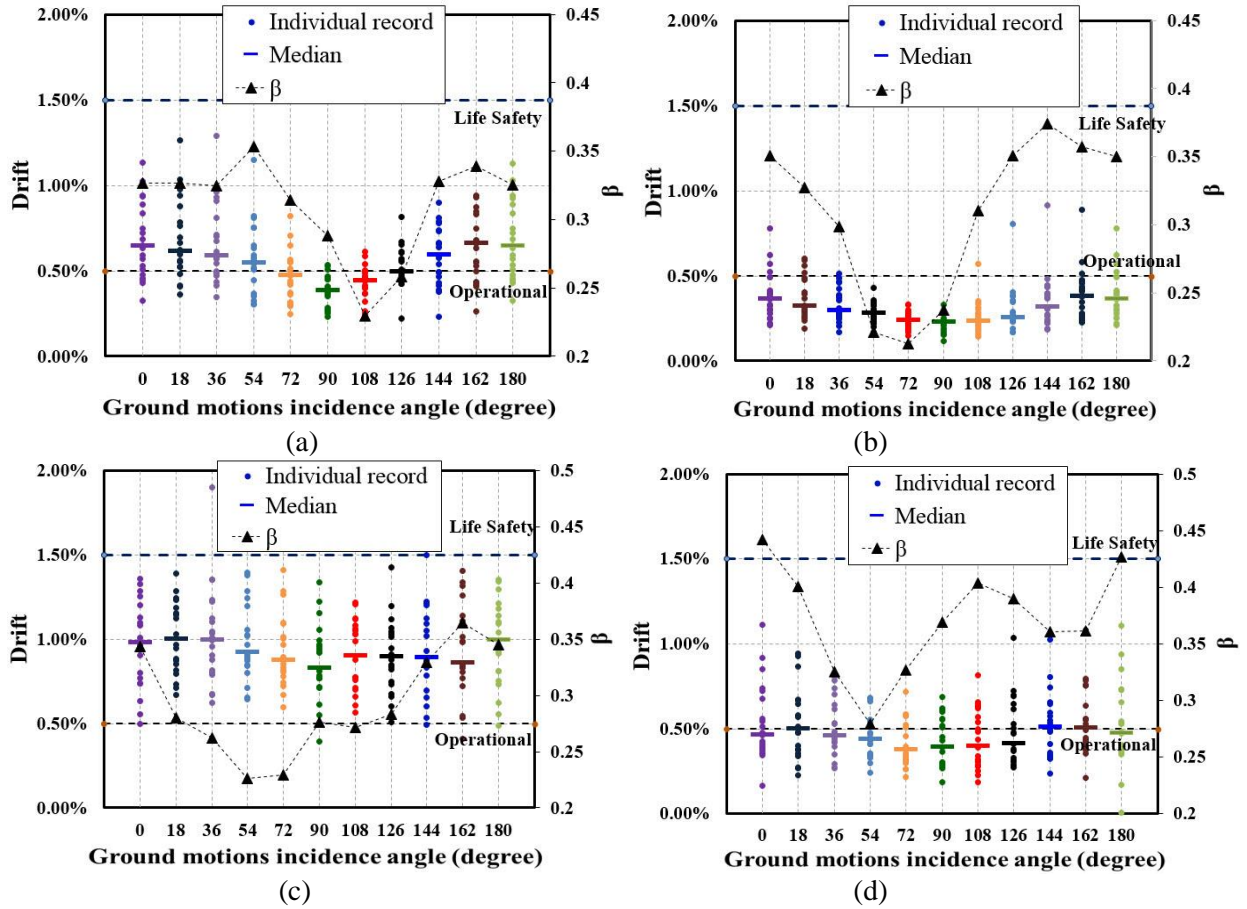


**Figure 4.43** Comparison of bent drift of straight and skewed bridges under 10 incidence angles:  
 (a) Original straight bridge; (b) straight bridge retrofitted with BRB; (c) Original 36° skewed bridge; (d) 36° skewed bridge retrofitted with BRB

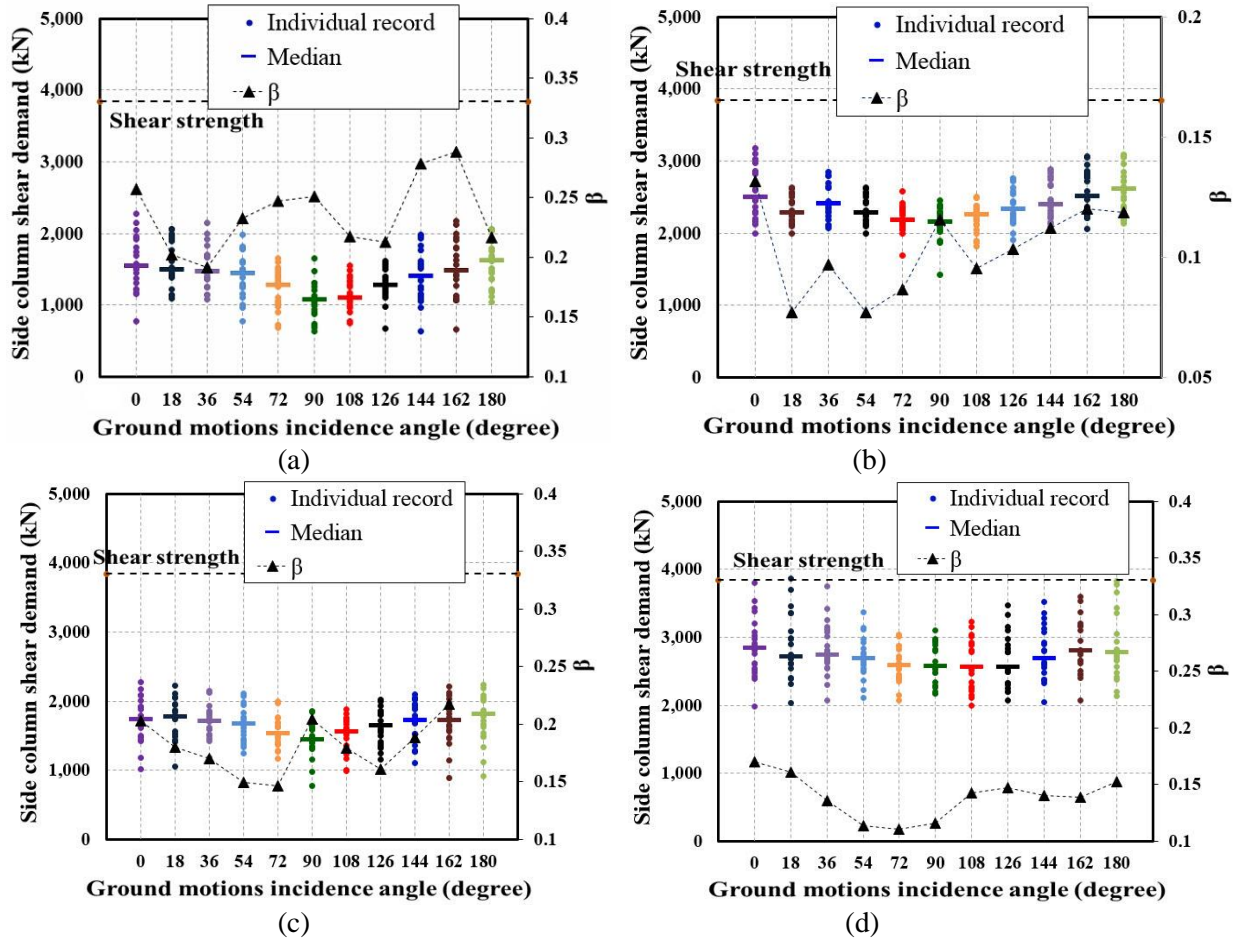


**Figure 4.44** Comparison of side column shear of straight and skewed bridges under 10 incidence angles: (a) Original straight bridge; (b) straight bridge retrofitted with BRB; (c) Original 36° skewed bridge; (d) 36° skewed bridge retrofitted with BRB

The shear demands of side columns in bridge bents are improved by the stiffness of BRB components. The side columns are exposed to higher demands for retrofitted bridges, but even in the worst case scenario (Figure 4.44d) the shear demands of side columns are still below the shear strength (Figure 2.7). As in the case of drifts, the influence of the incidence angle is smaller for straight and skewed bridges in the retrofitted bridges.

Regarding the strains at the RC columns, critical responses along skew direction from different incidence angles follow the drift response pattern. For straight bridges, the critical angle is close to 0° when the major GM component is closer to the transverse direction (Figure 4.45a). When the major GM component is close to the skew direction for skewed bridges (i.e., incidence angle is 144°), the GMs lead to more bent column damage (Figure 4.45c). However, when BRBs are implemented in straight and skewed BRB as a seismic fuse, most of the seismic energy is dissipated by BRB components. Figures 4.45b and 4.45d show that the mean response strain of all incidence angles decreases about 50% for straight and skewed bridges. The incidence angle effect decreases due to the large additional stiffness and hysteretic energy dissipation ability of BRBs. BRBs improve the concrete performance in skewed bridges, considering straight bridge bents are exposed to lower seismic demands. For retrofitted bridges, however, the concrete strain for straight and skewed bridge is similar.



Steel strain is also more vulnerable for reinforcement in columns when the GM incidence angle is close to 0° (Figure 4.46). Skewness would cause more damage at the column reinforcement of original skewed bridges. In general, BRB retrofit decreases the reinforcement steel strain for straight and skewed bridges. The moment capacity-to-demand ratio at the top of column exhibits a different pattern when compared to other demand parameters, exhibiting higher values at the incidence angle of 90°. One of the BRB benefits is the delay of the plastic hinge at the column to avoid further structural damage. As seen in Figures 4.47b and 4.47d, BRBs improve straight and skewed bridges' performance without developing plastic hinges at the top of columns.

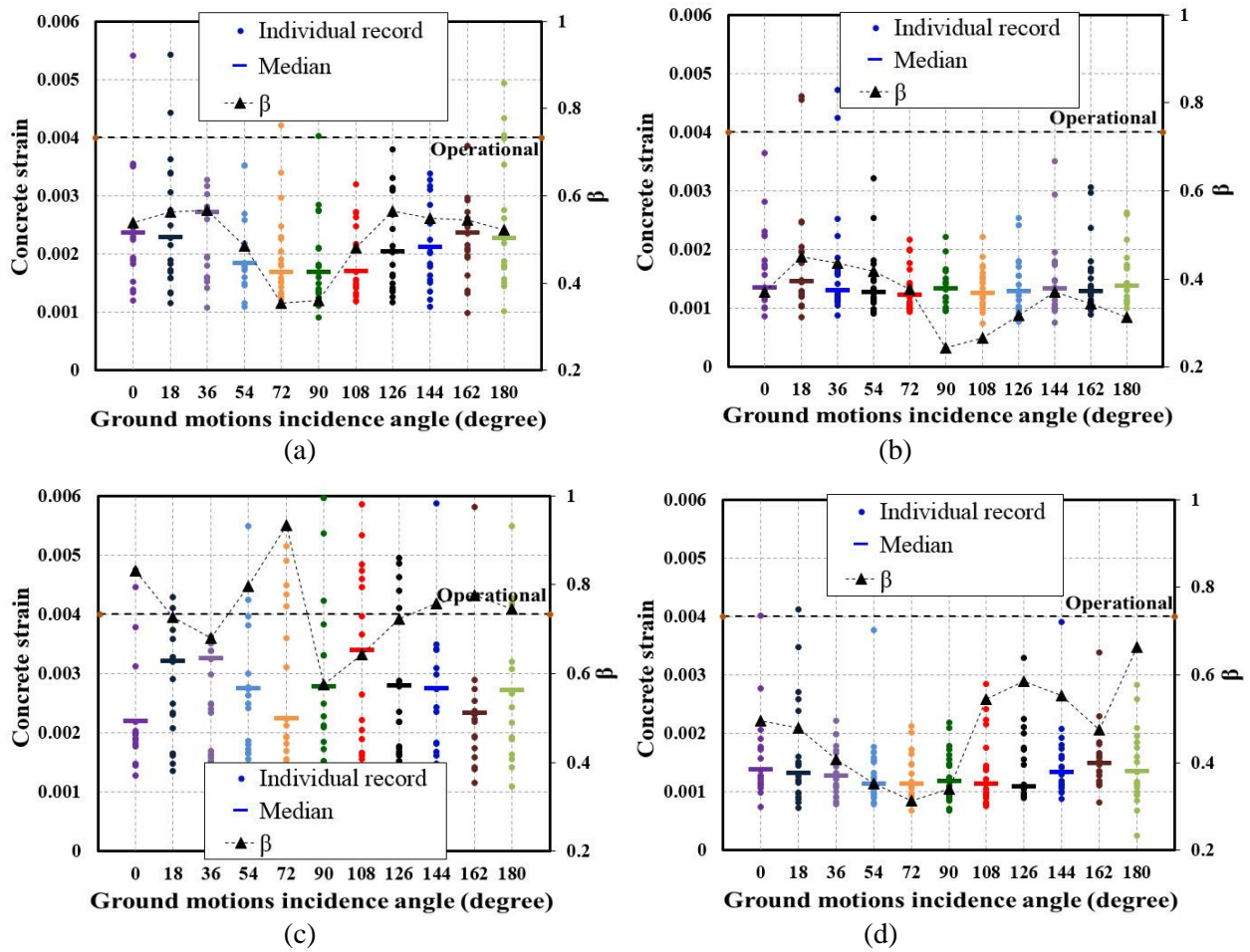


**Figure 4.45** Comparison of column concrete strain of straight and skewed bridges under 10 incidence angles: (a) Original straight bridge; (b) straight bridge retrofitted with BRB; (c) Original 36° skewed bridge; (d) 36° skewed bridge retrofitted with BRB

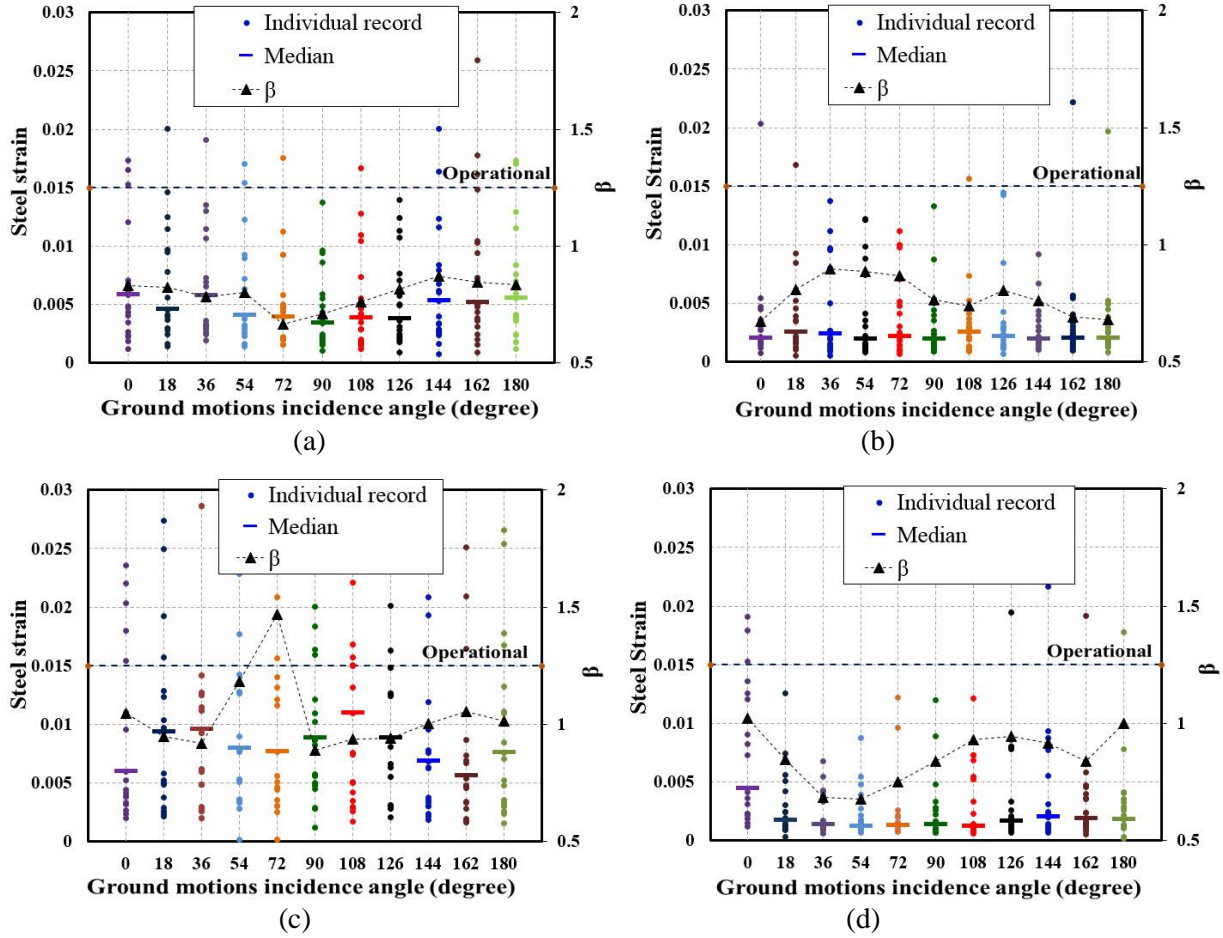


**Figure 4.46** Comparison of column steel strain of straight and skewed bridges under 10 incidence angles: (a) Original straight bridge; (b) straight bridge retrofitted with BRB; (c) Original 36° skewed bridge; (d) 36° skewed bridge retrofitted with BRB

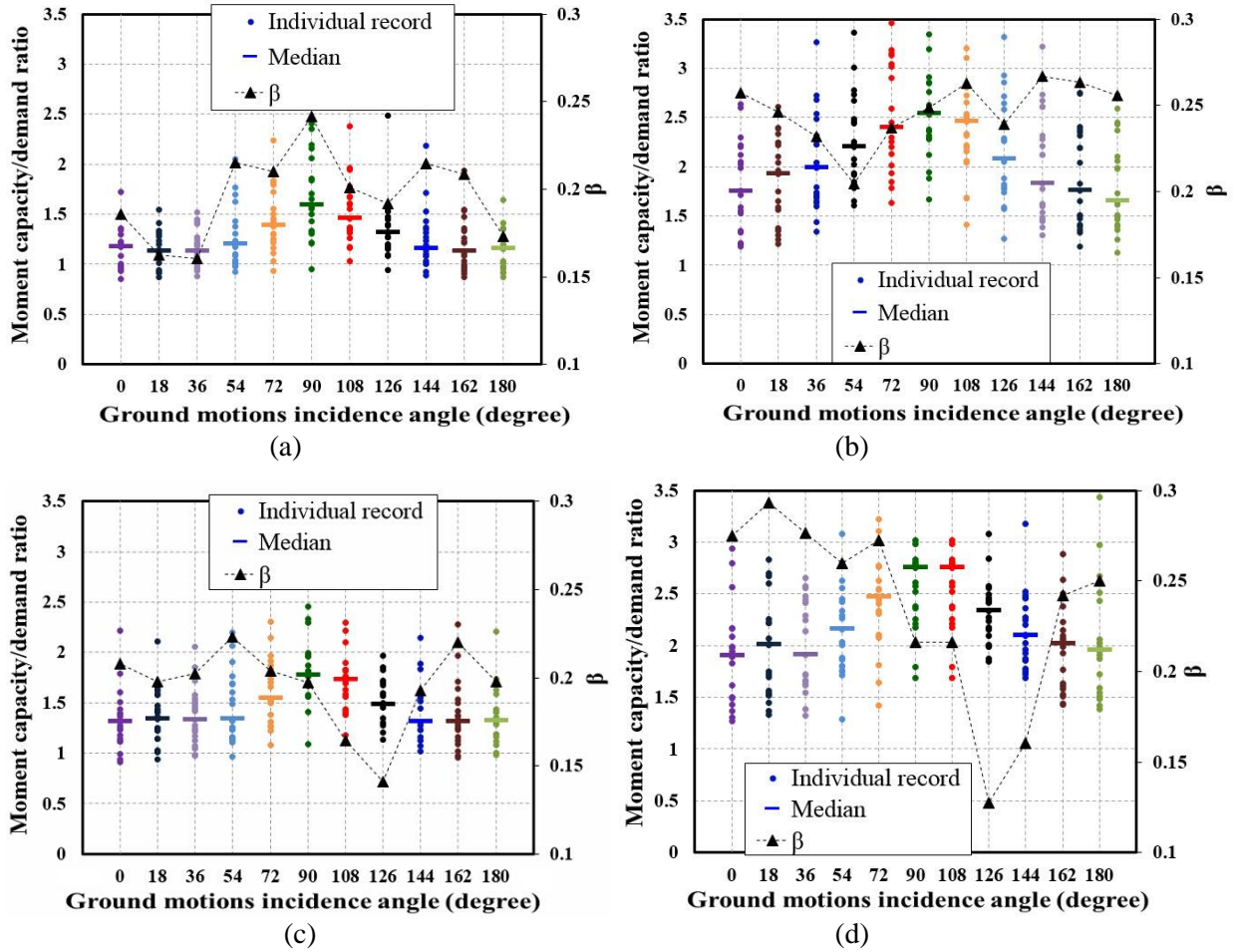


**Figure 4.47** Comparison of column moment capacity to demand ratio of straight and skewed bridges under 10 incidence angles: (a) Original straight bridge; (b) straight bridge retrofitted with BRB; (c) Original 36° skewed bridge; (d) 36° skewed bridge retrofitted with BRB

## 5. SIMPLIFIED BRB DESIGN PROCEDURE FOR ABUTMENT POUNDING

Selecting BRBs for bridges to prevent pounding between girders and abutment for a curved bridge is an iterative procedure. The design of BRBs for this procedure is force/strength controlled because the length of the BRB should be according to the expansion gap provided. BRBs are designed to develop a 1.5% to 2.0% strain in their core, and hence the maximum deformation in BRBs should be less than the expansion gap provided in the bridge to prevent pounding effectively. This iterative design procedure starts with analyzing the bridge in a structural analysis program (e.g., SAP 2000<sup>®</sup>) with a line beam model and assign mass to the nodes. A linear analysis is not sufficient to investigate pounding at the abutment. The engineer should ignore the friction resistance provided by the bearing on which girders are resting to idealize the situation as a roller support. The relative displacement of the deck node toward the abutment node in the analysis model should be checked. If this relative displacement ( $\Delta_{rel}$ ) is less than the expansion gap, for site-specific scaled ground acceleration data, the bridge is safe against the pounding. If the relative displacement ( $\Delta_{rel}$ ) is greater than the expansion gap provided, there will be pounding between the deck and the abutment, and BRBs are needed between abutment and the girder/deck.

A non-linear time-history analysis is necessary to take the yielding of BRBs into account. Design engineers should start with the BRBs calculated according to section 5.1.1 of this report. The aim should be to reduce the relative displacement ( $\Delta_{rel}$ ) and keep it below the expansion gap value. If the relative displacement is still greater than the expansion gap, the strength of BRB should be increased. If the relative displacement (after using BRB in analysis) is less than half of the expansion gap value, strength demand or the number of the BRBs should be decreased to optimize. A detailed process is summarized in Figure 5.1. The following are the notable points of the design process,

1.  $\Delta_{rel}$  is the relative displacement of girders/deck toward the abutment. Engineers should be careful with the sign convention while modeling and analyzing the results of time-history analysis.
2. Non-linear analysis is required to take the yielding of BRBs into account.

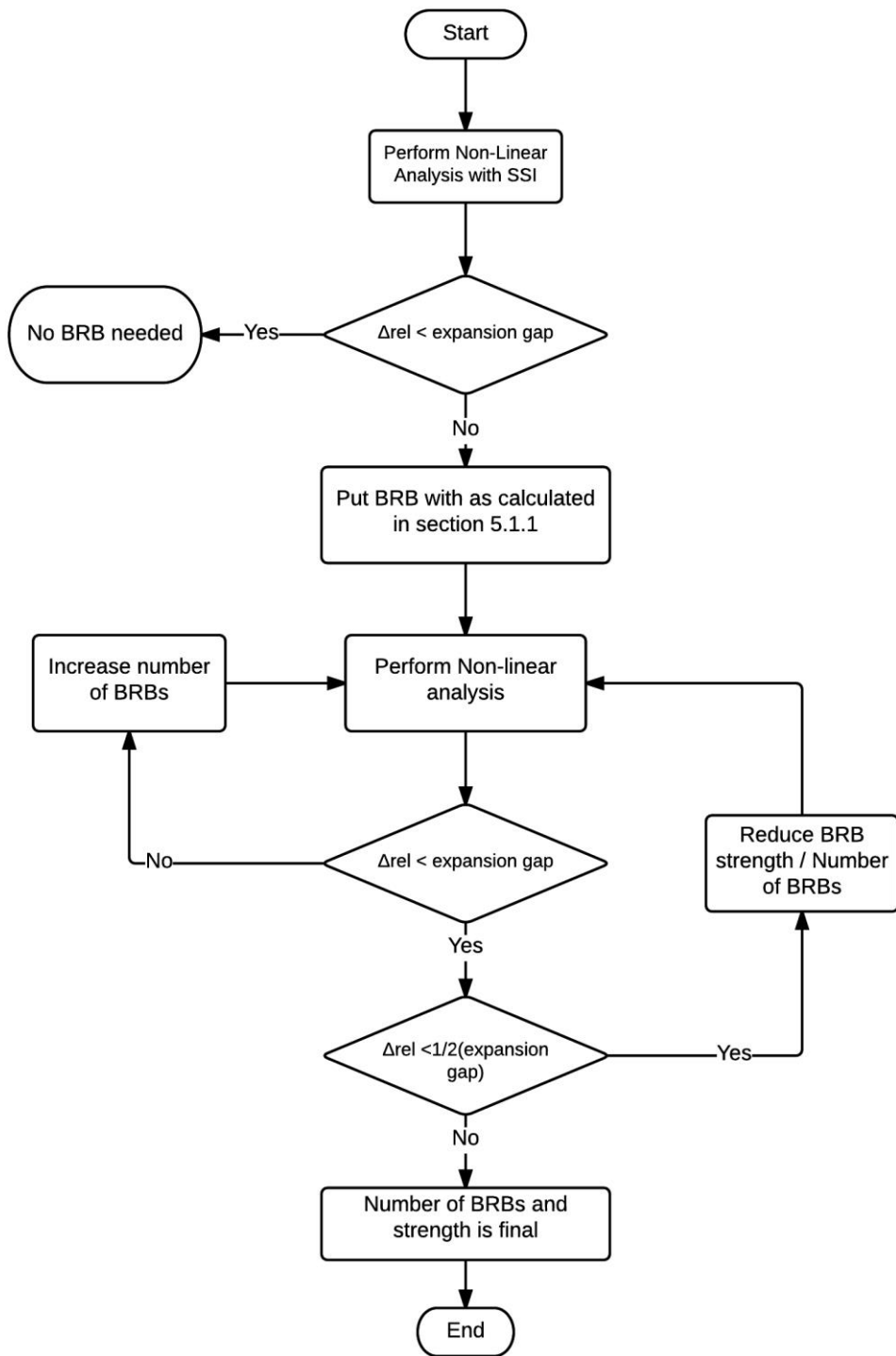


**Figure 5.1** Design procedure for BRBs at bridge abutments of curved bridge

## 5.1 Calculation for Initial BRB Strength

Consider the tributary weight of deck ( $W$ ) from expansion joint to expansion joint and the fundamental mode of vibration of the bridge,  $T_1$ . Calculate elastic seismic coefficient ( $C_{SM}$ ) corresponding to  $T_1$  using 5% damped AASHTO design response spectrum maps, as shown in Figure 5.2. Equivalent static seismic load can be calculated using weight of the deck, fundamental mode of vibration, and design spectral acceleration by following equation,

$$P_e = \frac{\phi C_{sm} W}{R}$$

$\Phi$  = Overstrength factor for given seismic zone. (AASHTO 3.10.9.4.3C)

$R$  = Response Modification Factor for substructures of the bridges. (AASHTO Table 3.10.7.1-1)

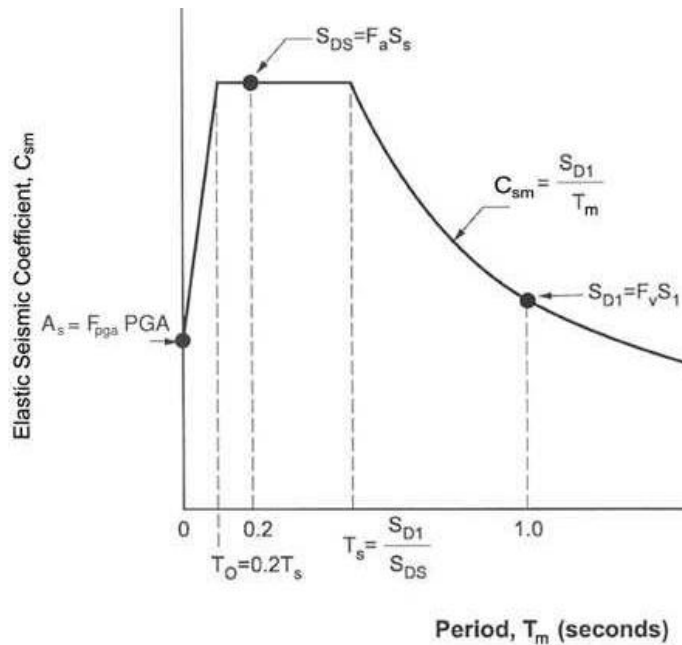


**Figure 5.2** Design Response Spectrum in AASHTO

The BRBs installed to the bridge abutment should be able to resist the equivalent static seismic force ( $P_e$ ) in order to prevent pounding between the abutment and the deck. As BRBs show a non-linear behavior, we should assume that BRBs will have  $P_e$  as the total ultimate compression force. Strength adjustment factors ( $\beta$  and  $\omega$ ) for the BRBs will be provided by the manufacturer.  $\beta$  is compression overstrength factor and  $\omega$  is strain-hardening factor for the buckling restrained braces. For a BRB with core area  $A_c$  and core yielding stress  $F_y$ , the following can be calculated,

$$\text{Yielding Force } (P_y) = A_c F_y$$

$$\text{Ultimate Compression Force } (P_{Uc}) = \beta \omega A_c F_y$$

$$\text{Ultimate Tension Force } (P_{Ut}) = \omega A_c F_y$$

$$\text{Hence Yield force, } P_y = P_{Uc} / \beta \omega$$

It is recommended to install one BRB at each girder to distribute stresses uniformly. As we know that ultimate compression force in each BRB should be equal to,

$$P_U = P_{Uc} = P_e / n \quad \text{Eq. 5.1}$$

Here n = number of girders in the bridge deck. Hence,

$$P_y = \frac{P_e}{n \beta \omega} \text{ (BRB yield force)} \quad \text{Eq. 5.2}$$

Also, the BRB should resist this force after showing non-linear behavior so that energy dissipation can be achieved. Therefore, we can assume that ultimate deformation in the BRB core is equal to the gap provided between abutment and the girder/deck, which can be taken from the design drawings.

$$\text{Ultimate Deformation in BRB } \Delta_u = \Delta_{\text{gap}} \quad \text{Eq. 5.3}$$

$$\begin{aligned} \text{Yield deformation in BRB } \Delta_{\text{yield}} &= 0.1 \Delta_u \\ \Delta_{\text{yield}} &= 0.1 \Delta_{\text{gap}} \end{aligned} \quad \text{Eq. 5.4}$$

After finalizing the yield force and yield deformations in the BRBs, these data are given to a BRB manufacturer that will design and manufacture BRBs accordingly. The backbone curve shown in Figure 5.3 can be used in SAP 2000 for a non-linear link element to be used as a BRB.

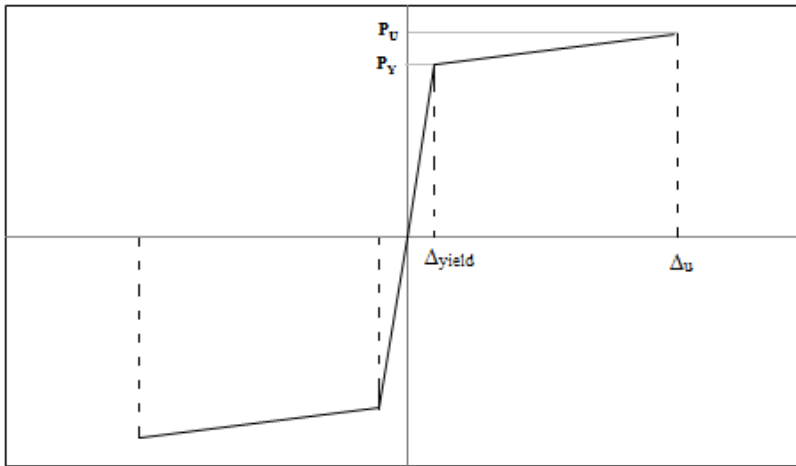


**Figure 5.3** BRB backbone curve for SAP 2000® non-linear analysis

## 6. CONCLUSIONS

### 6.1 Curved Bridge

The effects of pounding on curved bridges were studied considering soil-structure interaction (SSI). Time history analyses (THAs) showed that Buckling Restrained Braces (BRBs) can prevent structural pounding at the bridge abutments and expansion joints. A non-linear finite element model of the bridge was used to investigate structural pounding by performing several THAs of strong motion earthquake records scaled to the site conditions. In addition, Incremental Dynamic Analysis (IDA) was used to assess the bridge performance under various earthquake scenarios.

1. The bridge model was analyzed without SSI under DBE earthquake level, and it was found that girder displacements were less than the gap provided at the abutments and the expansion joints. No pounding was observed in this case and the columns had sufficient strength to resist the seismic forces.
2. The bridge model was re-analyzed including SSI, which lengthened the fundamental period of vibration. Displacement of the girders relative to the abutments increased due to SSI effects at a level higher than the construction gap, leading to pounding between the girders and the abutments. Restrainer rods at the expansion joints either buckled or fractured, which led to pounding between the girders. Shear keys experienced high pounding forces due to lateral movement of the girders.
3. IDAs showed that BRBs placed between the girders and abutments were able to reduce the relative displacement more effectively on the side of the bridge with the smallest radius of curvature; the relative displacement reduction at this location reached a median level of 50% for the 15 earthquakes considered.
4. BRBs placed between girders along the girder axis were able to prevent pounding at the expansion joints. In addition, BRBs placed in the lateral direction were able to prevent concrete shear key damage.
5. The DBE  $S_a$  for the site was 0.91g and the MCE was 1.2g. For the 15 earthquake records scaled to site DBE level, and including SSI effects, nonlinear analyses showed pounding was avoided for the as-built structure for a median acceleration below 0.91g; for the retrofitted structure, pounding was avoided for a median spectral acceleration below 1.56g.

### 6.2 Skewed Bridge

The study presents a comprehensive evaluation on the use of BRBs to seismically retrofit existing straight and 36° skewed RC bridges under 11 different incidence angles. BRBs are added to the bents as structural fuses, creating a dual lateral resistant system with larger strength and stiffness than that of the original bridge system. The results show that BRBs can prevent damage to the main components of the original bridge by dissipating seismic energy through hysteretic behavior and redistributing shear demand in the transverse direction. The main findings of this study are as follows:

1. The use of BRBs reduces the column bent drift about 50% in the evaluated straight and skewed bridges, and prevents deck unseating caused by shear key failure, which is the most likely type of failure in skewed bridges.
2. BRBs redistribute stiffness in the transverse direction between column bents and the abutments, and dissipate about 20% shear demand of the original seismic demands through BRB hysteretic behavior for both straight and skewed bridges.
3. The strain level of concrete and steel in columns is reduced within the operational limit for most evaluated retrofitted bridges. The addition of BRBs prevents or delays the occurrence of column plastic hinges near pier-cap joints.



4. BRBs improve the bent ductile response, but may result in larger demands on the bent columns due to the additional bent stiffness. A gusset plate directly attached to the foundation can mitigate this problem. On the other hand, the implementation of BRBs on bents always reduce the shear demands on the abutment of straight bridges.
5. Based on the results of this study, the concrete and steel strain performance limits from previous studies may overestimate the performance of bridge structures.
6. The evaluated bridges were optimized for dual systems DS-BRB50 (i.e., bents in which BRBs resist 50% of the elastic lateral demand). Based on pushover analyses, dual systems with larger BRBs capacity (e.g., DS-BRB75) do not exhibit significant hysteretic energy dissipation capabilities.
7. A ground motion scaling method was implemented by rotating the ground motion principal directions, using an approach similar to that recommended in ASCE 41-06 (2006)

## REFERENCES

- AASHTO. (1998). AASHTO LRFD bridge design specifications, 2nd Ed., American Association of State Highway and Transportation Officials, Washington, DC.
- AASHTO. (2012). AASHTO LRFD bridge design specifications, 6th Ed., American Association of State Highway and Transportation Officials, Washington, DC.
- AISC. (2014). “Seismic Design Manual.” American Institute of Steel Construction. Chicago, IL.
- Amjadian and Kalantari (2012), “A. Influence of Seismic Pounding on Dynamic Response of Skewed Highway Bridges.” 15th WCEE.
- Anagnostopoulos, S. A., and Karamaneas, C. E. (2008). “Use of collision shear walls to minimize seismic separation and to protect adjacent buildings from collapse due to earthquake-induced pounding.” *Earthquake Eng. Struct. Dyn.*, 37, 1371–1388.
- Andrawes, B. and DesRoches, R. (2007). “Comparison between Shape Memory Alloy Seismic Restrainers and Other Bridge Retrofit Devices,” *J. Bridge Eng.*, 10.1061/(ASCE)1084-0702(2007)12:6(700), 700-709.
- ASCE/SEI (2010). “Seismic Rehabilitation of Existing Buildings (ASCE/SEI 41-06).” Reston, VA.
- ASCE. (2013). “Minimum Design Loads For Buildings and Other Structures (ASCE/SEI 7-13)” Reston, VA.
- ASCE. (2014). “Seismic Rehabilitation of Existing Buildings.” 41-13, Reston, VA.
- Basu, S. B., and Shinozuka, M. (2011). “Effect of Ground Motion Directionality on Fragility Characteristics of a Highway Bridge.” *Advances in Civil Engineering*, Article ID 536171.
- Bhatnagar, U. R. (2013). “Seismic Performance of Skewed Bridges under Orthogonal Ground Motion Components.” M.S. Dissertation to Pennsylvania State University, State College, PA.
- Bi, K., and Hao, H. (2013). “Numerical simulation of pounding damage to bridge structures under spatially varying ground motions.” *Engineering Structures*, 46(5), 62–76.
- Bisadi, V., and Head, M. (2011). “Evaluation of Combination Rules for Orthogonal Seismic Demands in Nonlinear Time History Analysis of Bridges.” *J. Bridge Eng.*, 16(6), 711-717.
- Bruneau, M., Wilson, J. C., and Tremblay, R. (1996). “Performance of steel bridges during the 1995 Hyogo-ken Nanbu (Kobe, Japan) earthquake.” *Can. J. Civ. Eng.*, 23, 678-713.
- Buckle, I.G., Yen, W., Marsh, Lee, M., and Monzon, E., V. (2012). “Implications of bridge performance during Great East Japan earthquake for U.S. seismic design practice.” Proceedings of the International Symposium on Engineering Lessons Learned from the 2011 Great East Japan Earthquake, March 1-4, 2012, Tokyo, Japan, 1323-1332.
- Caltrans, S. D. C. (California Department of Transportation). (1999). “Caltrans Seismic Design Criteria version 1.1.,” Sacramento, California.

- Caltrans, S. D. C. (California Department of Transportation). (2010). "Caltrans Seismic Design Criteria version 1.6.," Sacramento, California.
- Capron, M. R. (1999). "Seismic Retrofit of the Poplar Street Bridge." Conference Proceedings, Structural Engineering in the 21<sup>st</sup> Century, Structures Congress, April 1-19, 1999, 37-40.
- Catacoli, S. S., Ventura, C. E., and Finn, W. D. L. (2012). "Displacement Demands for Performance Based Design of Skewed Bridges." Proceedings of the Fifteenth World Conference on Earthquake Engineering, September 24-28, 2012, Lisbon, Portugal.
- Celik, O. C., and Bruneau, M. (2009). "Seismic behavior of bidirectional-resistant ductile end diaphragms with buckling restrained braces in straight steel bridges." *Engineering Structures*, 31(2), 380–393.
- Celik, O. C., and Bruneau, M. (2011). "Skewed Slab-on-Girder Steel Bridge Superstructures with Bidirectional-Ductile End Diaphragms." *J. Bridge Eng.*, 10.1061/(ASCE)BE.1943-5592.0000141, 207-218.
- Computers and Structures Inc. (2013). "SAP 2000 v.16," Analysis software.  
<https://www.csiamerica.com/products/sap2000>.
- DesRoches, R., and Muthukumar, S. (2002). "Effect of Pounding and Restrainers on Seismic Response of Multiple-Frame Bridges." *J. Struct. Eng.*, 10.1061/(ASCE)0733-9445(2002)128:7(860), 860-869.
- Dicleli, M., and Bruneau, M. (1995). "Seismic Performance of Multispan Simply Supported Slab-on-girder Steel highway Bridges." *Engineering Structures*, 17(1), 4–14.
- Dusicka, P., Bazaez, R., and Knoles, S. (2015). "Bridge Seismic Retrofit Measures Considering Subduction Zone Earthquakes." FHWA Report No. FHWA-OR-RD-16-01, Oregon Department of Transportation, Portland State University.
- El-Bahey, S., and Bruneau, M. (2011). "Buckling restrained braces as structural fuses for the seismic retrofit of reinforced concrete bridge bents." *Engineering Structures*, 33(3), 1052-1061.
- El-Bahey, S., and Bruneau, M. (2012). "Bridge Piers with Structural Fuses and Bi-Steel Columns. I: Analytical Investigation." *J. Bridge Eng.*, 10.1061/(ASCE)BE.1943-5592.0000234, 25-35.
- FEMA 351 (2000). "Recommended Seismic Evaluation and Upgrade Criteria for Welded Steel Moment Frame Buildings." Report No. FEMA 351. Federal Emergency Management Agency, Washington, D.C.
- FEMA. (2000). "Seismic Rehabilitation Prestandards." FEMA 356, Federal Emergency Management Agency, Washington D.C.
- FEMA. (2009). "NEHRP Recommended Seismic Provisions." FEMA P-752, Federal Emergency Management Agency, Washington D.C.
- FEMA. (2009). "Quantification of Building Seismic Performance Factors." FEMA P-695, Federal Emergency Management Agency, Washington D.C.
- Goel, R.K. and Chopra, A.K. (2008). "Role of Shear Keys in Seismic Behavior of Bridges Crossing Fault-Rupture Zones." *J. Bridge Eng.*, 10.1061/(ASCE)1084-0702(2008)13:4(398), 398-408.

- Hao, H., and Chouw, N. (2008). "Seismic Design of Bridges for Prevention of Girder Pounding." e-JSE Special Issue, 133–141.
- Huo, Y. and Zhang, J. (2013). "Effects of Pounding and Skewness on Seismic Responses of Typical Multispan Highway Bridges Using the Fragility Function Method." J. Bridge Eng., 10.1061/(ASCE)BE.1943-5592.0000414, 499-515.
- Ibarra, L. F. and Krawinkler, H. (2005). "Global Collapse of Frame Structures under Seismic Excitations." PEER Report 2005/06, Pacific Earthquake Engineering Research Center, University of California, Berkeley.
- Itani, A. M., Bruneau, M., Carden, L., and Buckle, I. G. (2004). "Seismic Behavior of Steel Girder Bridge Superstructures." J. Bridge Eng., 10.1061/(ASCE)1084-0702(2004)9:3(243), 243-249.
- Jankowski, R. (2005). "Non-linear viscoelastic modelling of earthquake-induced structural pounding." Earthquake Eng. Struct. Dyn., 34, 595–611.
- Jennings, P. C., and Wood, J. H. (1971). "Earthquake damage to freeway structures." Engineering Features of the San Fernando Earthquake, 7102.
- Kanaji, H., Kitazawa, M., and Suzuki, N. (2005). "Seismic Retrofit Strategy using Damage Control Design Concept and the Response Reduction Effect for a Long-span Truss Bridge." Proceedings of 19<sup>th</sup> US-Japan Bridge Workshop, Tsukuba, Japan, October.
- Kaviani, P., Zareian, F., and Taciroglu, E. (2012). "Seismic Behavior of Reinforced Concrete Bridges with Skew-angled Seat-type Abutments." Engineering Structures, 45, 137-150.
- Konagai, K., Yin, Y., and Murono, Y. (2003). "Single beam analogy for describing soil-pile group interaction." Soil Dynamics and Earthquake Engineering, 23(3), 213–221.
- Kowalsky, M. J. (2000). "Deformation Limit States for Circular Reinforced Concrete Bridge Columns." J. Struct. Eng., 10.1061/(ASCE)0733-9445(2000)126:8(869), 869-878.
- Li, B., Bi, K., Chouw, N., Butterworth, J. W., and Hao, H. (2013). "Effect of abutment excitation on bridge pounding." Engineering Structures, 54, 57-68.
- Lu, Y., Gu, X., and Guan, J. (2005). "Probabilistic Drift Limits and Performance Evaluation of Reinforced Concrete Columns." J. Struct. Eng., 10.1061/(ASCE)0733-9445(2005)131:6(966), 966-978.
- Mackie, K. R., Cronin, K. J., and Nielson, B. G. (2011). "Response Sensitivity of Highway Bridges to Randomly Oriented Multi-Component Earthquake Excitation." Journal of Earthquake Engineering, 15(6), 850-876.
- Maleki, S., and Bisadi, V. (2006). "Orthogonal Effects in Seismic Analysis of Skewed Bridges." J. Bridge Eng., 10.1061/(ASCE)1084-0702(2006)11:1(122), 122-130.
- Mander, J. B., Priestley, M. J. and Park, R. (1988). "Theoretical Stress-strain Model for Confined Concrete." J. Struct. Eng., 10.1061/(ASCE)0733-9445(1988)114:8(1804), 1804-1826.

- Makris, N. and Zhang, J. (2002). "Structural Characterization and Seismic Response Analysis of a Highway Overcrossing Equipped with Elastomeric Bearings and Fluid Dampers: A Case Study." Report No. PEER – 2002/17, University of California, Berkeley, CA.
- Maragakis, E. A. and Jennings, P. C. (1987). "Analytical Models for the Rigid Body Motions of Skew Bridges." *Earthquake Eng. Struct. Dyn.*, 15(8), 923-944.
- Marsh, A. K. (2013). "Evaluation of Passive Force on Skewed Bridge Abutments with Large-Scale Tests." Ph.D. dissertation, Brigham Young University, Provo, UT.
- McKenna F., Fenves G.L., and Scott M.H. (2000). Open System for Earthquake Engineering Simulation (OpenSees) version 2.4.5 [Software]. Available from <http://opensees.berkeley.edu/>.
- Megally, S. H., Silva, P. F., and Seible, F. (2002) "Seismic Response of Sacrificial Shear Keys in Bridge Abutments." Report No. SSRP-2001/23. UC San Diego.
- NEHRP. (2012). "Selecting and Scaling Earthquake Ground Motions for Performing Response-History Analyses." NEHRP Synthesis 428. TRB, Washington D.C.
- Nielson, B. G., and DesRoches, R. (2006). "Influence of modeling assumptions on the seismic response of multi-span simply supported steel girder bridges in moderate seismic zones." *Engineering Structures*, 28(8), 1083-1092.
- OES (1995). "Vision 2000: Performance Based Seismic Engineering of Buildings." Prepared by Structural Engineers Association of California. California Office of Emergency Services.
- Pantelides, C. P., and Ma, X. (1998). "Linear and nonlinear pounding of structural systems." *Computers & Structures*, 66(1), 79–92.
- Padgett, J. E., and DesRoches R. (2008). "Three-dimensional nonlinear seismic performance evaluation of retrofit measures for typical steel girder bridges." *Engineering Structures*, 30(7), 1869-1878.
- Pan, Y., Agrawal, A., and Ghosn, M. (2007). "Seismic Fragility of Continuous Steel Highway Bridges in New York State." *J. Bridge Eng.*, 10.1061/(ASCE)BE.1943-5592.0000085, 448-461.
- Pan, Y., Agrawal, A., Ghosn, M., and Alampalli, S. (2010 a). "Seismic Fragility of Multispan Simply Supported Steel Highway Bridges in New York State. I: Bridge Modeling, Parametric Analysis, and Retrofit Design." *J. Bridge Eng.*, 10.1061/(ASCE)BE.1943-5592.0000085, 448-461.
- Pan, Y., Agrawal, A., Ghosn, M., and Alampalli, S. (2010 b). "Seismic Fragility of Multispan Simply Supported Steel Highway Bridges in New York State. II: Fragility Analysis, Fragility Curves, and Fragility Surfaces." *Journal of Bridge Engineering*, 10.1061/(ASCE)BE.1943-5592.0000055, 462-472.
- Penzien, J. and Watabe, M. (1975). "Characteristics of 3-D earthquake ground motions." *Earthquake Eng. Struct. Dyn.* 3, 365–373.
- PEER (2013). NGA-West2 database flatfile, Pacific Earthquake Engineering Research Center, available: <http://peer.berkeley.edu/ngawest2/databases/>. Last accessed 14 October 2014.
- Priestley, M. J. N. (2000) "Performance Based Seismic Design." *Bulletin of the New Zealand Society for Earthquake Engineering*, 33(3), 325-346.

- Raheem, A. S. E. (2009). "Pounding mitigation and unseating prevention at expansion joints of isolated multi-span bridges." *Engineering Structures*, 31(10), 2345–2356.
- Reno, M. and Pohll, M. N. (2013). "Incorporating Buckling Restrained Braces (BRB) as Part of the Auburn-Forest Hill Bridge Seismic Retrofit," The 29th US - Japan Bridge Engineering Workshop, Nov. 11-13, Tsukuba, Japan.
- Rollins, K. M., and Jessee, S. J. (2012). "Passive Force-Deflection Curves for Skewed Abutments." *J. Bridge Eng.*, 10.1061/(ASCE)BE.1943-5592.0000439, 1086-1094.
- SeismoSoft (2013) – "SeismoMatch v.2.1.2." [www.seismosoft.com](http://www.seismosoft.com).
- Soneji, B. B., and Jangid, R. S. (2008). "Influence of soil-structure interaction on the response of seismically isolated cable-stayed bridge." *Soil Dynamics and Earthquake Engineering*, 28(4), 245–257.
- Stewart, J. P., Taciroglu, E., Wallace, J. W., Ahlberg, E. R., Lemnitzer, A., Rha, C., and Salamanca, A. (2007). "Full Scale Cyclic Testing of Foundation Support Systems for Highway Bridges. Part II: Abutment backwalls." (UCLA-SGEL 2007/02), UCLA.
- Sun, L., Wei, J., and Xie, W. (2012). "Experimental Investigation on Energy Dissipation Subsidiary Piers for Long Span Cable-Stayed Bridges." Proceedings of 15<sup>th</sup> WCEE World Conference on Earthquake Engineering, Lisbon, Portugal.
- Takabatake, H., Yasui, M., Nakagawa, Y., and Kishida, A. (2014). "Relaxation method for pounding action between adjacent buildings at expansion joint." *Earthquake Eng. Struct. Dyn.*, 43, 1381–1400.
- Torbol, M., and Shinozuka, M. (2012). "Effect of the Angle of Seismic Incidence on the Fragility Curves of Bridges." *Earthquake Eng. Struct. Dyn.*, 41(14), 2111-2124.
- Uang, C., and Bertero, V. (1990) "Evaluation of Seismic Energy in Structures." *Earthquake Eng. Struct. Dyn.*, 19(1), 77–90.
- Upadhyay, A., Pantelides, C. P. and Ibarra, L. (2016). "Seismic Performance of Curved Bridges on Soft Soils Retrofitted with Buckling Restrained Braces." Geotechnical and Structural Engineering Congress 2016, 118-137.
- Upadhyay, A., Pantelides, C. P. and Ibarra, L. (2016). "Seismic Pounding Mitigation using BRBs for Curved Bridges on Soft Soils." *J. Bridge Eng.* (Submitted).
- US DOT (U.S. Department of Transportation, Bureau of Transportation). (2014). "National Transportation Statistics." <<http://www.rita.dot.gov/bts/sites/rita.dot.gov/bts/>>.
- USGS. (2014). "Seismic Design Map Tools." US Geological Survey. <http://earthquake.usgs.gov/designmaps/us/application.php>
- Wakefield, R., Nazmy, A. S., and Billington, D. P. (1991). "Analysis of Seismic Failure in Skew RC Bridge." *J. Struct. Eng.*, 10.1061/(ASCE)0733-9445(1991)117:3(972), 972-986.
- Wang, Y., Ibarra, L., and Pantelides, C. (2016). "Seismic Retrofit of a Three-Span RC Bridge with Buckling-Restrained Braces." *Journal of Bridge Engineering*, 10.1061/(ASCE)BE.1943-5592.0000937, 04016073.

Wang, Y., Ibarra, L., and Pantelides, C. (2017). "Seismic Assessment for Retrofitted Skewed Reinforced Concrete Bridges with Buckling Restrained Braces." Accepted by 16<sup>th</sup> WCEE, Chile.

Watanabe, G., and Kawashima, K. (2004). "Effectiveness of Cable-restrainer for Mitigating Rotation of a Skewed Bridge Subjected to Strong Ground Shaking." Proceedings of the 13<sup>th</sup> World Conference on Earthquake Engineering, Vancouver, British Columbia, Canada 2004.

Wilson, T., Mahmoud, H., and Chen, S. (2014). "Seismic performance of skewed and curved reinforced concrete bridges in mountainous states." *Eng. Struct.*, 70, 158-167.

Van Mier, J., Pruijssers, A., Reinhardt, H., and Monnier, T. (1991). "Load-Time Response of Colliding Concrete Bodies." *J. Struct. Eng.*, 10.1061/(ASCE)0733-9445(1991)117:2(354), 354-374.

Xu, W. (2016). "Experiments, Analysis and Design Improvements for New Generation BRBs." PhD Dissertation, Salt Lake City, University of Utah.

Yashinsky, M., Oviedo, R., Ashford, S.A., Fargier-Gabaldon, L., and Hube, M. (2010). "Performance of highway and railway structures during the February 27, 2010, Maule Chile earthquake."

EERI/PEER/FHWA Bridge Team Report:

<[http://peer.berkeley.edu/publications/chile\\_2010/reports\\_chile.html](http://peer.berkeley.edu/publications/chile_2010/reports_chile.html)>

Zhou, G. L. and Meng, Q. L., (2011). "Using Cable Restrainers to Mitigate the Seismic Pounding between Adjacent Structure Members." *Applied Mechanics and Materials*, Vol 71-78, pp. 598-602.

**APPENDIX A. CURVED BRIDGE DRAWINGS AND SITE PHOTOGRAPH**



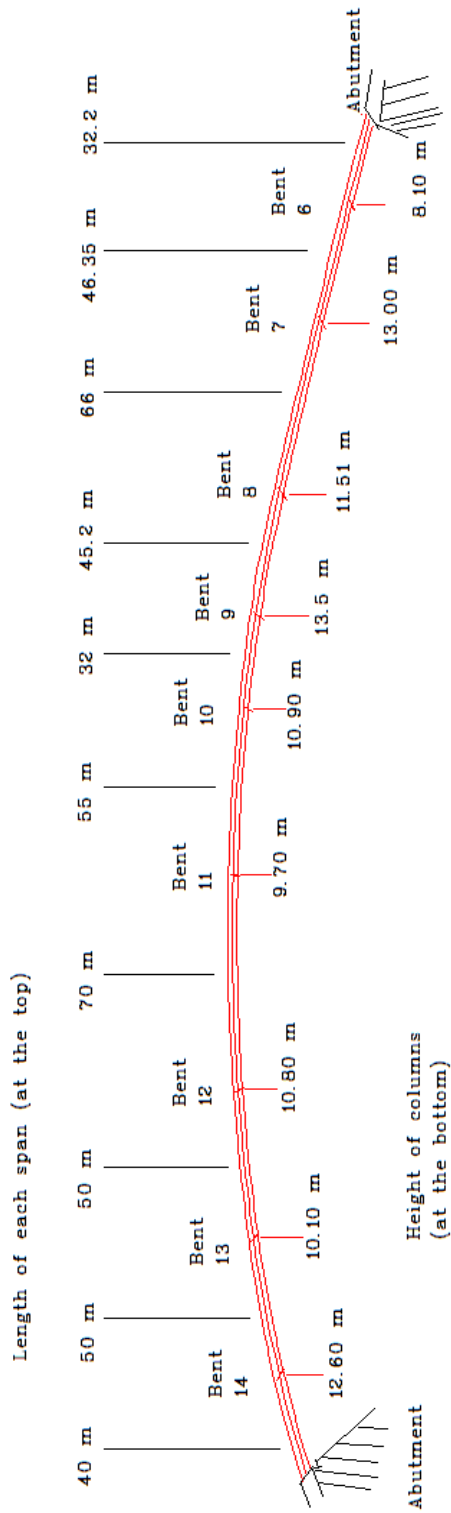


**Figure A.1** Plan and elevation of curved bridge spans

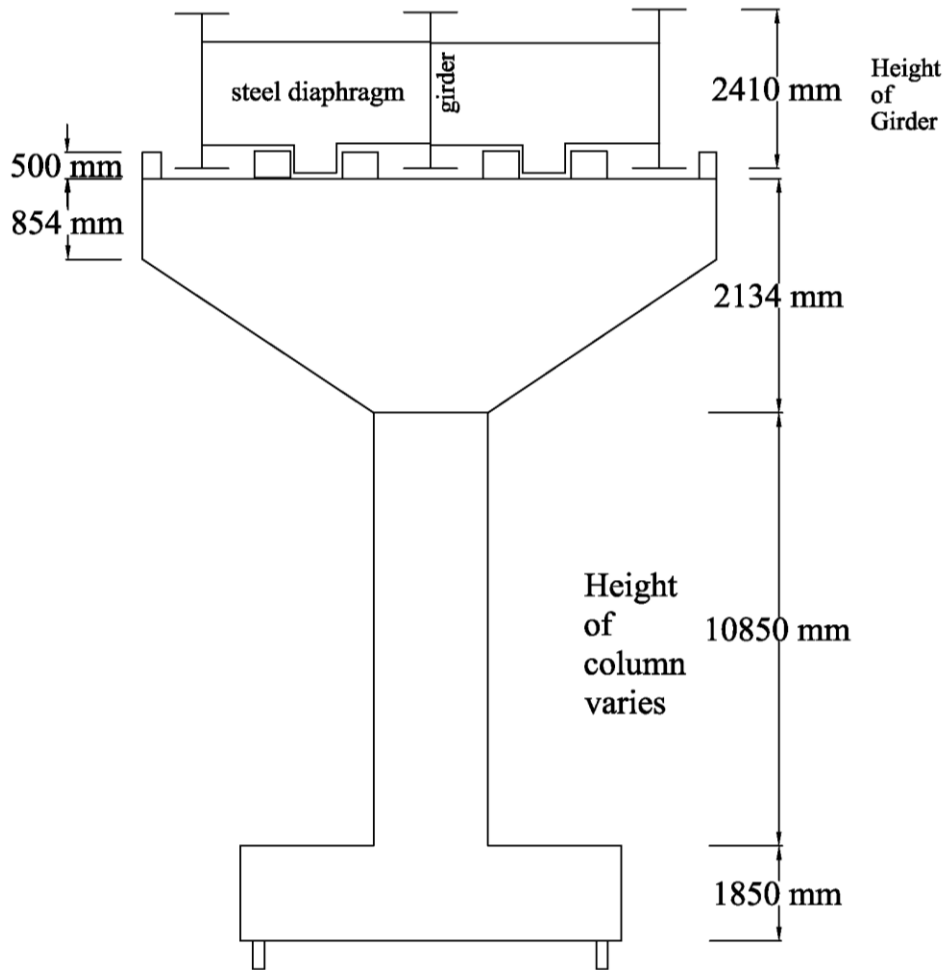
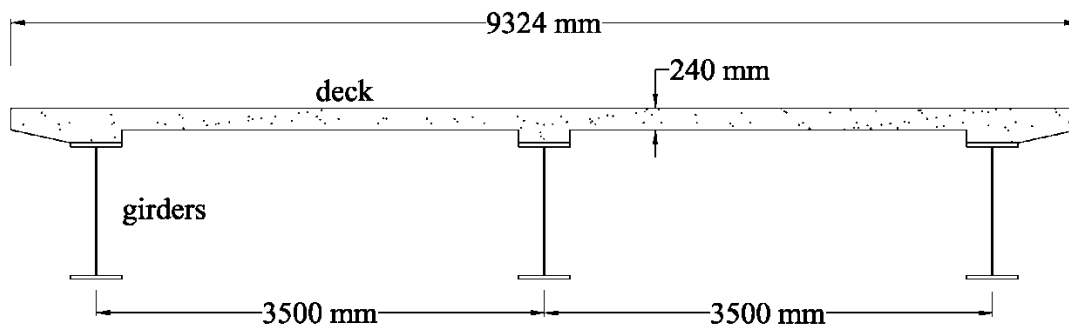
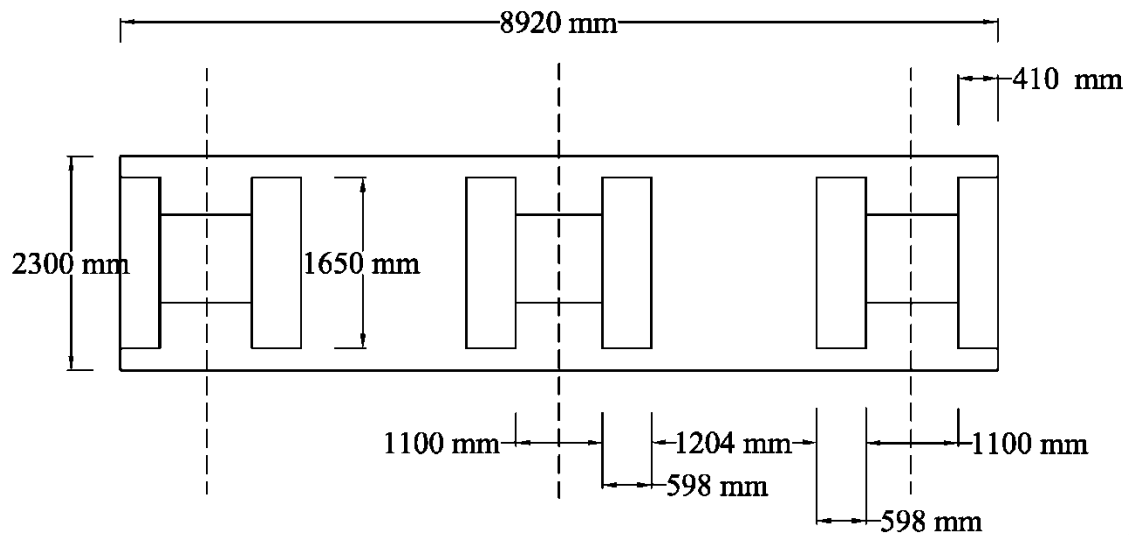


Figure A.2 Elevation of bent 10 of curved bridge



A.3 Dimensions of the concrete deck of curved bridge

Figure



**Figure**

**A.4** Top view of the bent 10 beam of curved bridge

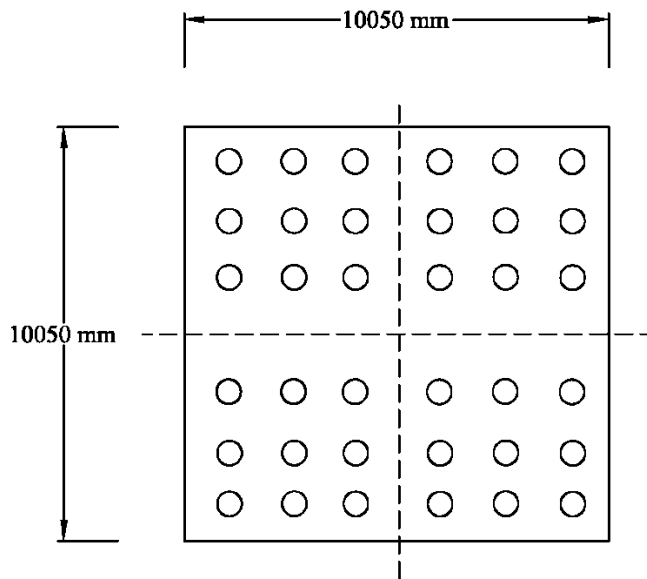


**Figure A.5** Pile group and pile cap at bent 11 of curved bridge (see Table A.1 for more details)

**Table A.1** Details of pile groups and pile caps at various bents of curved bridge

Bent No.	Length	Width	Thickness	No. of Piles	Pile Dia.
	mm	mm	mm		mm
2	7920	7920	1850	24	324
3	7920	7920	1850	24	324
4	7920	7920	1850	24	324
5	7920	7920	1850	24	324
6	7920	7920	1850	24	324
7	7920	7920	1850	24	324
8	7920	7920	1850	24	324
9	10050	10050	1850	36	324
10	7920	7920	1850	26	324
11	7920	7920	1850	32	324
12	10050	10050	1850	24	324
13	10050	10050	1850	32	324
14	10050	10050	1850	42	324

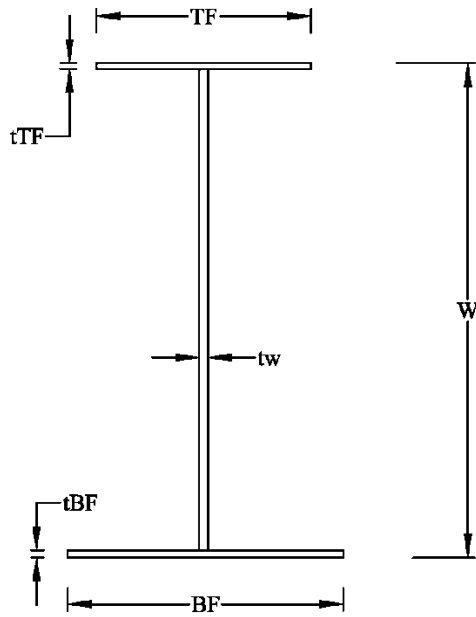


**Figure A.6** Section of steel girder used in the curved bridge (see Table A.2 for details)

**Table A.2** Steel girder sections used in curved bridge

<b>S. No.</b>	<b>W</b>	<b>TF</b>	<b>tTF</b>	<b>tw</b>	<b>BF</b>	<b>tBF</b>
	<b>m</b>	<b>m</b>	<b>m</b>	<b>m</b>	<b>m</b>	<b>m</b>
1	2.336	0.350	0.020	0.020	0.684	0.030
2	2.356	0.350	0.035	0.020	0.684	0.035
3	2.426	0.684	0.070	0.020	0.684	0.070
4	2.396	0.610	0.055	0.018	0.684	0.055
5	2.396	0.684	0.055	0.018	0.684	0.550
6	2.344	0.458	0.028	0.016	0.684	0.030
7	2.366	0.458	0.030	0.016	0.684	0.050
8	2.341	0.458	0.020	0.016	0.684	0.035
9	2.356	0.350	0.020	0.016	0.684	0.050
10	2.341	0.458	0.020	0.016	0.684	0.035
11	2.366	0.508	0.030	0.018	0.684	0.050
12	2.336	0.350	0.020	0.016	0.684	0.030
13	2.356	0.458	0.035	0.020	0.684	0.035
14	2.346	0.350	0.025	0.022	0.684	0.035
15	2.374	0.458	0.038	0.022	0.684	0.050
16	2.461	0.684	0.080	0.022	0.684	0.095
17	2.411	0.690	0.060	0.020	0.684	0.065
18	2.411	0.690	0.060	0.020	0.684	0.065
19	2.341	0.350	0.020	0.018	0.684	0.035



**Figure A.7** Site photograph of curved bridge (Bents 11, 12, 13 and 14)

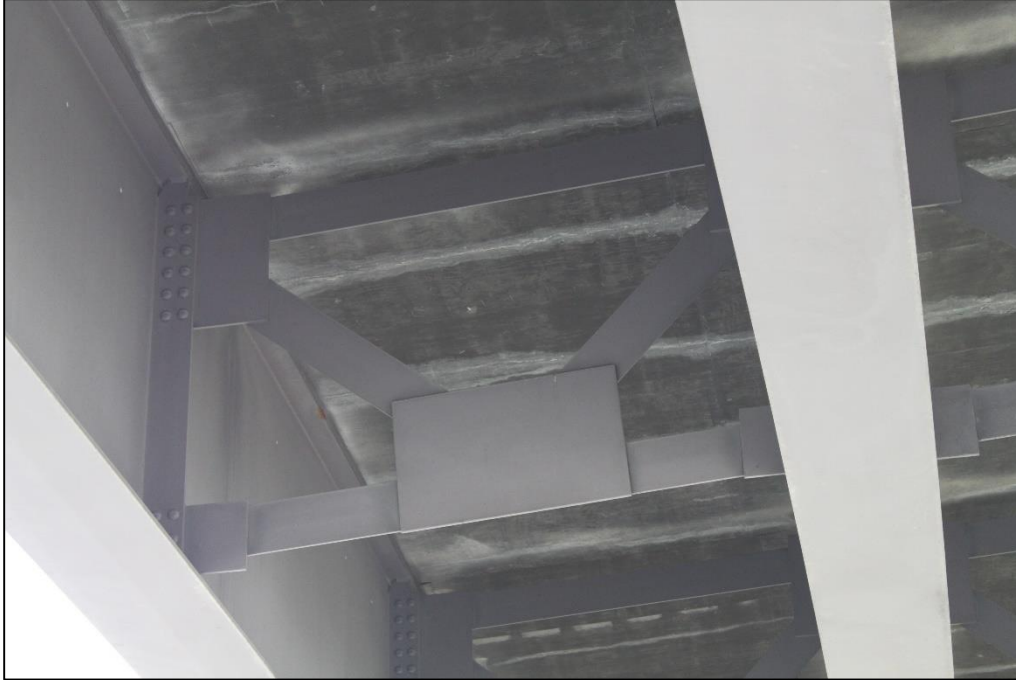


**Figure A.8** Site photograph of diaphragms connecting the girders of curved bridge



**Figure A.9** Site photograph of fixed bearing condition at bent 9 of curved bridge

## **APPENDIX B. CURVED BRIDGE SOIL SPRING CONSTANTS**

### **Pile Cap-Soil Spring Constant**

Soil spring constants for pile caps were calculated based on the directions given in FEMA 356 document in chapter 4 (Foundations and Geologic Site Hazards). These spring constants are based on the values of soil shear modulus, Poisson's ratio, dimension of the pile-cap and depth of the foundation from the soil surface. From the soil bore-log data (Figures B.1 and B.2) it is safe to assume the modulus of elasticity of the soil to be 200 MPa and Poisson's ratio 0.2. Effective shear modulus can be calculated using Table 4.7 of the FEMA document. However, shear modulus is a function of peak ground acceleration (PGA) and the value of shear modulus decreases with the increasing value of PGA. This is because the shear waves traveling through a soil stratum change the physical properties of that particular soil stratum resulting in reduction in shear modulus. For simplification the shear modulus was considered to be constant in this study. Figure B.3 shows the equations recommended by FEMA 356 document to calculate the soil spring constants for shallow foundations. This value of spring constant should be added to the pile-soil spring constants in parallel combination to get true value. If pile-soil spring constant is comparatively low than the pile cap-soil spring constant, pile-soil spring constant can be neglected.

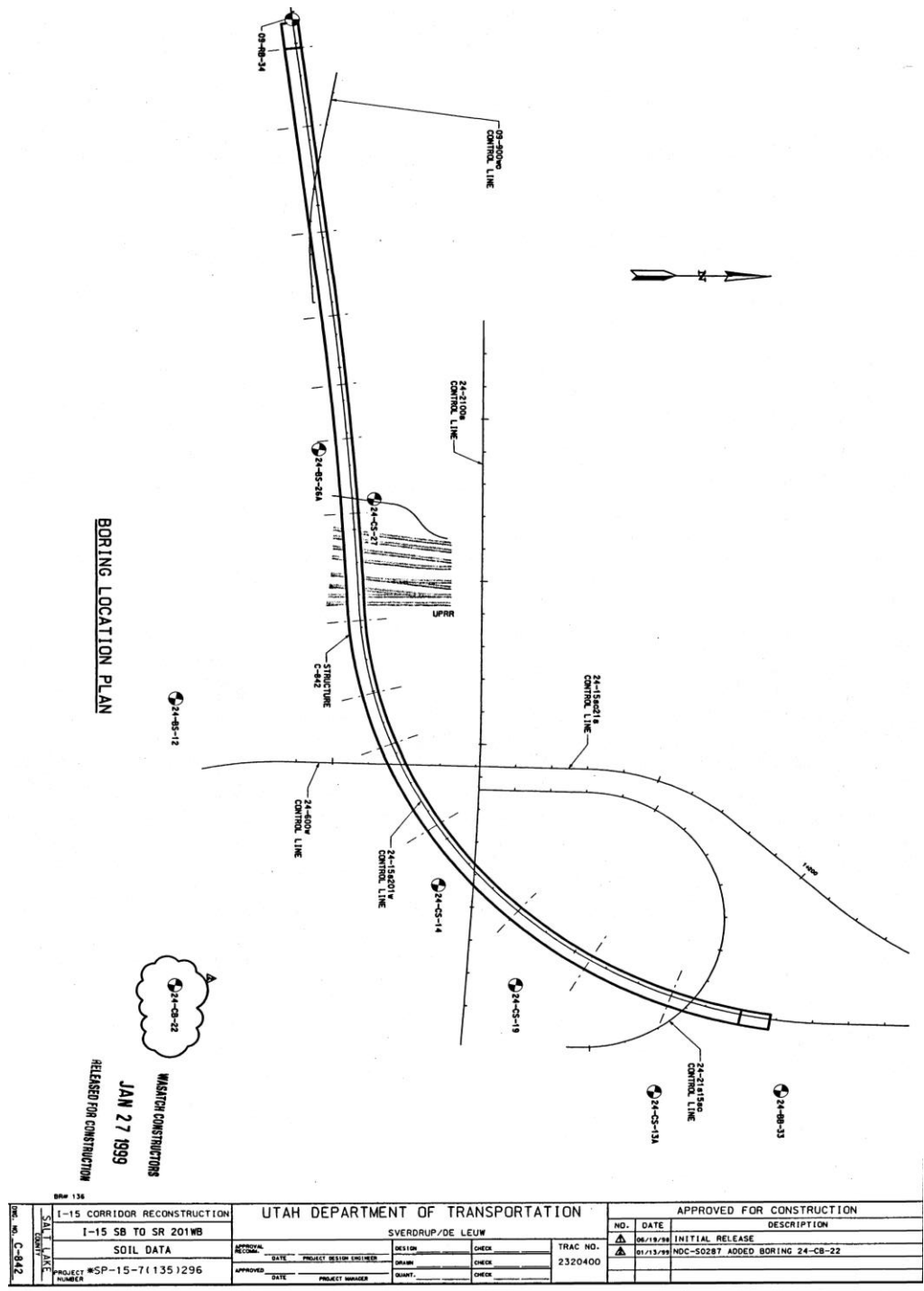


Figure B.1 Location of Bore holes at curved bridge site



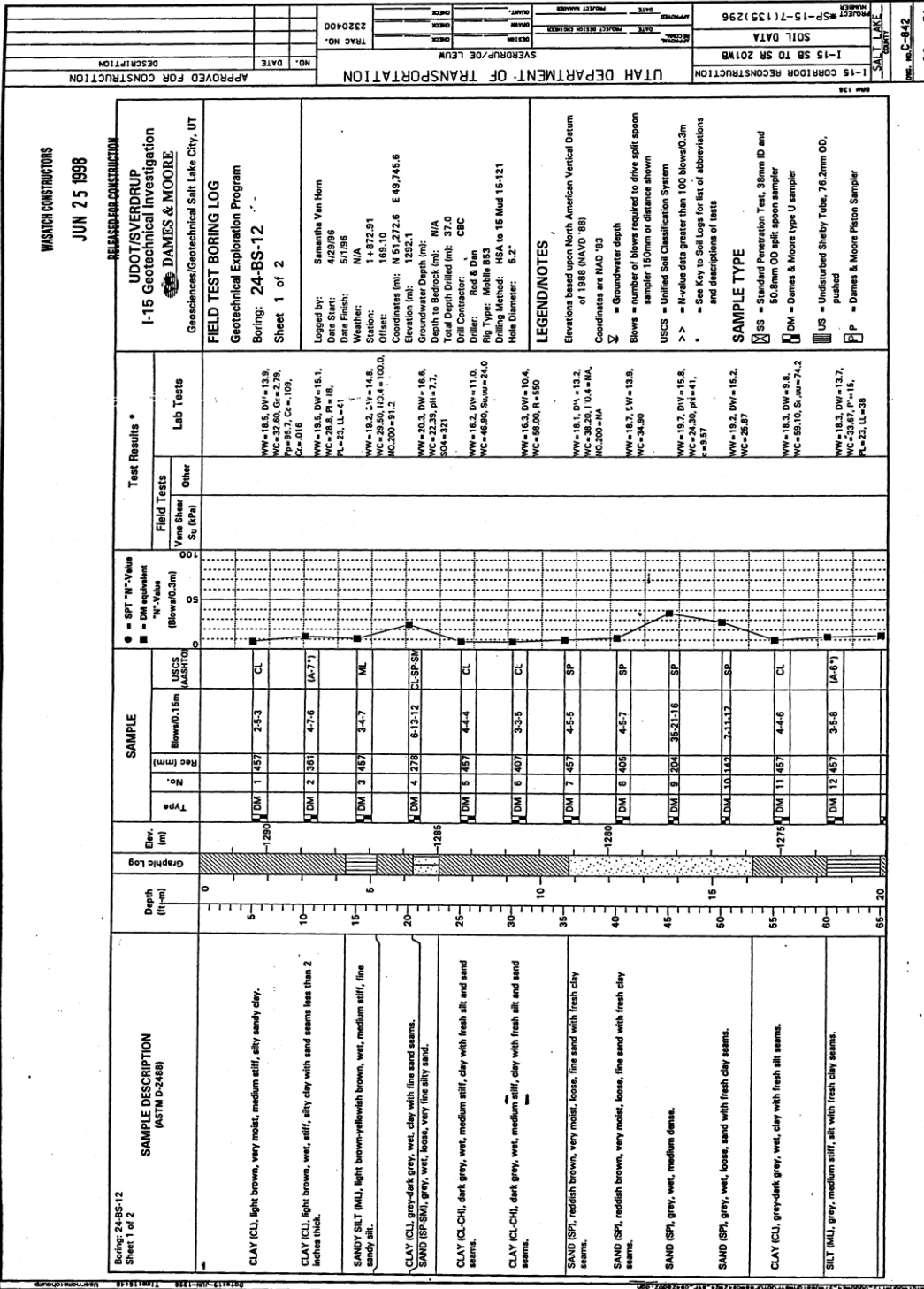
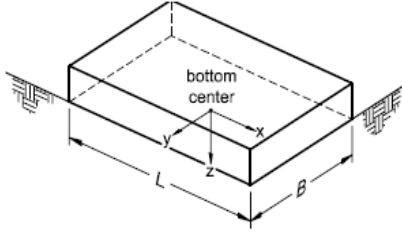
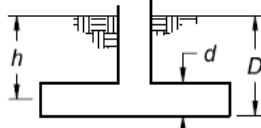


Figure B.2 Soil bore log data at curved bridge

Degree of Freedom	Stiffness of Foundation at Surface	Note
Translation along x-axis	$K_{x, sur} = \frac{GB}{2-\nu} \left[ 3.4 \left( \frac{L}{B} \right)^{0.65} + 1.2 \right]$	 <p>bottom center</p> <p>Orient axes such that <math>L \geq B</math></p>
Translation along y-axis	$K_{y, sur} = \frac{GB}{2-\nu} \left[ 3.4 \left( \frac{L}{B} \right)^{0.65} + 0.4 \frac{L}{B} + 0.8 \right]$	
Translation along z-axis	$K_{z, sur} = \frac{GB}{1-\nu} \left[ 1.55 \left( \frac{L}{B} \right)^{0.75} + 0.8 \right]$	
Rocking about x-axis	$K_{xx, sur} = \frac{GB^3}{1-\nu} \left[ 0.4 \left( \frac{L}{B} \right) + 0.1 \right]$	
Rocking about y-axis	$K_{yy, sur} = \frac{GB^3}{1-\nu} \left[ 0.47 \left( \frac{L}{B} \right)^{2.4} + 0.034 \right]$	
Torsion about z-axis	$K_{zz, sur} = GB^3 \left[ 0.53 \left( \frac{L}{B} \right)^{2.45} + 0.51 \right]$	
Degree of Freedom	Correction Factor for Embedment	Note
Translation along x-axis	$\beta_x = \left( 1 + 0.21 \sqrt{\frac{D}{B}} \right) \cdot \left[ 1 + 1.6 \left( \frac{hd(B+L)}{BL^2} \right)^{0.4} \right]$	 <p><math>d</math> = height of effective sidewall contact (may be less than total foundation height)</p> <p><math>h</math> = depth to centroid of effective sidewall contact</p> <p>For each degree of freedom, calculate  <math>K_{emb} = \beta K_{sur}</math></p>
Translation along y-axis	$\beta_y = \beta_x$	
Translation along z-axis	$\beta_z = \left[ 1 + \frac{1}{21} \frac{D}{B} \left( 2 + 2.6 \frac{B}{L} \right) \right] \cdot \left[ 1 + 0.32 \left( \frac{d(B+L)}{BL} \right)^{2/3} \right]$	
Rocking about x-axis	$\beta_{xx} = 1 + 2.5 \frac{d}{B} \left[ 1 + \frac{2d}{B} \left( \frac{d}{D} \right)^{-0.2} \sqrt{\frac{B}{L}} \right]$	
Rocking about y-axis	$\beta_{yy} = 1 + 1.4 \left( \frac{d}{L} \right)^{0.6} \left[ 1.5 + 3.7 \left( \frac{d}{L} \right)^{1.9} \left( \frac{d}{D} \right)^{-0.6} \right]$	
Torsion about z-axis	$\beta_{zz} = 1 + 2.6 \left( 1 + \frac{B}{L} \right) \left( \frac{d}{B} \right)^{0.9}$	

**Figure B.3** Equations used to calculate foundation-soil spring constants (FEMA 356)

## File Group

Lateral stiffness of pile group was calculated using procedure (Figure B.4) to develop P-y curves for piles in clay with no free water given by Welch and Reese (1972). Following is the summary of the procedure.

<b>Static Loading</b>	
1. Compute ultimate soil resistance, $P_u$ (using the smaller values)	$P_u = \left[ 3 + \frac{\gamma'}{C_u} z + \frac{J}{D} z \right] C_u D$ $P_u = 9C_u D$
2. Compute deflection at one-half the ultimate soil resistance, $y_{50}$	$y_{50} = 2.5 \varepsilon_{50} D$
3. Develop $p$ - $y$ curves using the following expression	$\frac{P}{P_u} = 0.5 \left( \frac{y}{y_{50}} \right)^{1/4} \quad \text{for } y \leq 16y_{50}$ $P = P_u \quad \text{for } y > 16y_{50}$
<b>Cyclic Loading</b>	
1. Develop $p$ - $y$ curves for static loading	Follow step 1 to 3
2. Determine parameter describing effect of repeated loading, $C$	$C = 9.6 \left( \frac{P}{P_u} \right)^4$
3. Determine $y$ for cyclic loading, $y_c$	$y_c = y_s + y_{50} C \log N$
<p>Where: <math>C_u</math> = Undrained shear strength  <math>D</math> = Pile diameter  <math>J</math> = Constant = 0.5  <math>N</math> = Number of cycles  <math>P_{ult}</math> = Ultimate soil resistance  <math>y_{50}</math> = Deflection at One-half the ultimate soil resistance  <math>y_c</math> = Deflection under N-cycles of load  <math>y_s</math> = Deflection under short-term static  <math>Z</math> = Depth  <math>\varepsilon_{50}</math> = Strain at one-half ultimate soil resistance 0.020 for soft clay,  0.010 for medium clay, and 0.005 for stiff clay  <math>\gamma'</math> = Effective soil unit weight</p>	

**Figure B.4** P-y curve calculation procedure

Table B.1 shows the calculation for  $Y_s$ ,  $Y_c$  and  $P$  for soil springs at various depth from the surface. P-y curves for each spring were then calculated as shown in Table B.2 and a simplified curve was calculated based on equal area method, for SAP 2000 input as shown Table B.3 and Figure B.5.

**Table B.1** Calculation of  $Y_s$ ,  $Y_c$  and  $P$  at various pile depth of curved bridge

Depth Z	Unit weight	$S_{U,uu}$	Pile Dia. D	J	$P_{U,1}$	$P_{U,2}$	$\epsilon_{50}$	$Y_{50}$	Pu
m	kN/cum	kN/m <sup>2</sup>	m		kN	kN		m	
2	19.00	25.00	0.324	0.5	61.60	72.90	0.005	0.00405	72.90
3	19.00	25.00	0.324	0.5	80.20	72.90	0.005	0.00405	80.26
4	19.00	25.00	0.324	0.5	98.90	72.90	0.005	0.00405	98.92
5	19.00	24.00	0.324	0.5	114.10	69.90	0.005	0.00405	114.10
6	19.00	24.00	0.324	0.5	132.20	69.90	0.005	0.00405	132.26
7	19.00	25.00	0.324	0.5	154.80	72.90	0.005	0.00405	154.89
8	19.00	25.00	0.324	0.5	173.50	72.90	0.005	0.00405	173.54
9	19.00	30.46	0.324	0.5	222.10	88.80	0.005	0.00405	222.11
10	19.00	35.93	0.324	0.5	276.10	104.70	0.005	0.00405	276.15
11	19.00	41.39	0.324	0.5	335.60	120.70	0.005	0.00405	335.65
12	19.00	46.86	0.324	0.5	400.60	136.60	0.005	0.00405	400.62
13	19.00	52.30	0.324	0.5	471.00	152.60	0.005	0.00405	471.06
14	19.00	57.79	0.324	0.5	546.90	168.50	0.005	0.00405	546.96
15	19.00	63.26	0.324	0.5	628.30	184.40	0.005	0.00405	628.33
16	19.00	68.73	0.324	0.5	715.20	200.40	0.005	0.00405	715.17
17	19.00	74.2	0.324	0.5	807.40	216.30	0.005	0.00405	807.47

**Table B.2** Calculation of P-y curve at depth Z = 2 m. for curved bridge

$Y_s$	$Y_{50}$	$P_U$	P	N	C	$Y_C$	Area under curve
m	m	kN/m	kN/m			m	
0	0.00405	61.61	0	20	0	0	
0.001	0.00405	61.61	21.71	20	0.148	0.001	0.0193
0.002	0.00405	61.61	25.82	20	0.296	0.003	0.0423
0.003	0.00405	61.61	28.57	20	0.444	0.005	0.0484
0.004	0.00405	61.61	30.71	20	0.592	0.007	0.0527
0.008	0.00405	61.61	36.52	20	1.185	0.014	0.2394
0.012	0.00405	61.61	40.41	20	1.777	0.021	0.2739
0.016	0.00405	61.61	43.43	20	2.370	0.028	0.2986
0.02	0.00405	61.61	45.92	20	2.962	0.035	0.3182
0.024	0.00405	61.61	48.06	20	3.555	0.042	0.3347
0.028	0.00405	61.61	49.95	20	4.148	0.049	0.3490
0.032	0.00405	61.61	51.64	20	4.740	0.056	0.3618
0.036	0.00405	61.61	53.19	20	5.333	0.064	0.3733
0.04	0.00405	61.61	54.61	20	5.925	0.071	0.3839
0.044	0.00405	61.61	55.92	20	6.518	0.078	0.3936
0.048	0.00405	61.61	57.15	20	7.111	0.085	0.4027
0.052	0.00405	61.61	58.31	20	7.703	0.092	0.4112
0.056	0.00405	61.61	59.40	20	8.296	0.099	0.4192
0.06	0.00405	61.612	60.4379	20	8.88	0.106837	0.4267867
0.064	0.00405	61.612	61.612	20	9.60	0.114584	0.4727582
0.068	0.00405	61.612	61.612	20	9.60	0.118584	0.246448
0.072	0.00405	61.612	61.612	20	9.60	0.122584	0.246448
0.076	0.00405	61.612	61.612	20	9.60	0.126584	0.246448
0.08	0.00405	61.612	61.612	20	9.60	0.130584	0.246448
0.084	0.00405	61.612	61.612	20	9.60	0.134584	0.246448
0.088	0.00405	61.612	61.612	20	9.60	0.138584	0.246448
0.092	0.00405	61.612	61.612	20	9.60	0.142584	0.246448
0.096	0.00405	61.612	61.612	20	9.60	0.146584	0.246448
0.1	0.00405	61.612	61.612	20	9.60	0.150584	0.246448

Total area under the curve = 7.8404 kN-m/m (to generate a tri-linear curve)

**Table B.3** Tri-linear curve points for P-y curve at Z=2 m. for curved bridge

Point	Y (kN/m)	P (m)	Area
1	0	0	
2	0.007122	30.806	0.1097
3	0.079412	61.612	3.340446
4	0.15058	61.612	4.384806

Total area under the tri-linear curve = 7.8349 kN-m/m

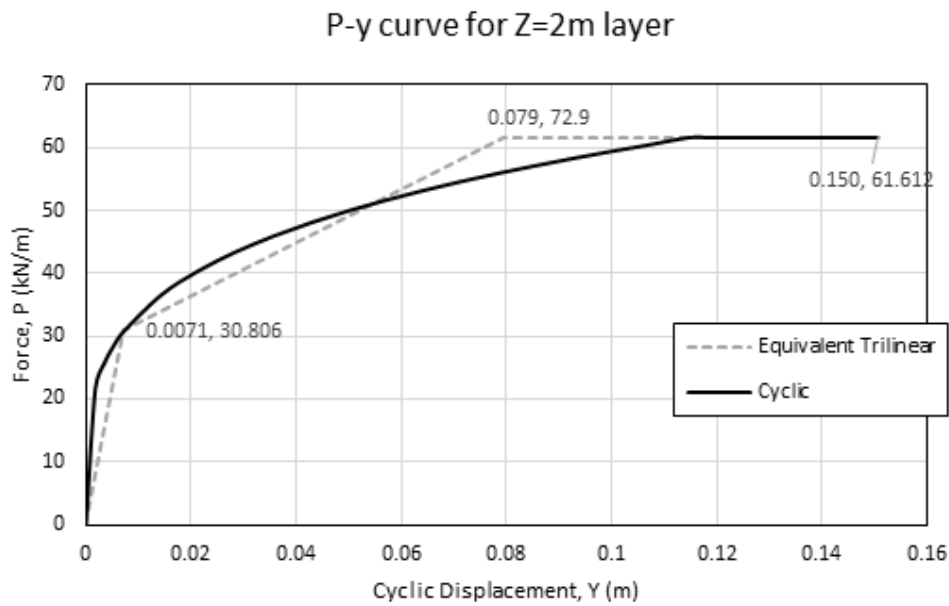


**Figure B.5** P-y curve for pile at Z=2

# APPENDIX C. SKEWED BRIDGE DRAWINGS AND SITE PHOTOGRAPHS

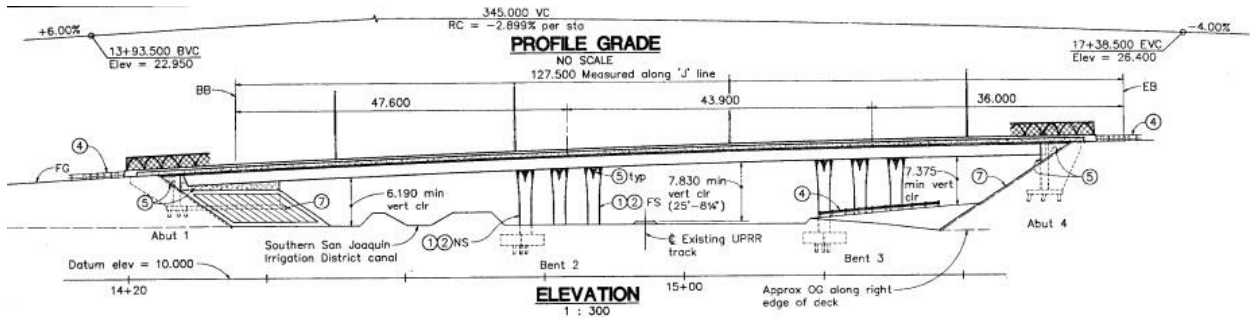


Figure C.1 Elevation and side view of skewed bridge



Figure C.2 Picture of on-site bridge (Image capture July 2012, Map data ©2015 Google)

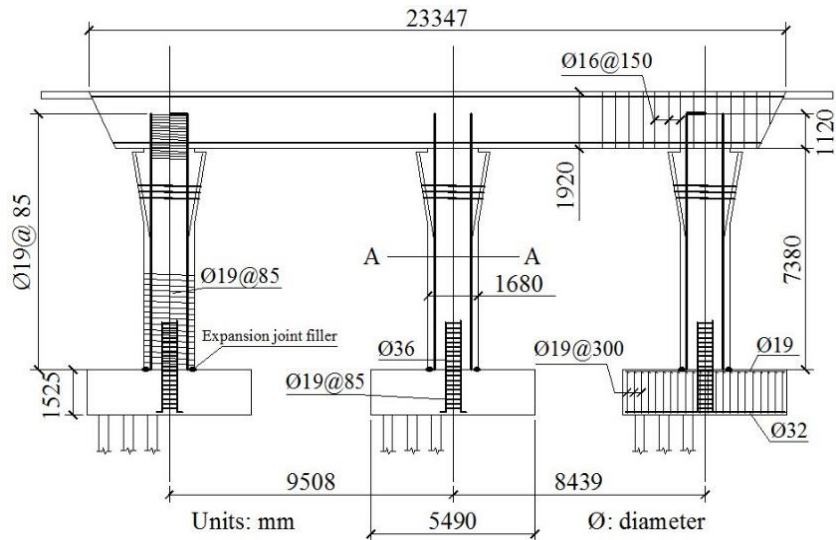


Figure C.3 Bent design details (adapted from Caltrans, 2008)

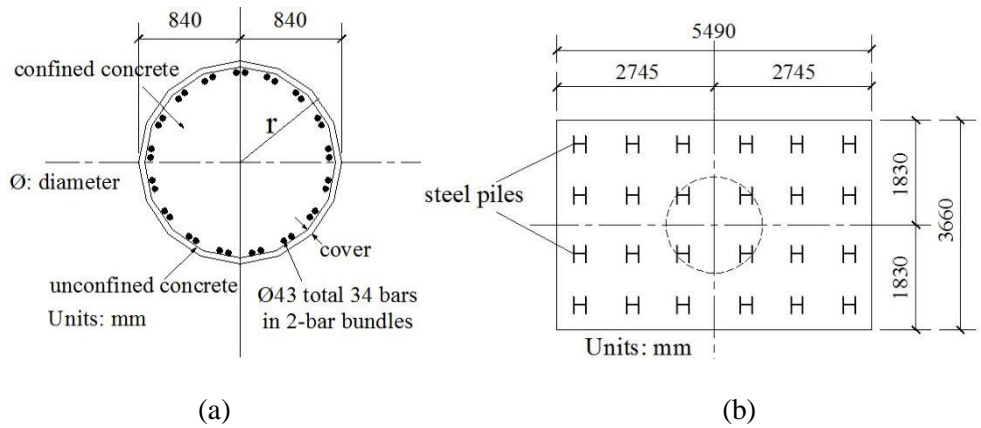


Figure C.4 Bent detail: (a) Column cross section; (b) Footing plan (adapted from Caltrans, 2008)

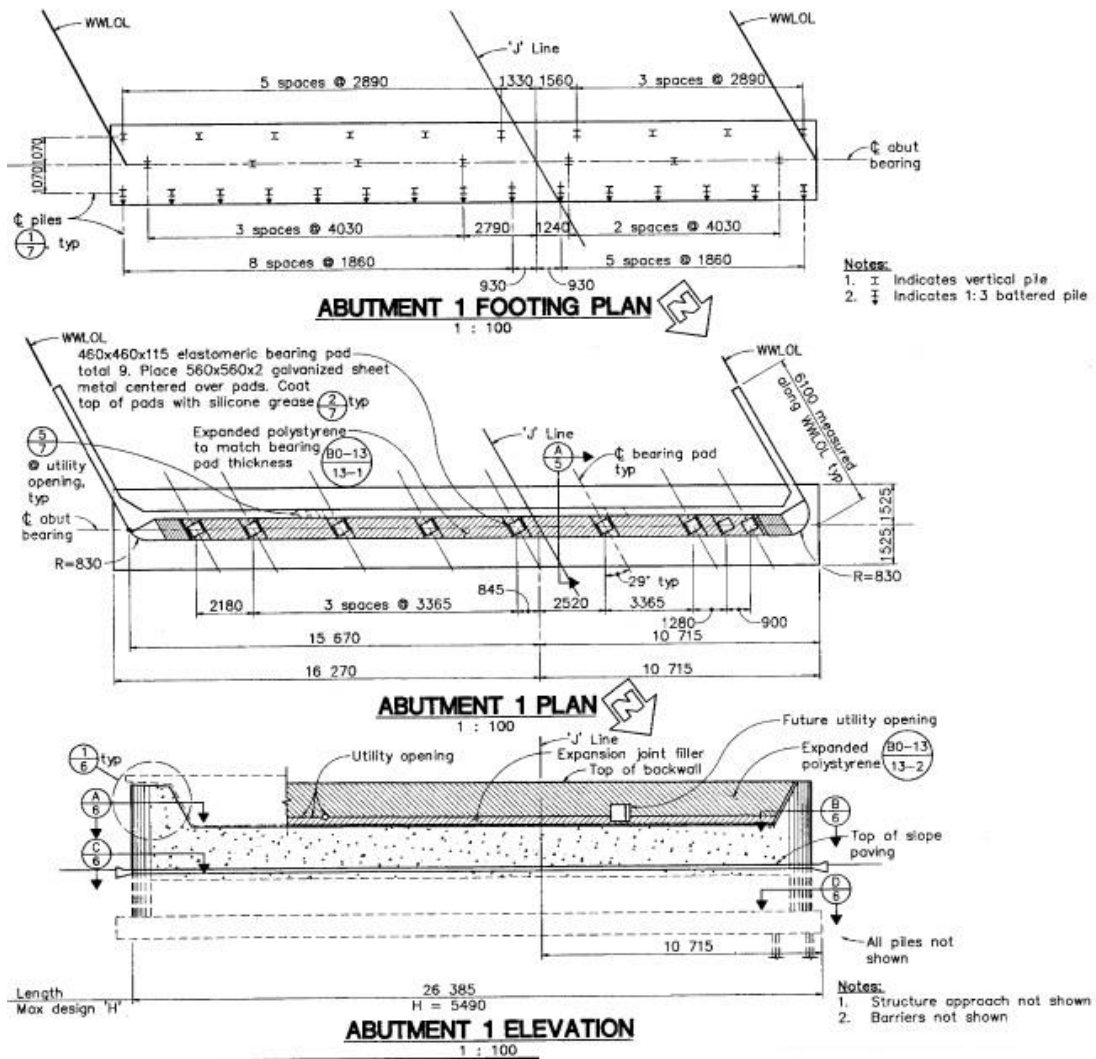


Figure C.5 Abutment plan and elevation